

Electronic Supplementary Information

Modulating the ground state, stability and charge transport in OFETs of biradicaloid Hexahydro-diindenopyrene derivatives and a proposed method to estimate the biradical character

Tanguy Jousselin-Oba,^a Masashi Mamada,^{*b} Atsushi Okazawa,^c Jérôme Marrot,^a Takayuki Ishida,^d Chihaya Adachi,^{b,e} Abderrahim Yassar,^f Michel Frigoli^{*a}

^{a.} UMR CNRS 8180, UVSQ, Institut Lavoisier de Versailles, Université Paris-Saclay, 45 avenue des Etats-Unis, 78035 Versailles Cedex, France. michel.frigoli@uvsq.fr

^{b.} Center for Organic Photonics and Electronics Research (OPERA), JST ERATO Adachi Molecular Exciton Engineering Project, and Academia-Industry Molecular Systems for Devices Research and Education Center, Kyushu University, Kyushu University, Nishi, Fukuoka, 819-0395 Japan. mamada@opera.kyushu-u.ac.jp

^{c.} Division of Chemistry, Institute of Liberal Education, Nihon University School of Medicine, Itabashi, Tokyo 173-8610, Japan.

^{d.} Department of Engineering Science, The University of Electro-Communications, Chofu, Tokyo 182-8585, Japan.

^{e.} International Institute for Carbon Neutral Energy Research (WPI-I2CNER), Kyushu University, Nishi, Fukuoka 819-0395, Japan.

^{f.} Ecole Polytechnique, Institut Polytechnique de Paris, LPICM, CNRS, route de Saclay, 91128 Palaiseau, France.

Content

GENERAL METHODS FOR SYNTHESIS	S3
INSTRUMENTS	S3
SYNTHESIS	S4
X-RAY STRUCTURE OF alcohol by product (CCDC: 1987611)	S14
X-RAY STRUCTURE OF HDIP (CCDC: 1987607).....	S15
X-RAY STRUCTURE OF <i>LINEAR</i> -HDIP (CCDC: 1987608).....	S16
X-RAY STRUCTURE OF <i>Syn</i> -HDIP (CCDC: 1987609).....	S17
X-RAY STRUCTURE OF <i>Anti</i> -HDIP (CCDC: 1987610).....	S18
VARIABLE TEMPERATURE ¹ H NMR of HDIP in <i>o</i> -DCB (d ₄)	S19
VARIABLE TEMPERATURE ¹ H NMR of <i>linear</i> -HDIP in <i>o</i> -DCB (d ₄) with COSY and NOESY.....	S20
VARIABLE TEMPERATURE ¹ H NMR of <i>syn</i> -HDIP in <i>o</i> -DCB (d ₄).....	S22
VARIABLE TEMPERATURE ¹ H NMR of <i>anti</i> -HDIP in <i>o</i> -DCB (d ₄) with COSY and NOESY	S23
ESR and SQUID MEASUREMENTS.....	S25
STABILITY TESTS OF HDIP DERIVATIVES	S27
THERMOGRAVIMETRY ANALYSIS OF HDIP derivatives under N ₂	S29
THEORITICAL CALCULATIONS	S30
HDIP: Bond length comparison of X-ray structure and calculations	S32
<i>Linear</i> -HDIP: Bond length comparison of X-ray structure and calculations.....	S34
<i>Syn</i> -HDIP: Bond length comparison of X-ray structure and calculations	S36
<i>Anti</i> -HDIP: Bond length comparison of X-ray structure and calculations	S38
TIPS-octazethrene: Bond length comparison of X-ray structure and calculations.....	S40
TIPS-heptazethrene: Bond length comparison of X-ray structure and calculations	S42
<i>Linear</i> -DIAn: Bond length comparison of X-ray structure and calculations	S44
ODD-ELECTRON DENSITY MAPS FOR FF DERIVATIVES.....	S53
OFET DEVICES	S54
RMN SPECTRA	S56
INFRARED SPECTRA	S63
MALDI (TOF) of HDIP derivatives.....	S67
REFERENCES	S71

GENERAL METHODS FOR SYNTHESIS

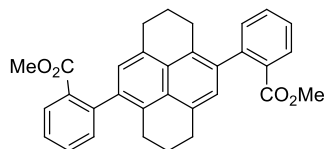
All reactions were carried out under argon. Dichloromethane was distilled from P₂O₅, THF and Toluene were distilled over Na/benzophenone. Dichloromethane and Toluene were kept over activated 3 Å molecular sieves. All commercial reagents were used without further purification. 4,9-dibromo-1,2,3,6,7,8-hexahydropyrene, ⁱ methyl 2-(4,4,5,5-tetramethyl-1,3,2-dioxaborolan-2-yl)benzoate, ⁱⁱ methyl 1-(4,4,5,5-tetramethyl-1,3,2-dioxaborolan-2-yl)-2-naphthoate, ⁱⁱⁱ 3-(4,4,5,5-tetramethyl-1,3,2-dioxaborolan-2-yl)-2-naphthoate, ^{iv} and methyl 3-(4,4,5,5-tetramethyl-1,3,2-dioxaborolan-2-yl)-2-naphthoate,^v were obtained according to procedures described from literature. ¹H and ¹³C NMR spectra were recorded at room temperature on Bruker Avance-300 MHz NMR spectrometer. ¹H NMR spectra were recorded at 300 MHz and ¹³C NMR spectra were recorded at 75 MHz. Chloroform residual peak was taken as internal reference at 7.26 ppm for ¹H NMR and 77 ppm for ¹³C NMR. *o*-Dichlorobenzene-d₄ residual peak was taken as internal reference at 7.20 ppm for ¹H NMR. Infrared spectra were recorded from Nicolet 6700 FT-IR spectrometer. High-resolution mass spectra were obtained by using Waters Xevo Q-ToF using positive mode. MALDI High-resolution mass spectra and Elementary analysis were performed by the analysis platform of ICSN (Centre de Recherche de Gif - www.icsn.cnrs-gif.fr).

INSTRUMENTS

Thermogravimetry-differential thermal analysis (TG-DTA) and differential scanning calorimetry (DSC) were performed on a TA Instruments SDT Q600 unit under a N₂ atmosphere with a heating rate of 10 °C per minute. Cyclic voltammetry was performed with BAS Electrochemical system in a three-electrode single-compartment cell with platinum working electrode, a platinum wire counter electrode, and an Ag/AgNO₃ reference electrode. The measurements were carried out in dry chlorobenzene using a 0.1 M tetrabutylammonium hexafluorophosphate (TBAPF₆) electrolyte, the solution being purged with nitrogen prior to measurement. All potentials were internally referred to the ferrocene/ferrocenium couple. Ultraviolet-visible (UV-vis) absorption spectra were recorded on UV-vis (Lambda 950-PKA, PerkinElmer) spectrophotometer. The thickness of CYTOP was measured by surface profiler Bruker Dektak XT. The channel width and length were measured optically with a laser scanning microscope (Olympus LEXT).

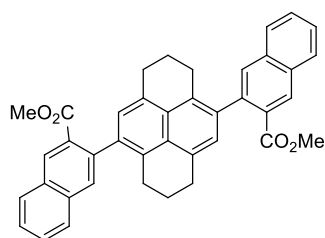
SYNTHESIS

Compound 1a



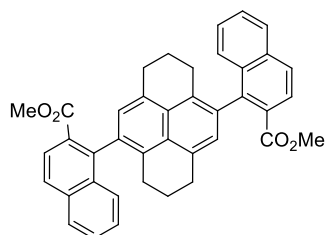
A solution of 4,9-dibromo-1,2,3,6,7,8-hexahydropyrene (1 g, 2.73 mmol), methyl 2-(4,4,5,5-tetramethyl-1,3,2-dioxaborolan-2-yl)benzoate (2.12 g; 8.1 mmol), K_3PO_4 (3.44 g; 16.2 mmol) and toluene/water (36/4 mL) was degassed for 30 min with argon. Tris(dibenzylideneacetone)dipalladium (0) ($Pd_2(dba)_3$) (124 mg; 0.135 mmol) and S-Phos (111 mg; 0.270 mmol) were then added. The resulting solution was heated at 100°C for 36 hours. The crude mixture was left to return to room temperature, diluted with chloroform. The solution was heated and then filtered through a pad of silica gel with hot chloroform several times. The resulting solution was concentrated under vacuum. The crude product was precipitated in DCM/MeOH. The solid obtained was then pass through a pad of silica gel eluted first with Petroleum ether / DCM (50/50) then with DCM to obtain a mixture of atropisomers (white solid, 1.20 g, 92%). Only 1H NMR could be performed due to low solubility. 1H NMR (300 MHz, $CDCl_3$) δ 7.97 (d, $J = 7.8$ Hz, 2H), 7.59 – 7.52 (m, 2H), 7.44 (td, $J = 7.6, 1.2$ Hz, 2H), 7.34 – 7.27 (m, 2H), 7.02 (d, $J = 7.8$ Hz, 2H), 3.64 (s, 2.7H), 3.62 (s, 3.3H), 3.10 – 3.00 (m, 4H), 2.75 – 2.70 (m, 4H), 2.00-1.90 (m, 4H). IR (cm^{-1}) = 1719 (COOMe); Elementary analysis: calculated for %C: 80.65; %H: 5.92; found for %C: 80.38; %H: 5.94.

Compound 1b

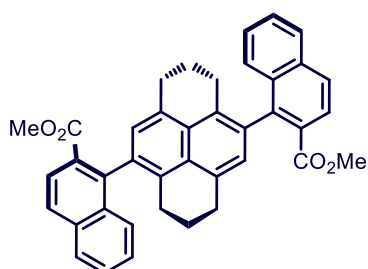


The synthesis of **1b** follows the same recipe as described for **1a** with 4,9-dibromo-1,2,3,6,7,8-hexahydropyrene (1 g, 2.70 mmol), methyl 1-(4,4,5,5-tetramethyl-1,3,2-dioxaborolan-2-yl)-2-naphthoate (2.53 g; 8.10 mmol), K_3PO_4 (5.16 g; 24.3 mmol), toluene/water (54/6 mL), $Pd_2(dba)_3$ (186 mg; 0.203 mmol) and S-Phos (167 mg; 0.407 mmol). Only 1H NMR could be performed due to low solubility. Yield 90% (2.13 g); 1H NMR (300 MHz, $CDCl_3$) δ 8.55 (s, 2H), 8.00 (d, $J = 7.7$ Hz, 2H), 7.86 (t, $J = 7.0$ Hz, 2H), 7.77 (s, 1.1H), 7.73 (s, 0.9H), 7.65 – 7.54 (m, 4H), 7.14 (d, $J = 7.5$ Hz, 2H), 3.71 (s, 2.7H), 3.69 (s, 3.3H), 3.10-3.09 (m, 4H), 2.81-2.77 (m, 4H), 2.02 – 1.90 (m, 4H); IR (cm^{-1}) = 1718 (COOMe); Elementary analysis: calculated for %C: 83.31; %H: 5.59; found for %C: 82.96; %H: 5.63.

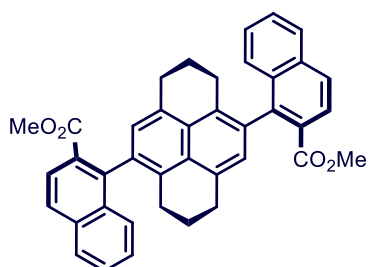
Compound 1c



The synthesis of **1c** follows the same recipe as described for **1a** with 4,9-dibromo-1,2,3,6,7,8-hexahydropyrene (1 g, 4.10 mmol), methyl 3-(4,4,5,5-tetramethyl-1,3,2-dioxaborolan-2-yl)-2-naphthoate (2.53 g; 8.10 mmol), K_3PO_4 (3.44 g; 16.2 mmol), toluene/water (36/4 mL), $Pd_2(dba)_3$ (124 mg; 0.135 mmol) and S-Phos (111 mg; 0.270 mmol). The crude product was purified by column chromatography using as eluent first EP/DCM (50/50) to collect first diastereoisomers (*trans*-configuration, 745 mg) then with dichloromethane to collect the second diastereoisomers (*cis*-configuration, 519 mg). The global yield is of 90 % with a ratio *trans/cis* of 59/41.



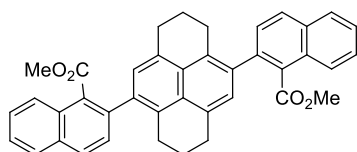
First diastereoisomer (*trans*): *Rf*: 0.54 (30/70, PE/DCM), 1H NMR (300 MHz, $CDCl_3$) δ 8.03 (d, $J = 8.6$ Hz, 2H), 7.94 (d, $J = 8.5$ Hz, 4H), 7.62 – 7.51 (m, 4H), 7.48 – 7.41 (m, 2H), 7.02 (s, 2H), 3.73 (s, 6H), 3.06-3.02 (m, 4H), 2.74-2.65 (m, 2H), 2.53-2.44 (m, 2H), 1.98 – 1.85 (m, 4H); ^{13}C NMR (75 MHz, $CDCl_3$) δ 168.06, 142.49, 134.85, 133.65, 132.64, 132.60, 131.82, 129.72, 128.24, 127.86, 127.60, 127.49, 127.41, 126.68, 125.70, 125.53, 52.10, 31.35, 28.86, 23.10; ^{13}C NMR (75 MHz, $CDCl_3$) δ 168.06, 142.49, 134.85, 133.65, 132.64, 132.60, 131.82, 129.72, 128.24, 127.86, 127.60, 127.49, 127.41, 126.68, 125.70, 125.53, 52.10, 31.35, 28.86, 23.10; IR (cm^{-1}) = 1723 (COOMe); Elementary analysis: calculated for %C: 83.31; %H: 5.59; found for %C: 83.15; %H: 5.61.



Second diastereoisomer (*cis*): *Rf*: 0.30 (30/70, PE/DCM), 1H NMR (300 MHz, $CDCl_3$) δ 7.94 (dd, $J_{AB} = 16.0$, 8.5 Hz, 6H), 7.58 – 7.48 (m, 4H), 7.43 – 7.35 (m, 2H), 7.02 (s, 2H), 3.56 (s, 6H), 3.05 - 3.99 (m, 2H), 2.74

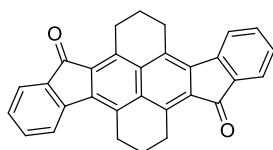
– 2.62 (m, 2H), 2.52 – 2.45 (m, 2H), 2.0 – 1.85 (m, 4H); Elementary analysis: calculated for %C: 83.31; %H: 5.59; found for %C: 83.17; %H: 5.61.

Compound 1d



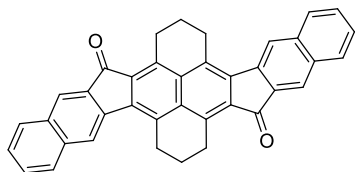
The synthesis of **1d** follows the same recipe as described for **1a** with 4,9-dibromo-1,2,3,6,7,8-hexahydropyrene (1 g, 4.10 mmol), methyl 3-(4,4,5,5-tetramethyl-1,3,2-dioxaborolan-2-yl)-2-naphthoate (2.53 g; 8.10 mmol), K₃PO₄ (3.44 g; 16.2 mmol), toluene/water (36/4 mL), Pd₂(dba)₃ (124 mg; 0.135 mmol) and S-Phos (111 mg; 0.270 mmol). Only ¹H NMR could be performed due to low solubility. Yield 85% (1.11 g); ¹H NMR (300 MHz, CDCl₃) δ 7.99 (td, *J* = 8.1, 2.1 Hz, 6H), 7.67 – 7.57 (m, 4H), 7.50 (d, *J* = 8.4 Hz, 1.1H), 7.45 (d, *J* = 8.4 Hz, 0.9H), 7.20 (s, 2H), 3.66 (s, 3H), 3.65 (s, 3H), 3.12–3.08 (m, 4H), 2.90–2.87 (m, 4H), 2.11 – 1.90 (m, 4H); IR (cm⁻¹) = 1727 (COOMe); Elementary analysis: calculated for %C: 83.31; %H: 5.59; found for %C: 83.14; %H: 5.61.

Compound 2a



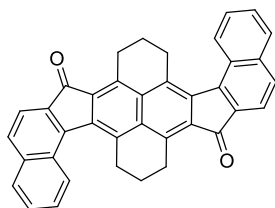
Compound **1a** (900 mg, 1.89 mmol) was put in suspension in 1,2-Dichloroethane (72 mL). TfOH (5.83 mL, 66 mmol) was then added dropwise. The resulting mixture was stirred at room temperature overnight then was transferred to an Erlenmeyer flask with a minimum amount of dichloromethane. MeOH (150 mL) was carefully added followed by a saturated aq. NaHCO₃ solution until neutral pH then diluted with plenty of water. The resulting precipitate was filtered, washed with water and MeOH. After drying under vacuum, compound **2a** was obtained as orange solid (677 mg, 78%). Due to the insolubility of the compound, only IR was measured. IR (cm⁻¹) = 1692 (C=O stretching of 5-membered ring); Elementary analysis: calculated for %C: 87.36; %H: 4.89; found for %C: 86.99; %H: 4.93.

Compound 2b



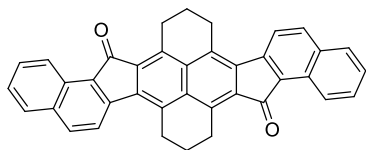
Compound **1b** (1.5 g, 2.60 mmol) was put in suspension in 1,2-Dichloroethane (100 mL). TfOH (8 mL, 91 mmol) was then added dropwise. The resulting mixture was stirred at room temperature for 5h then was transferred to an Erlenmeyer flask with a minimum amount of dichloromethane. MeOH (200 mL) was carefully added followed by a saturated aq. NaHCO₃ solution until neutral pH then diluted with plenty of water. The resulting precipitate was filtered, washed with water and MeOH. After drying under vacuum, compound **2b** was obtained as orange solid (1.29 g, 98%). Due the insolubility of the compound, only IR was measured. IR (cm⁻¹) = 1691 (C=O stretching of 5-membered ring); Elementary analysis: calculated for %C: 89.04; %H: 4.72; found for %C: 88.65; %H: 4.75.

Compound 2c



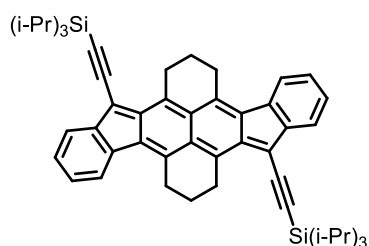
Compound **2c** (408 mg, 0.708 mmol) was put in suspension in 1,2-Dichloroethane (27 mL). TfOH (4.38 mL, 49.6 mmol) was then added dropwise. The resulting mixture was stirred at room temperature overnight then was transferred to an Erlenmeyer flask with a minimum amount of dichloromethane. MeOH (60 mL) was carefully added followed by a saturated aq. NaHCO₃ solution until neutral pH then diluted with plenty of water. The resulting precipitate was filtered, washed with water and MeOH. After drying under vacuum, compound **2c** was obtained as orange-red solid (323 mg, 89%). Due the insolubility of the compound, only IR was measured. IR (cm⁻¹) = 1688 (C=O stretching of 5-membered ring); Elementary analysis: calculated for %C: 89.04; %H: 4.72; found for %C: 88.25; %H: 4.77.

Compound 2d



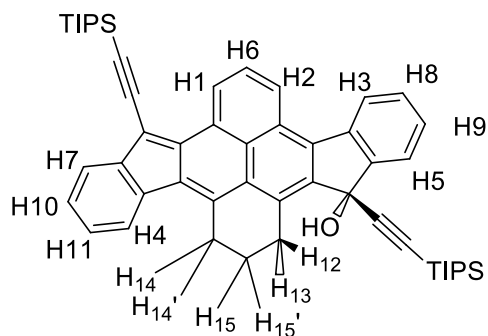
Compound **1d** (850 mg, 1.47 mmol) was put in suspension in 1,2-Dichloroéthane (56 mL). TfOH (8 mL, 91 mmol) was then added dropwise. The resulting mixture was stirred at room temperature for 5h than was transferred to an Erlenmeyer flask with a minimum amount of dichloromethane. MeOH (110 mL) was carefully added followed by a saturated aq. NaHCO₃ solution until neutral pH then diluted with plenty of water. The resulting precipitate was filtered, washed with water and MeOH. After drying under vacuum, compound **2d** was obtained as orange-red solid (766 mg, 75%). Due the insolubility of the compound, only IR was measured. IR (cm⁻¹) = 1676 (C=O stretching of 5-membered ring); Elementary analysis: calculated for %C: 89.04; %H: 4.72; found for %C: 88.60; %H: 4.75.

HDIP



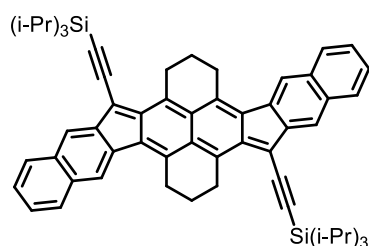
(Triisopropylsilyl)acetylene (0.46 g, 2.45 mmol) in THF (6 mL) was cooled to 0 °C. *n*-BuLi (1.51 mL, 2.41 mmol, 1.6 M) was added and the mixture stirred at 0 °C for 30 min. In a separate flask, **compound 2a** (206 mg, 0.049 mmol) in THF (60 mL) was sonicated for 30 min and then cooled to 0 °C. The lithiate solution was cannulated into the cold diene suspension and the reaction was stirred for 3h30 at room temperature. The reaction was quenched by addition of saturated aq. NH₄Cl solution and extracted with Et₂O. The organic layer was washed with water and dried (MgSO₄), filtered, and concentrated under vacuum keeping the temperature below 40°C. The crude product was precipitated purified by filtration on an alumina gel pad, eluting with different mixture of solvent: petroleum ether/Dichloromethane/diethyl ether/methanol: starting with 10/0/0/0 to remove the excess of TIPS-acetylene, then 0/8/2/0 to collect the first diol diastereoisomer, and then 0/9/0/1 to collect the second diol diastereoisomer. The obtain diols after concentration under vacuum at temperature below 40°C were then precipitated in a mixture of dichloromethane/petroleum ether, filtered and dried under vacuum to afford the crude diols: 98 mg of the trans diol and 232 mg of the cis diol.

The diol (330 mg, 0.424 mmol) was dissolved in anhydrous toluene (126 ml), degassed for 30 min with Ar under sonication, then SnCl₂ (322 mg, 1.69 mmol) was added. The resulting mixture was stirred at room temperature for 1h20 then filtered over a pad of silica gel eluted with dichloromethane. After concentration the product was precipitated with CH₂Cl₂ and MeCN and filtered. The filtrate is purified by column chromatography eluted with petroleum ether/dichloromethane: 9/1 to afford a bit of HDIP and the partially aromatized monoalcohol (39 mg, 12%). The fraction of the HDIP obtain by chromatography is putted together with the previously obtained precipitate, and is precipitated in a mixture of dichloromethane/petroleum ether to afford the expected HDIP (163 mg, 48%) as a blue solid. Due to the low solubility of HDIP, only the ¹H NMR was recorded. ¹H NMR (300 MHz, CDCl₃) δ 7.70 (dd, *J* = 6.2, 2.0 Hz, 2H), 7.53 – 7.45 (m, 2H), 7.23 – 7.14 (m, 4H), 3.58 (t, *J* = 6.1 Hz, 4H), 3.27 (t, *J* = 6.2 Hz, 4H), 2.16 – 1.92 (m, 4H), 1.35 – 1.12 (m, 42H); HRMS (MALDI-TOF): calculated for C₅₂H₆₂Si₂ (M⁺): 742.43901; found: 742.43850.



^1H NMR (300 MHz, CD_2Cl_2) δ 9.64 (d, $J = 7.5$ Hz, H1), 8.67 (d, $J = 8.3$ Hz, H2), 8.22 (d, $J = 7.6$ Hz, H3), 7.94 (d, $J = 7.6$ Hz, H4), 7.77 (d, $J = 7.2$ Hz, H5), 7.70 (t, $J = 8.0$ Hz, H6), 7.65 (d, $J = 7.2$ Hz, H7), 7.49 (t, $J = 6.9$ Hz, H8), 7.43 (t, $J = 7.1$ Hz, H9), 7.37 (t, $J = 7.1$ Hz, H10), 7.28 (t, $J = 7.0$ Hz, H11), 3.95 – 3.80 (m, H12), 3.68 – 3.53 (m, H13), 3.52 – 3.35 (m, H14, H14'), 2.59 (s, OH), 2.31 – 2.04 (m, H15, H15'), 1.33 – 1.21 (m, 21H, TIPS), 1.01 (s, 21H, TIPS).

Linear-HDIP



(Triisopropylsilyl)acetylene (0.854 g, 4.68 mmol) in THF (12 mL) was cooled to 0 °C. *n*-BuLi (2.8 mL, 4.53 mmol, 1.6 M) was added and the mixture stirred at 0 °C for 30 min. In a separate flask, **compound 2b** (390 mg, 0.76 mmol) in THF (120 mL) was sonicated for 30 min and then cooled to 0 °C. The lithiated solution was cannulated into the cold dione suspension and the reaction was stirred for 4h at room temperature. The reaction was quenched by addition of saturated aq. NH_4Cl solution and extracted with Et_2O . The organic layer was washed with water and dried (MgSO_4), filtered, and concentrated under vacuum keeping the temperature below 40°C. The crude product was precipitated purified by filtration on an alumina gel pad, eluting with different mixture of solvent: petroleum ether/dichloromethane/diethyl ether/methanol: starting with 10/0/0/0 to remove the excess of TIPS-acetylene, then 0/8/2/0 to collect the first *trans*-diastereoisomer, and then 0/9/0/1 to collect the *cis*-diol diastereoisomer. The obtain diols after concentration under vacuum at temperature below 40°C were then precipitated in a mixture of dichloromethane/petroleum ether, filtered and dried under vacuum to afford the crude diols 175 mg of the *trans*-diol and 474 mg of the *cis*-diol.

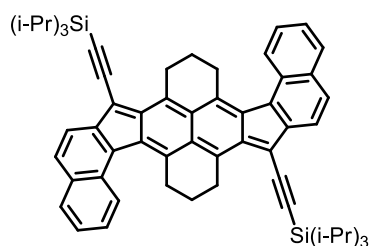
The *trans*-diol (175 mg, 0.200 mmol) was dissolved in anhydrous toluene (70 ml), degassed for 30 min with Ar under sonication, then SnCl_2 (151 mg, 0.798 mmol) was added. The resulting mixture was stirred at room temperature for 2h30, and then filtered over a pad of silica gel eluted with dichloromethane. After concentration the product was precipitated with CH_2Cl_2 and MeCN and

filtered. The precipitate is solubilized in dichloromethane and precipitated with petroleum ether upon evaporation of the dichloromethane under vacuum and then filtrated. The MeCN and petroleum ether filtrate are put together and purified by column chromatography eluted with petroleum ether/dichloromethane: 9/1 to afford a bit of linear-HDIP. The fraction of the *linear*-HDIP obtain by chromatography is putted together with the previously obtained precipitate, and is precipitated again twice in a mixture of dichloromethane/petroleum ether to afford the expected *linear*-HDIP (73mg, 41%) as a dark blue solid.

Starting with the *cis*-diol (474 mg, 0,540 mmol) under the same condition, the reaction time is 1h20 until completion and afford the about the same yield (191mg, 40%).

Due to the low solubility of *linear*-HDIP, only the ^1H NMR was recorded. ^1H NMR (300 MHz, CDCl_3) δ 8.08 (s, 2H), 7.85 (s, 2H), 7.83 – 7.69 (m, 4H), 7.40-7.34 (m, 4H), 3.67 (t, $J = 5.8$ Hz, 4H), 3.40 (t, $J = 6.1$ Hz, 4H), 2.12 (dt, $J = 12.2, 6.1$ Hz, 4H), 1.29 (dd, $J = 16.8, 3.9$ Hz, 42H); HRMS (MALDI-TOF): calculated for $\text{C}_{60}\text{H}_{66}\text{Si}_2$ (M^+): 842.47031; found: 842.47138.

Syn-HDIP



(Triisopropylsilyl)acetylene (0.854 g, 4.68 mmol) in THF (12 mL) was cooled to 0 °C. *n*-BuLi (2.8 mL, 4.53 mmol, 1.6 M) was added and the mixture stirred at 0 °C for 30 min. In a separate flask, **compound 2b** (400 mg, 0,78 mmol) in THF (120 mL) was sonicated for 30 min and then cooled to 0 °C. The lithiated solution was cannulated into the cold dione suspension and the reaction was stirred for 4h at room temperature. The reaction was quenched by addition of saturated aq. NH_4Cl solution and extracted with Et_2O . The organic layer was washed with water and dried (MgSO_4), filtered, and concentrated under vacuum keeping the temperature below 40°C. The crude product was precipitated purified by filtration on an alumina gel pad, eluting with different mixture of solvent: petroleum ether/dichloromethane/diethyl ether: starting with 10/0/0 to remove the excess of TIPS-acetylene, then 5/5/0 to collect the *trans*-diol diastereoisomer and then 0/5/5 to collect the *cis*-diol diastereoisomer. The obtain diols after concentration under vacuum at temperature below 40°C were then precipitated twice in a mixture of dichloromethane/petroleum ether, filtered and dried under vacuum to afford the crude diols 268 mg of the *trans*-diol and 173 mg of the *cis*-diol.

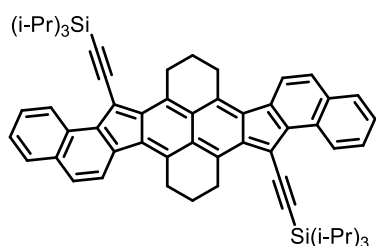
The *cis*-diol (170 mg, 0.194 mmol) was dissolved in anhydrous toluene (70 ml), degassed for 30 min with Ar under sonication, then SnCl_2 (147 mg, 0.775 mmol) was added. The resulting mixture was stirred at room temperature for 1h30, and then filtered over a pad of silica gel eluted with dichloromethane. After concentration the product was precipitated with CH_2Cl_2 and MeCN and

filtered and precipitated again in dichloromethane/methanol. The precipitate is purified by column chromatography eluted with petroleum ether/dichloromethane: 9/1 to afford a *syn*-HDIP. The fraction of the *syn*-HDIP obtain by chromatography is putted together with the previously obtained precipitate, and is precipitated again twice in a mixture of dichloromethane/petroleum ether to afford the expected *syn*-HDIP (31mg, 13%) as a dark blue solid.

Starting with the *trans*-diol (268 mg, 0.305 mmol) under the same condition, the reaction time is 1h50 until completion and afford about the same yield (61 mg, 8%).

Due to the low solubility of *syn*-HDIP, only the ^1H NMR was recorded. ^1H NMR (300 MHz, CDCl_3) δ 8.18 (d, $J = 8.3$ Hz, 2H), 7.75 (d, $J = 7.1$ Hz, 2H), 7.63 (s, 4H), 7.44 (t, $J = 7.0$ Hz, 2H), 7.36 (t, $J = 7.2$ Hz, 2H), 3.63 (t, $J = 5.8$ Hz, 4H), 3.36 – 3.23 (m, 4H), 2.04 – 1.80 (m, 4H), 1.34 – 1.12 (m, 42H); HRMS (MALDI-TOF): calculated for $\text{C}_{60}\text{H}_{66}\text{Si}_2$ (M^+): 842.47031; found: 842.47254.

Anti-HDIP



(Triisopropylsilyl)acetylene (1.07 g, 5.85 mmol) in THF (16 mL) was cooled to 0 °C. *n*-BuLi (3.53 mL, 5.64 mmol, 1.6 M) was added and the mixture stirred at 0 °C for 30 min. In a separate flask, **compound 2b** (500 mg, 0,98 mmol) in THF (150 mL) was sonicated for 30 min and then cooled to 0 °C. The lithiated solution was cannulated into the cold dione suspension and the reaction was stirred for 4h at room temperature. The reaction was quenched by addition of saturated aq. NH_4Cl solution and extracted with Et_2O . The organic layer was washed with water and dried (MgSO_4), filtered, and concentrated under vacuum keeping the temperature below 40°C. The crude product was precipitated purified by filtration on an alumina gel pad, eluting with different mixture of solvent: petroleum ether/dichloromethane/diethyl ether/methanol: starting with 10/0/0/0 to remove the excess of TIPS-acetylene, then 0/8/2/0 to collect the *trans*-diol diastereoisomer, and then 0/8/0/2 to collect the *cis*-diol diastereoisomer. The obtain diols after concentration under vacuum at temperature below 40°C were then precipitated in a mixture of dichloromethane/petroleum ether, filtered and dried under vacuum to afford the crude diols: 244 mg of the *trans*-diol and 478 mg of the *cis*-diol.

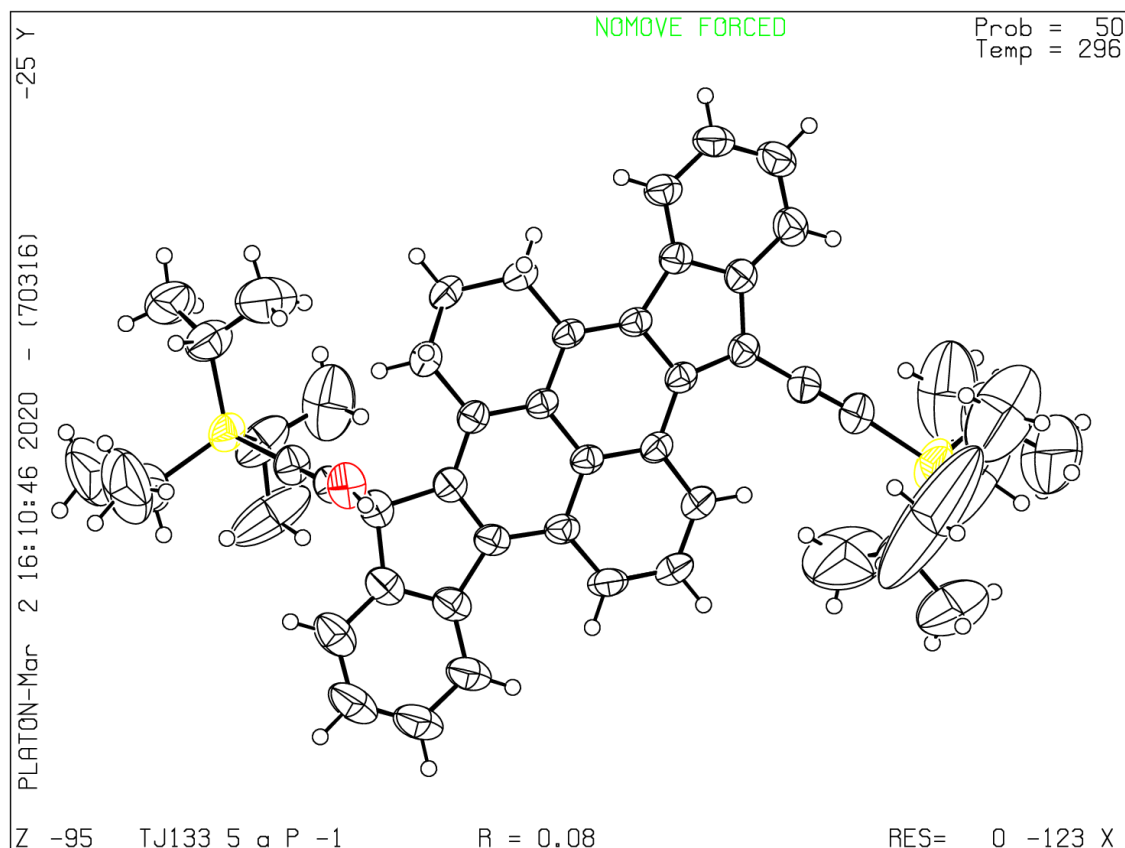
The *trans*-diol (100 mg, 0.114 mmol) was dissolved in anhydrous toluene (40 ml), degassed for 30 min with Ar under sonication, then SnCl_2 (87 mg, 0.456 mmol) was added. The resulting mixture was stirred at room temperature for 4h30, and then filtered over a pad of silica gel eluted with dichloromethane and then hot toluene. After concentration the product was precipitated twice with

CH₂Cl₂ and MeCN, filtered, washed with MeCN, methanol, petroleum ether and acetone and dried under vacuum to afford *anti* HDIP (53 mg, 51%) as a dark blue solid.

Starting with the *trans*-diol (100 mg, 0.114 mmol) under the same condition, the reaction time is 2h30 until completion and afford about the same yield (52 mg, 52%).

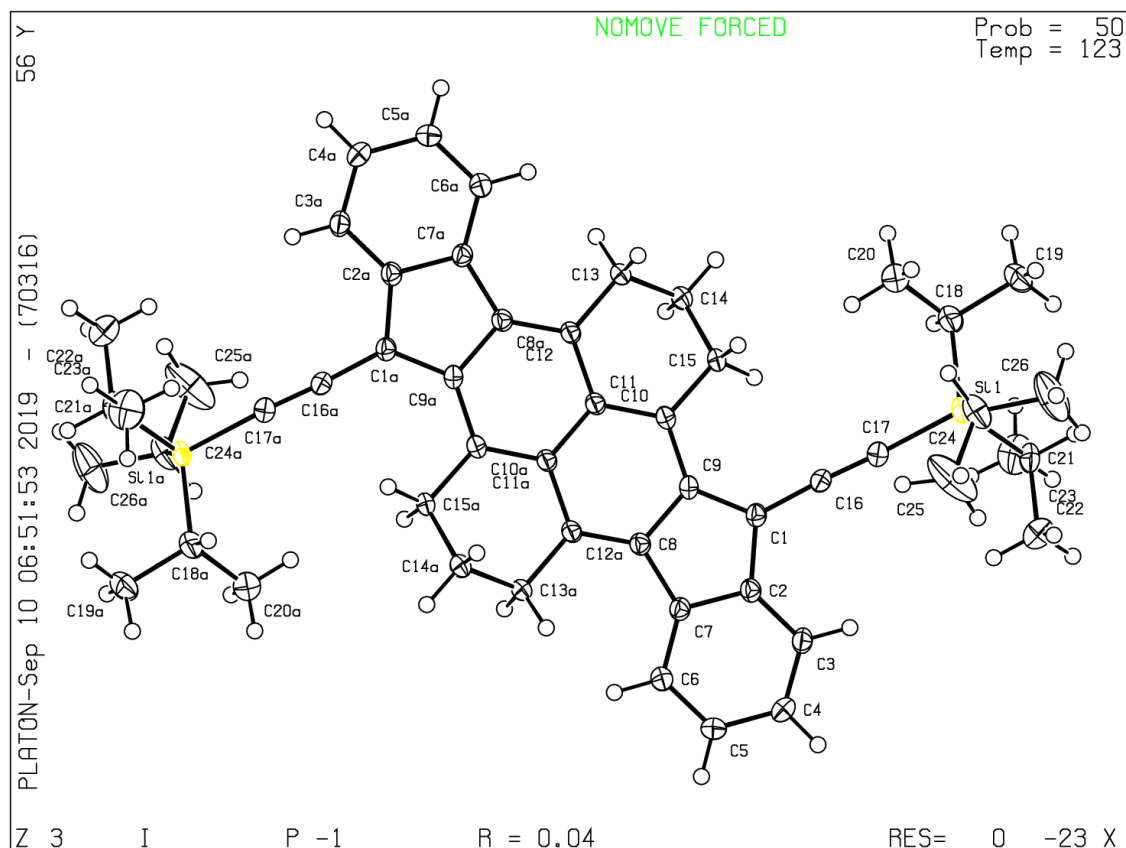
Due to the low solubility of *Anti*-HDIP, only the ¹H NMR was recorded; ¹H NMR (300 MHz, CDCl₃) δ 9.68 – 9.63 (m, 2H), 7.83 (d, *J* = 8.8 Hz, 2H), 7.72 (dd, *J* = 6.3, 3.3 Hz, 2H), 7.55 (d, *J* = 8.3 Hz, 2H), 7.41-7.36 (m, 3H), 3.69 (t, *J* = 5.9 Hz, 4H), 3.35 (t, *J* = 6.5 Hz, 4H), 2.15 – 1.94 (m, 4H), 1.60 – 0.96 (m, 42H); HRMS (MALDI-TOF): calculated for C₆₀H₆₆Si₂ (M⁺): 842.47031; found: 842.47270.

X-RAY STRUCTURE OF alcohol by product (CCDC: 1987611)



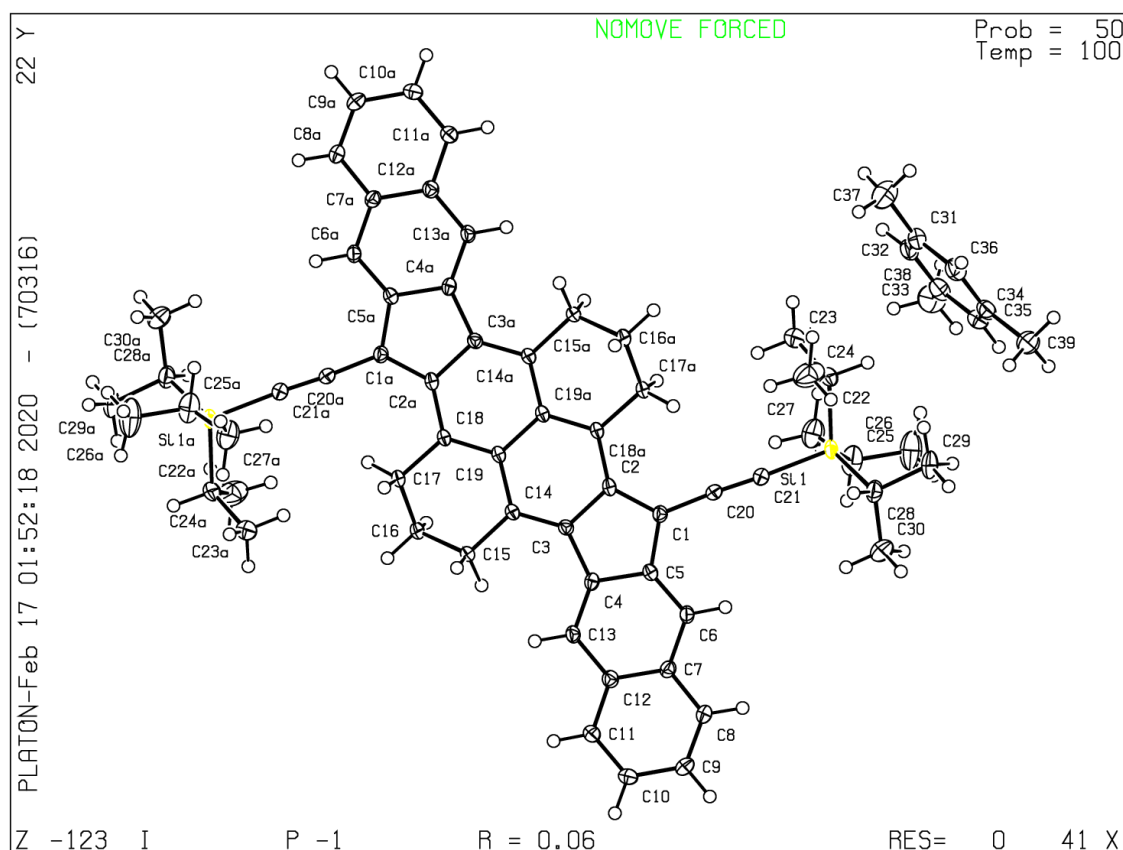
Crystal data for alcohol by product : $C_{52}H_{60}OSi_2$, $M_w = 757.18$, triclinic, space group $P-1$; dimensions: $a = 11.6952(3) \text{ \AA}$, $b = 12.3024(3) \text{ \AA}$, $c = 18.2803(5) \text{ \AA}$, $\alpha = 72.922(1)^\circ$, $\beta = 72.859(1)^\circ$, $\gamma = 66.635(1)^\circ$, $V = 2259.89(10) \text{ \AA}^3$; $Z = 2$; $\mu = 0.11 \text{ mm}^{-1}$; 55136 reflections measured at 296 K; independent reflections: 10425 [$7533 F_o > 4\sigma(F_o)$]; data were collected up to a $2\theta_{max}$ value of 55.2° (99.6 % coverage). Number of variables: 509; $R_1 = 0.080$, $wR_2 = 0.232$, $S = 1.05$; highest residual electron density 0.64 e.\AA^{-3} ; CCDC = 1987611.

X-RAY STRUCTURE OF HDIP (CCDC: 1987607)



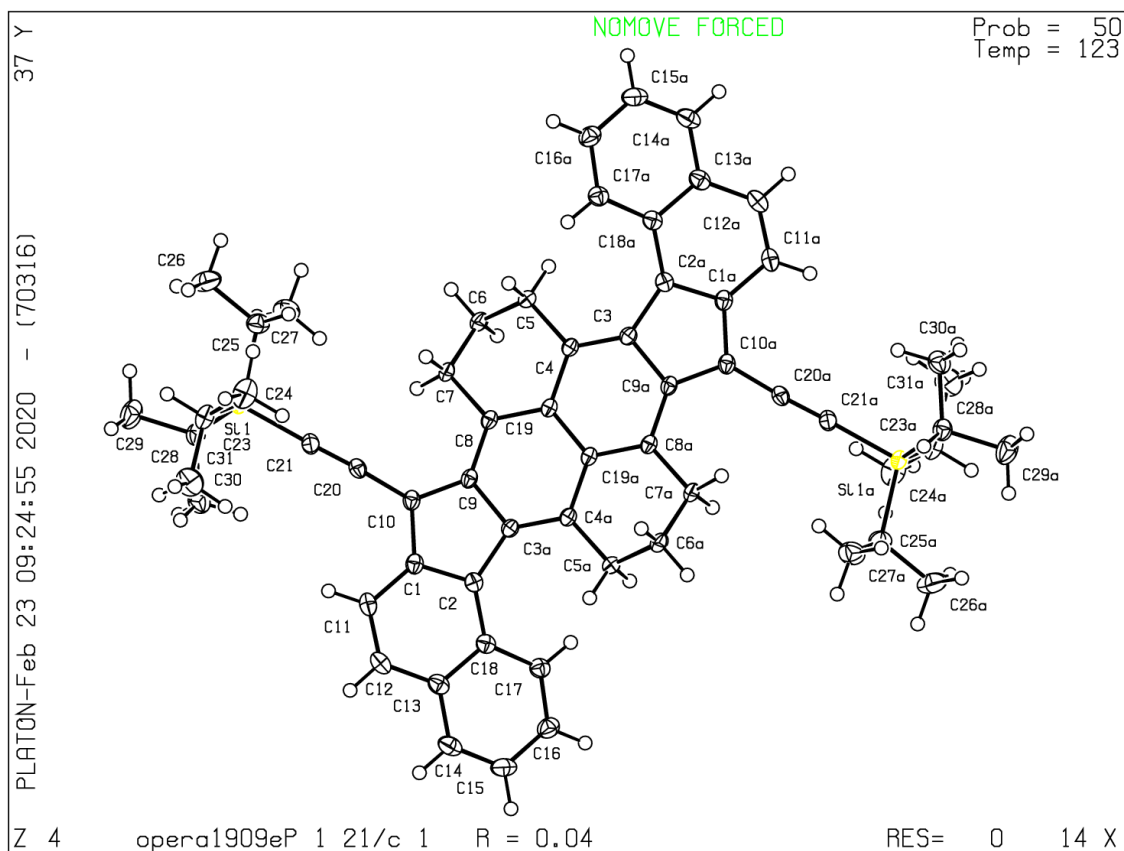
Crystal data for HDIP : $C_{52}H_{62}Si_2$, $M_w = 743.19$, triclinic, space group $P-1$; dimensions: $a = 7.7000$ (5) Å, $b = 8.2465$ (5) Å, $c = 17.9156$ (8) Å, $\alpha = 89.138$ (4)°, $\beta = 79.878$ (4)°, $\gamma = 75.346$ (5)°, $V = 1082.95$ (11) Å³; $Z = 1$; $\mu = 0.12$ mm⁻¹; 17540 reflections measured at 123 K; independent reflections: 4955 [3978 $F_o > 4\sigma(F_o)$]; data were collected up to a $2\theta_{max}$ value of 54.8° (99.9 % coverage). Number of variables: 250; $R_1 = 0.045$, $wR_2 = 0.123$, $S = 1.05$; highest residual electron density 0.51 e.Å⁻³; CCDC = 1987607.

X-RAY STRUCTURE OF *LINEAR-HDIP* (CCDC: 1987608)



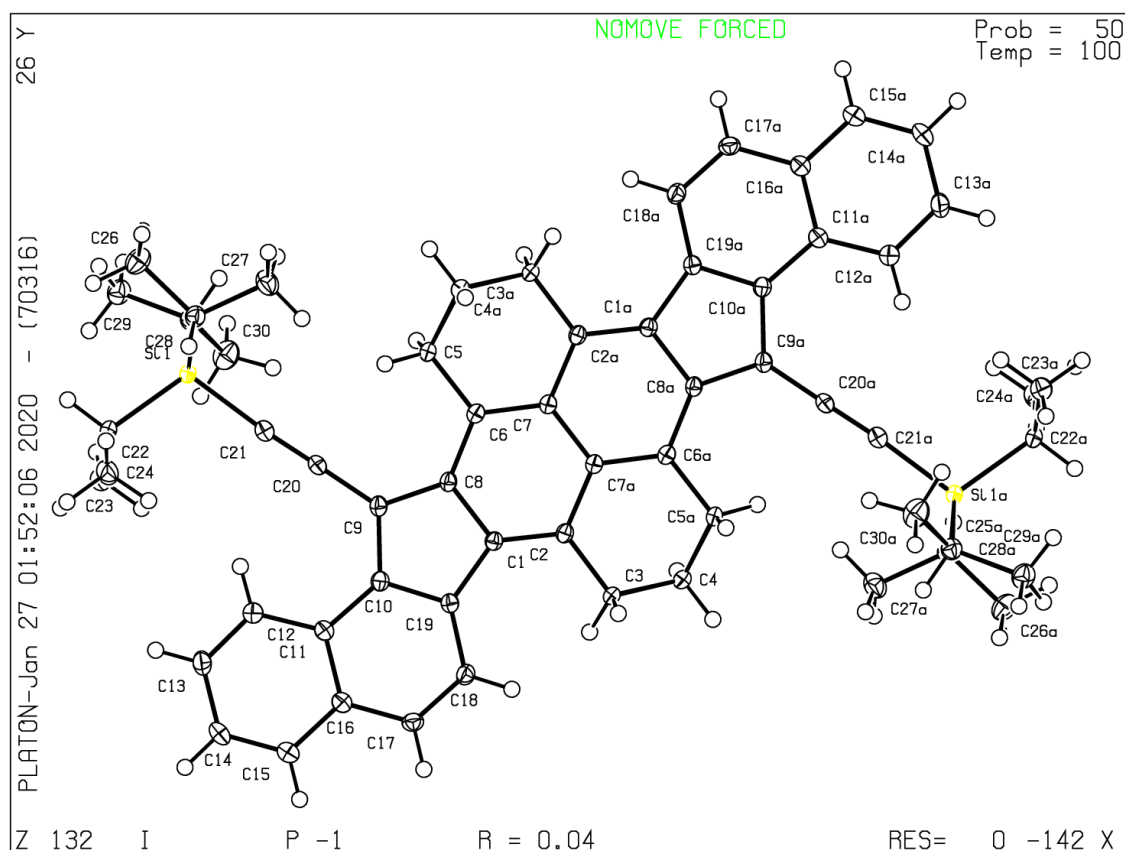
Crystal data for *linear-HDIP*: $C_{78}H_{90}Si_2$, $M_w = 1083.67$, triclinic, space group $P-1$; dimensions: $a = 8.8789(6) \text{ \AA}$, $b = 12.7356(5) \text{ \AA}$, $c = 14.6701(9) \text{ \AA}$, $\alpha = 99.626(4)^\circ$, $\beta = 104.748(6)^\circ$, $\gamma = 98.811(4)^\circ$, $V = 1547.92(16) \text{ \AA}^3$; $Z = 1$; $\mu = 0.10 \text{ mm}^{-1}$; 17632 reflections measured at 100 K; independent reflections: 6212 [4914 $F_o > 4\sigma(F_o)$]; data were collected up to a $2\theta_{\text{max}}$ value of 52.6° (98.3 % coverage). Number of variables: 370; $R_1 = 0.059$, $wR_2 = 0.144$, $S = 1.03$; highest residual electron density 0.86 e.\AA^{-3} ; CCDC = 1987608.

X-RAY STRUCTURE OF *Syn*-HDIP (CCDC: 1987609)



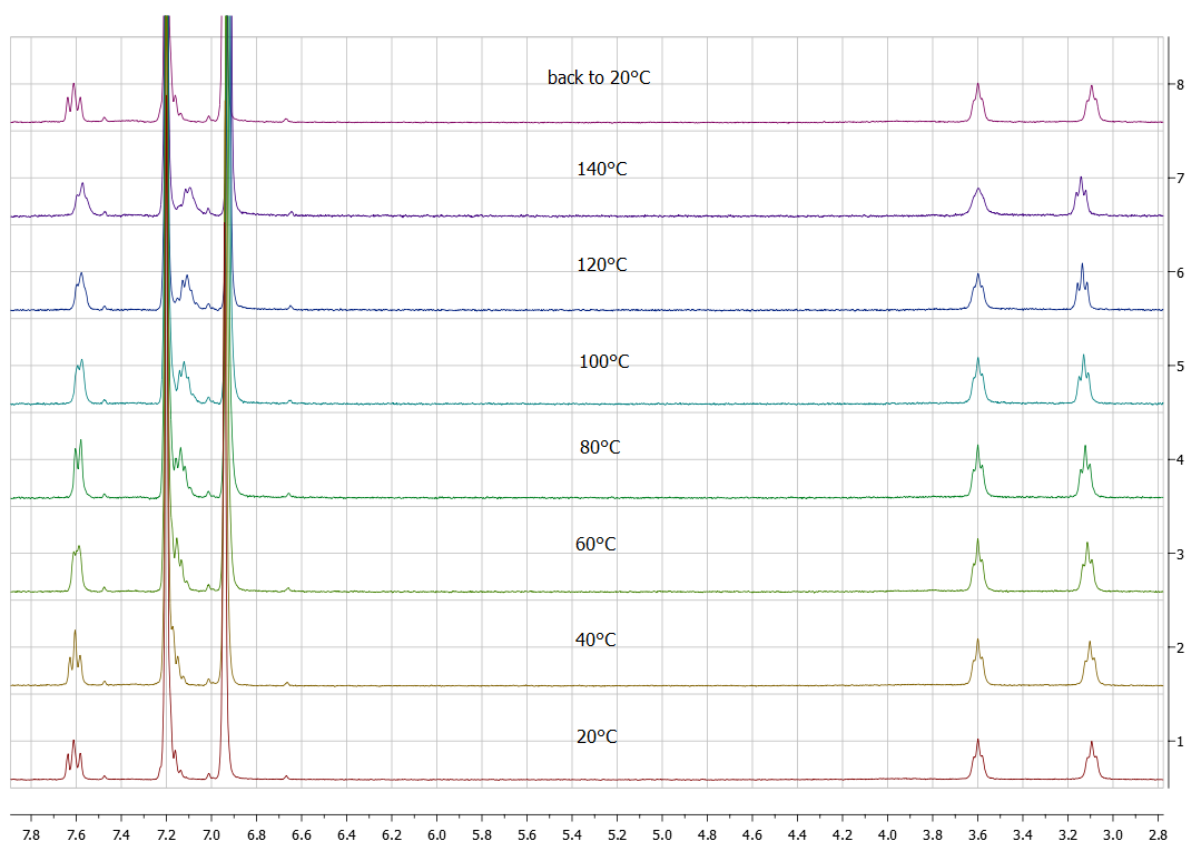
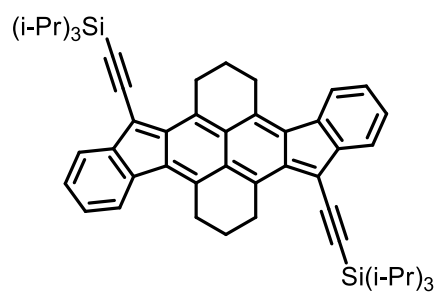
Crystal data for *syn*-HDIP : $C_{60}H_{66}Si_2$, $M_w = 843.30$, monoclinic, space group $P2_1/c$; dimensions: $a = 8.1631(3) \text{ \AA}$, $b = 13.8454(6) \text{ \AA}$, $c = 21.1693(8) \text{ \AA}$, $\beta = 91.995(4)^\circ$, $V = 2391.13(18) \text{ \AA}^3$; $Z = 2$; $\mu = 0.11 \text{ mm}^{-1}$; 21124 reflections measured at 123 K; independent reflections: 5474 [$4380 F_o > 4\sigma(F_o)$]; data were collected up to a $2\theta_{\text{max}}$ value of 54.9° (99.8 % coverage). Number of variables: 286; $R_1 = 0.042$, $wR_2 = 0.103$, $S = 1.03$; highest residual electron density 0.37 e.\AA^{-3} ; CCDC = 1987609.

X-RAY STRUCTURE OF *Anti*-HDIP (CCDC: 1987610)

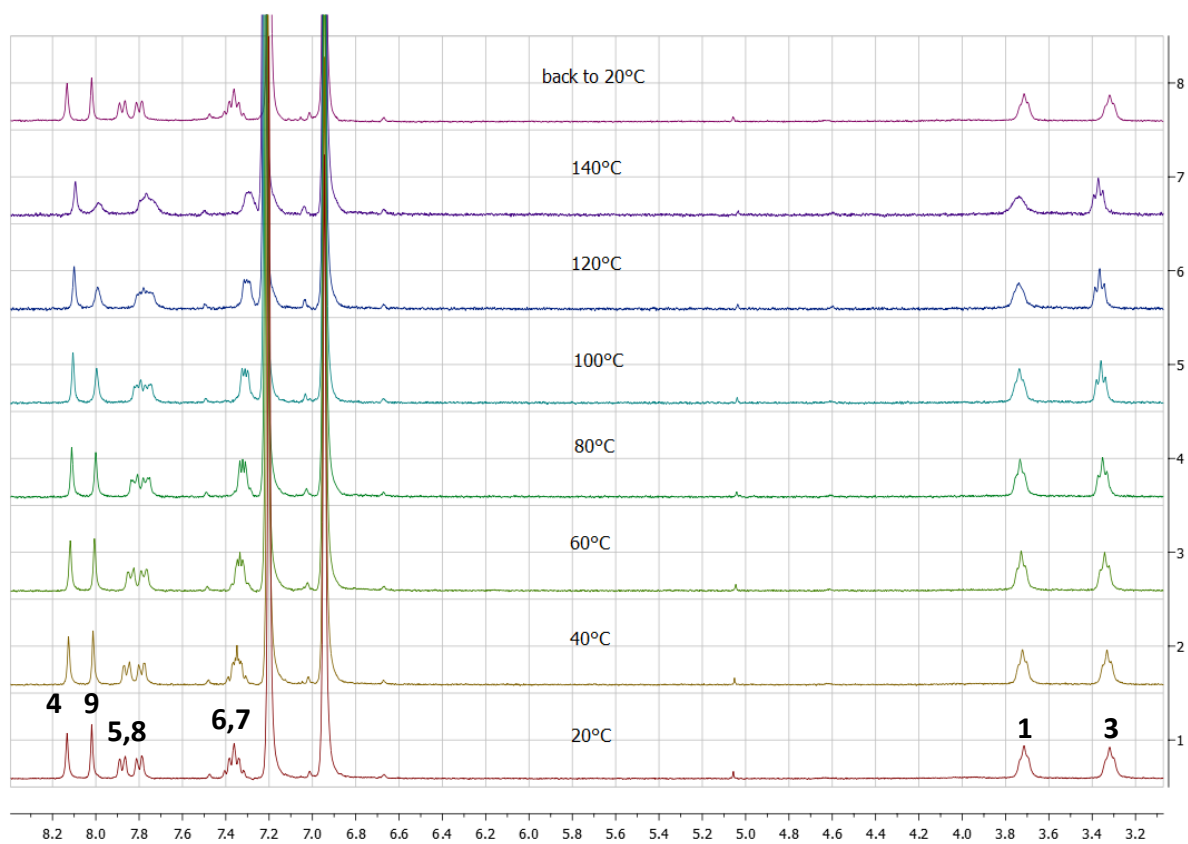
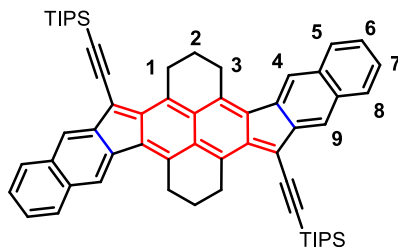


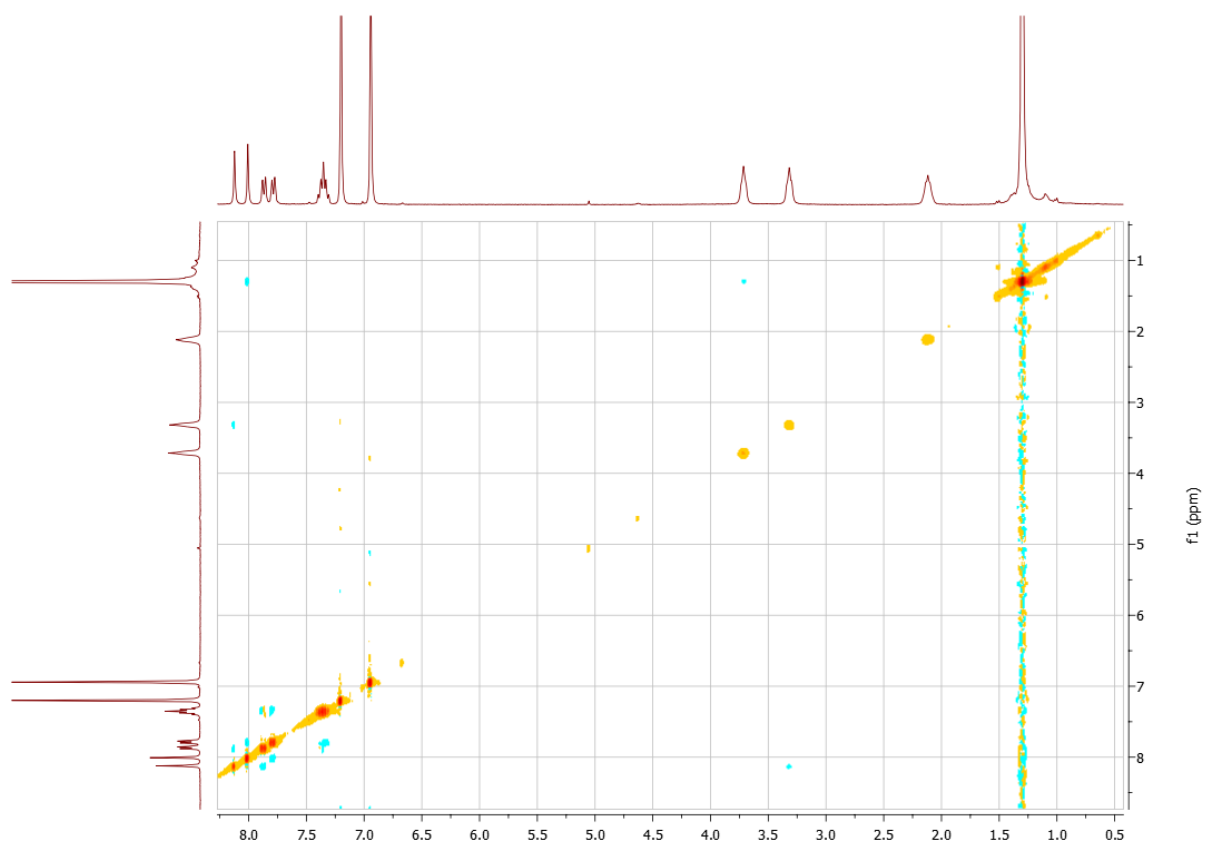
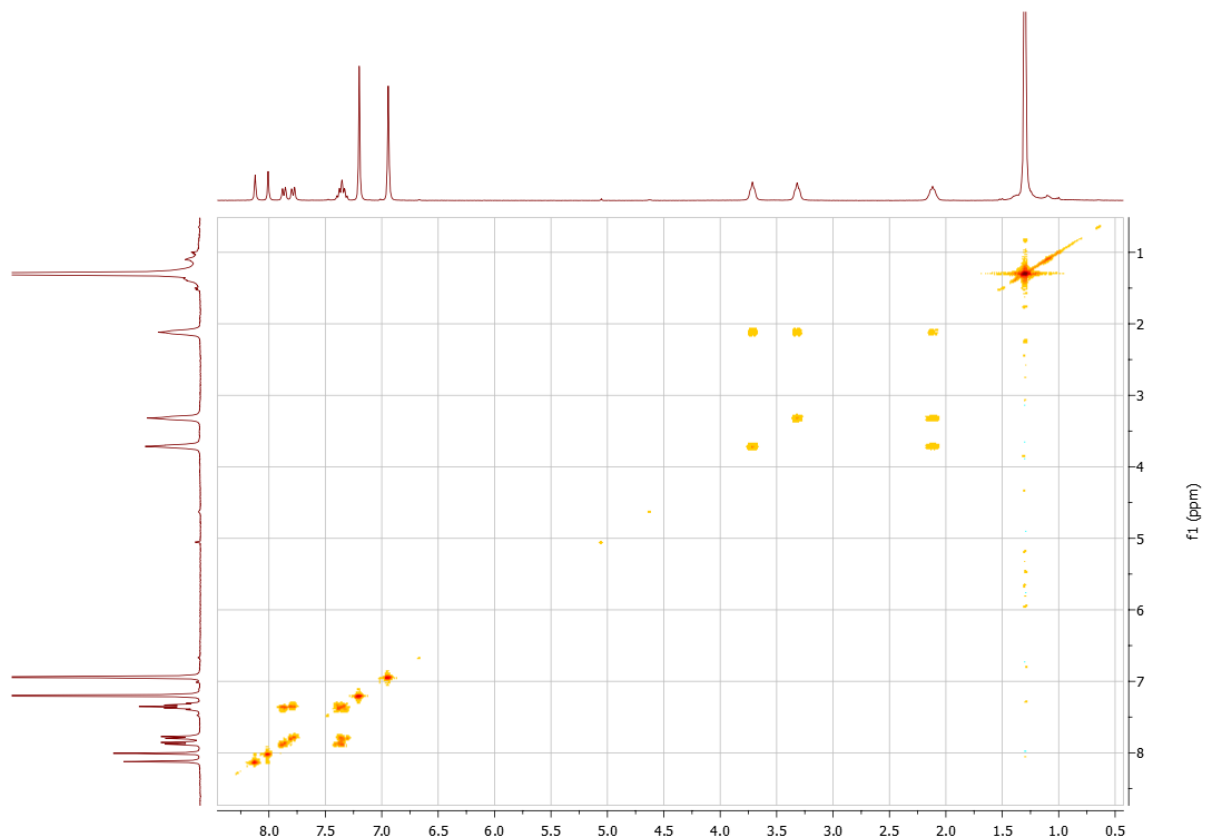
Crystal data for *anti*-HDIP : $C_{60}H_{66}Si_2$, $M_w = 843.30$, triclinic, space group $P-1$; dimensions: $a = 8.2869$ (3) Å, $b = 9.3544$ (4) Å, $c = 15.0106$ (7) Å, $\alpha = 83.361$ (4)°, $\beta = 81.878$ (4)°, $\gamma = 89.500$ (3)°, $V = 1144.18$ (8) Å³; $Z = 1$; $\mu = 0.12$ mm⁻¹; 26342 reflections measured at 100 K; independent reflections: 5252 [4265 $F_o > 4\sigma(F_o)$]; data were collected up to a $2\theta_{max}$ value of 54.9° (99.9 % coverage). Number of variables: 286; $R_1 = 0.041$, $wR_2 = 0.107$, $S = 1.04$; highest residual electron density 0.29 e.Å⁻³; CCDC = 1987610.

VARIABLE TEMPERATURE ^1H NMR of HDIP in *o*-DCB (d_4)

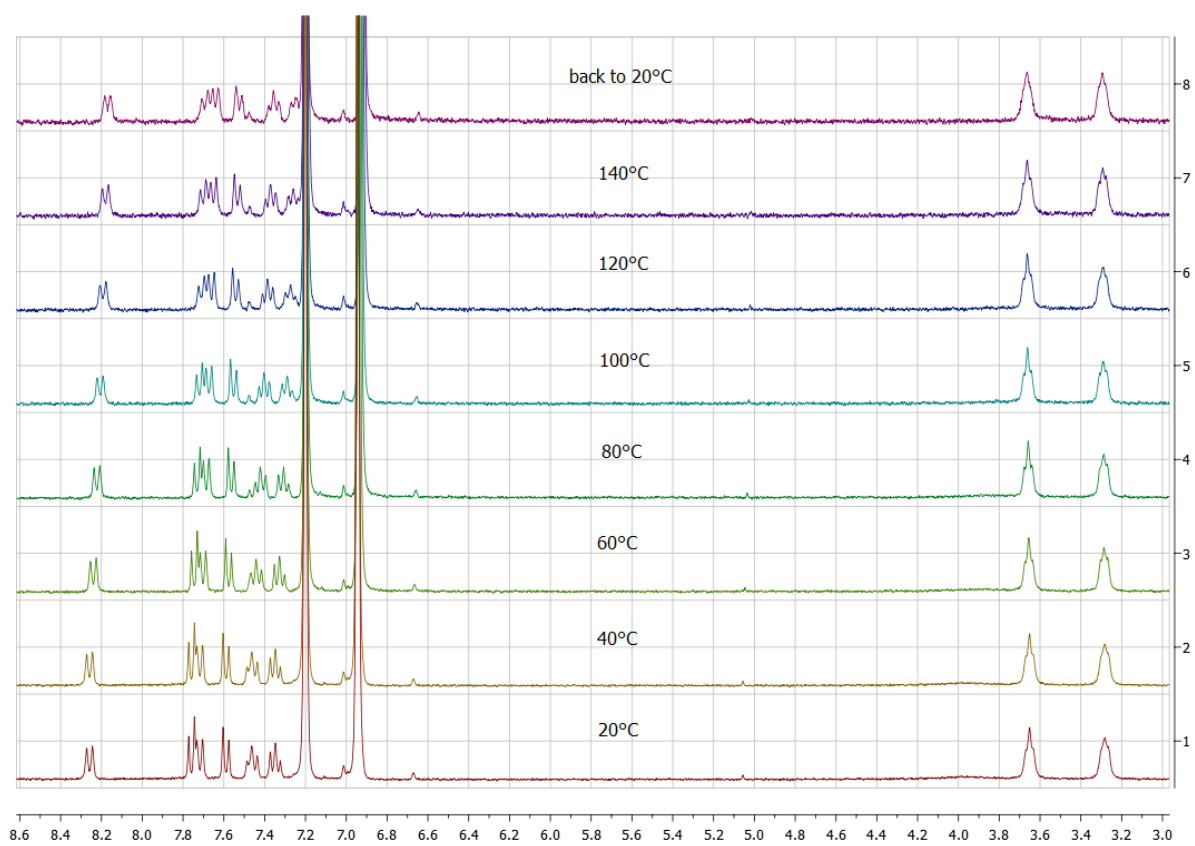
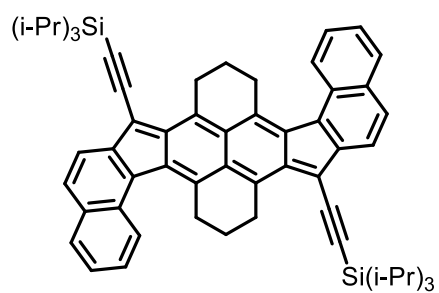


VARIABLE TEMPERATURE ^1H NMR of *linear*-HDIP in *o*-DCB (d_4) with COSY and NOESY

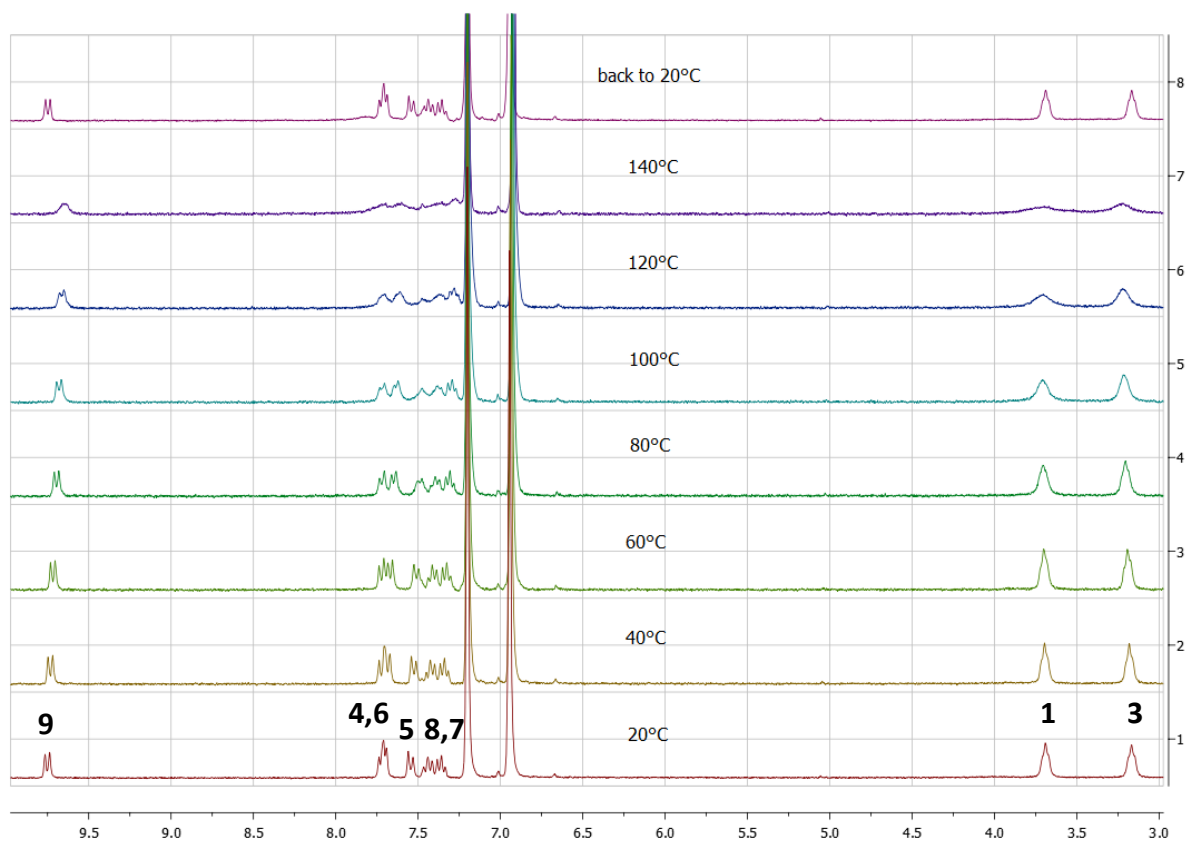
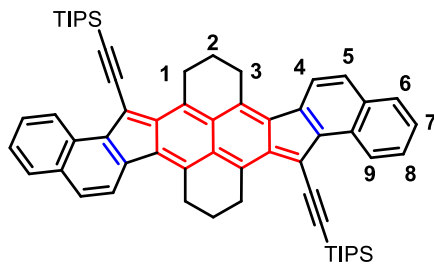


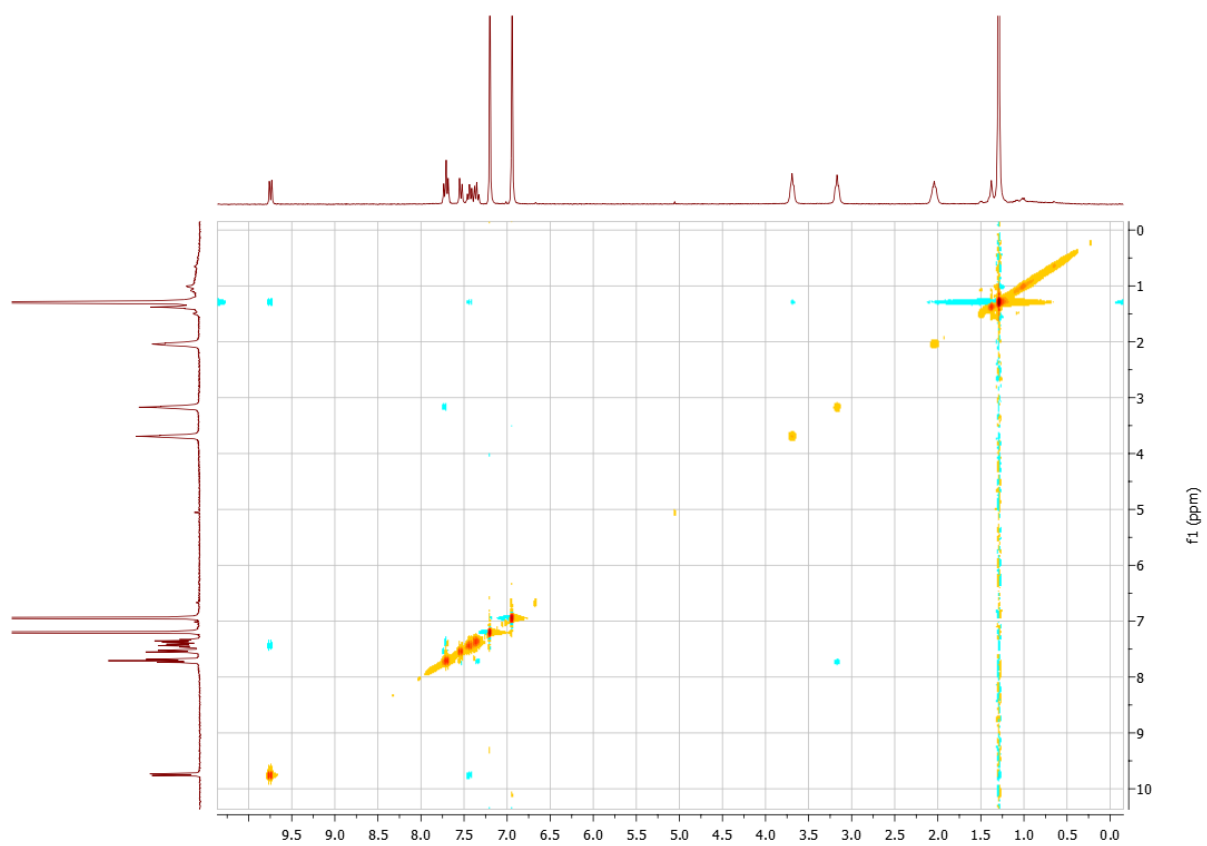
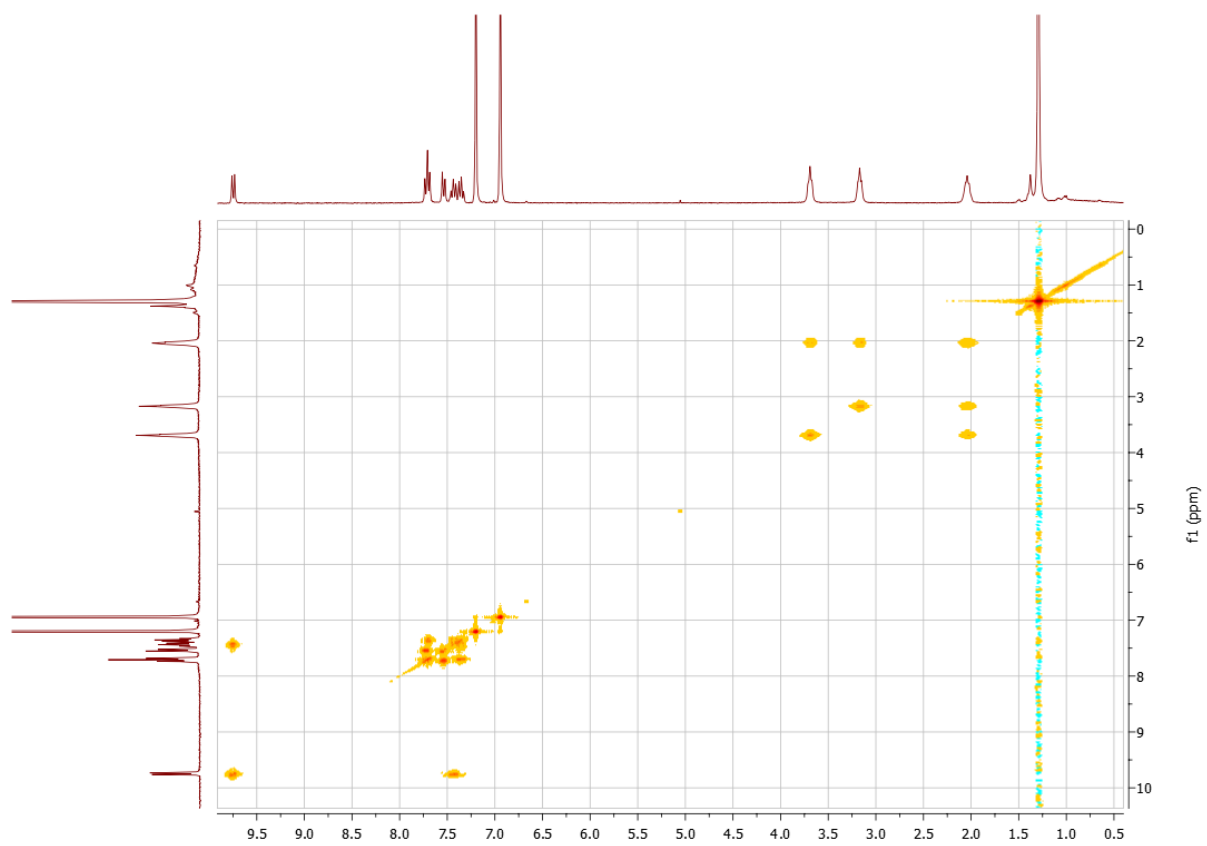


VARIABLE TEMPERATURE ^1H NMR of *syn*-HDIP in *o*-DCB (d_4)



VARIABLE TEMPERATURE ^1H NMR of *anti*-HDIP in *o*-DCB (d_4) with COSY and NOESY





ESR and SQUID MEASUREMENTS

Magnetic susceptibilities of the samples were measured using a Quantum Design MPMS-XL7 SQUID magnetometer in a temperature range of 200–400 K at an applied magnetic field of 1 T. The magnetic response was corrected with diamagnetic blank from the sample holder measured separately. The diamagnetism of the sample itself was estimated from Pascal's constant. Electron spin resonance (ESR) measurements were carried out on a Bruker ELEXSYS X-band (9.7 GHz) spectrometer. The ESR spectra of the polycrystalline samples were recorded in a temperature range from 200–500 K, where a cryostat (Oxford) was applied using liquid nitrogen. The samples were contained in a glass tube where inner gasses were removed in vacuum and sealed by using flame in order to prevent oxygen containing. Unfortunately, a detectable response derived from the excited spin triplet state in the samples cannot be found in SQUID and ESR results in the measuring temperature range, because the magnetic susceptibility and ESR responses for all the HDIP samples showed anomalous paramagnetic behavior quite similar to those in the previous report.^{vi} According to the reference, the anomalous behavior was derived from a small concentration of radical cations generated through exposure to ambient atmosphere (oxygen, water) and light even for extra-purified samples. The broadening ($\Delta H_{pp} = \sim 15$ G) of ESR signals is supportive of such anomalous behavior, which seems to be a nature of aggregated samples different from a chemically oxidized radical cation showing a sharp signal. The unexpected paramagnetic response was not avoided in our magnetic experiments, which masks the contribution of the inherent excited triplet state in the HDIP singlet biradicals.

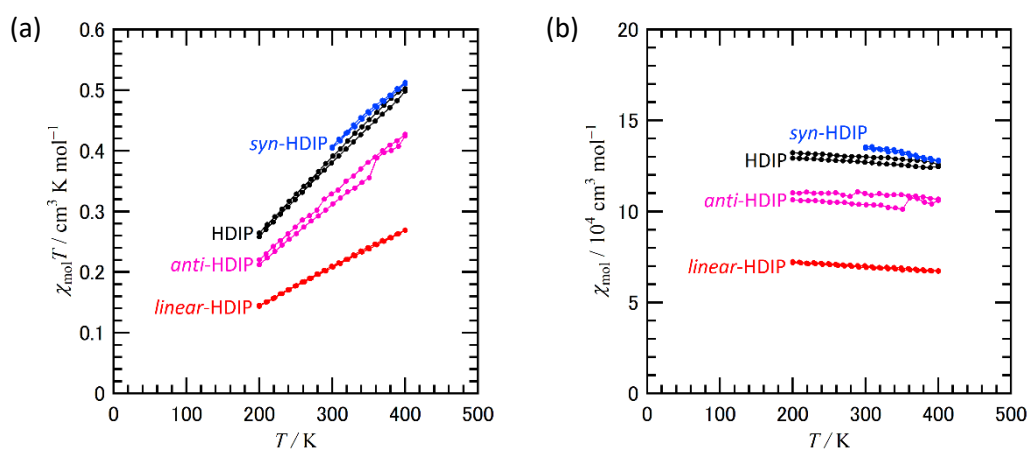


Figure S1. Temperature dependences (a) of $\chi_{\text{mol}} T$ and (b) of χ_{mol} for the HDIP derivatives.

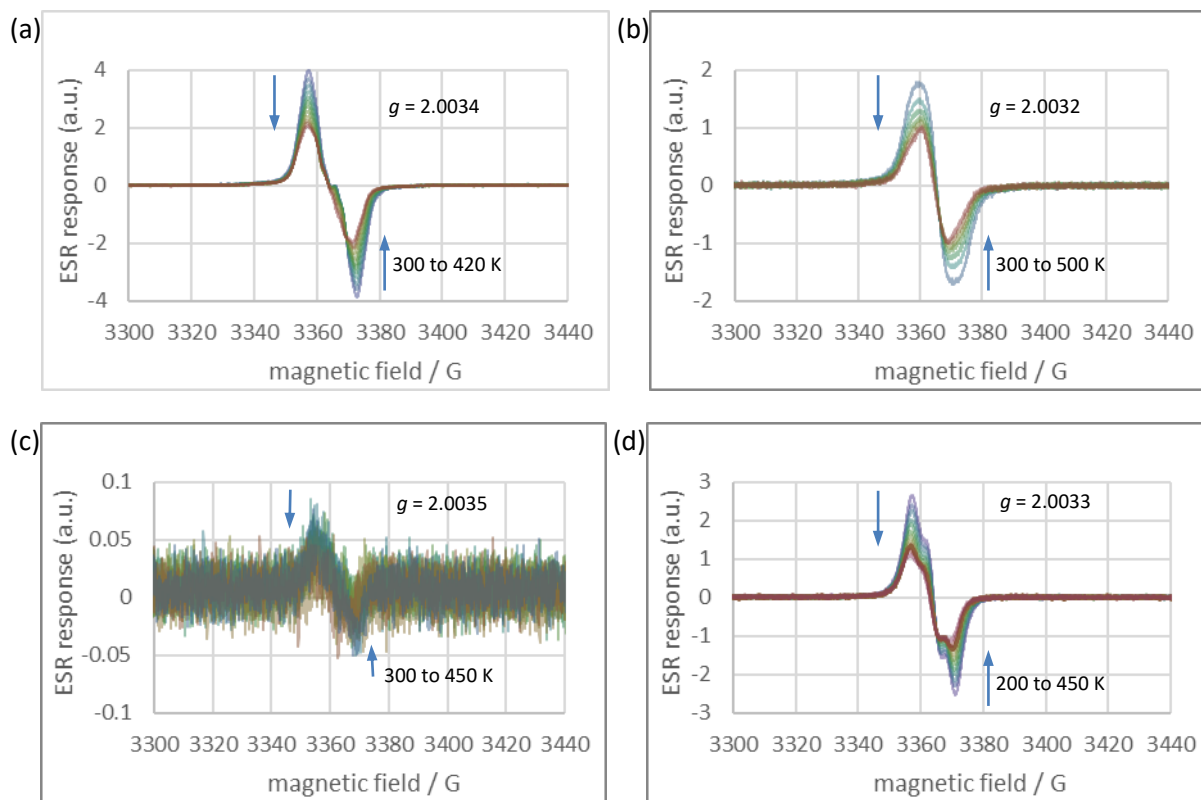
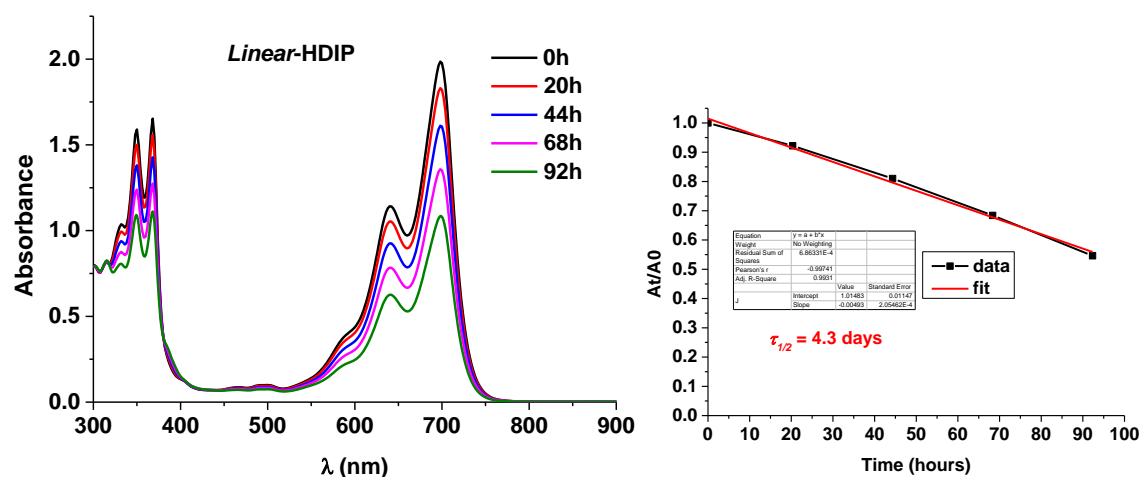
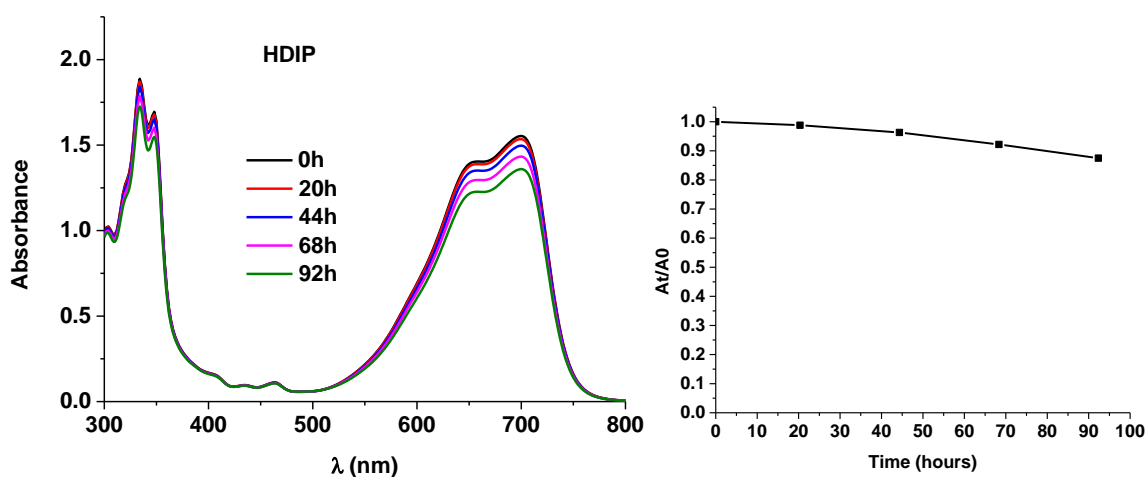


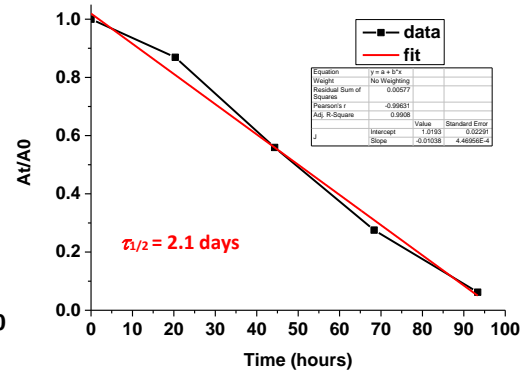
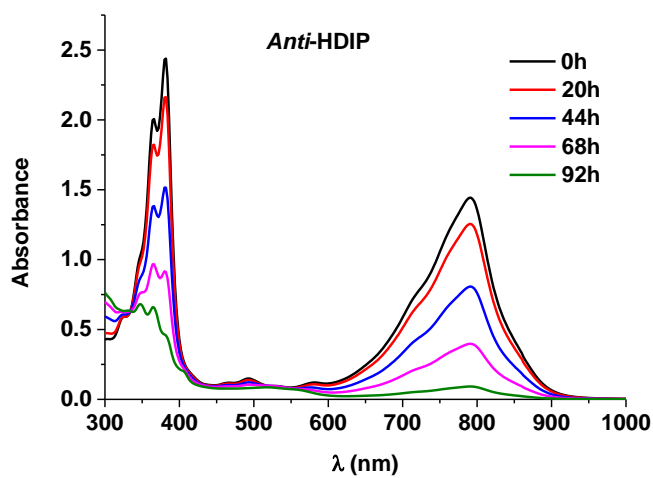
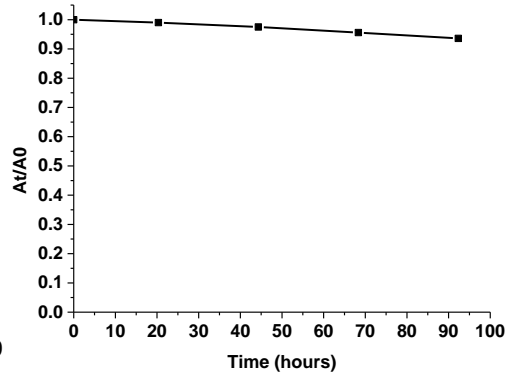
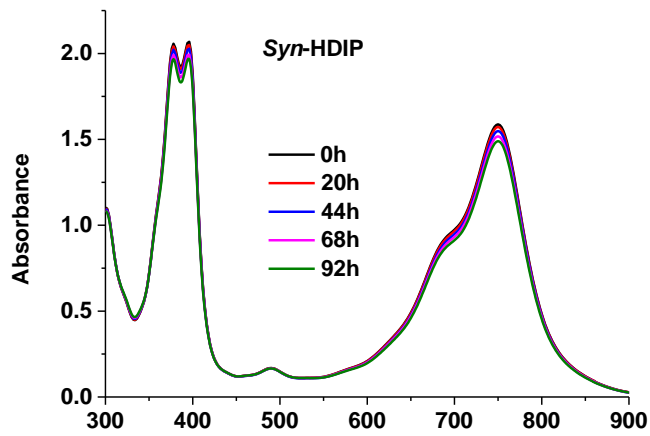
Figure S2. Temperature dependences of ESR spectra on the polycrystalline samples of (a) HDIP, (b) *linear*-HDIP, (c) *syn*-HDIP, and (d) *anti*-HDIP.

STABILITY TESTS OF HDIP DERIVATIVES

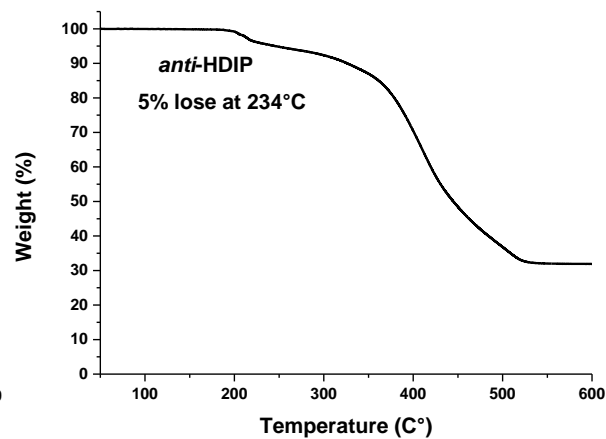
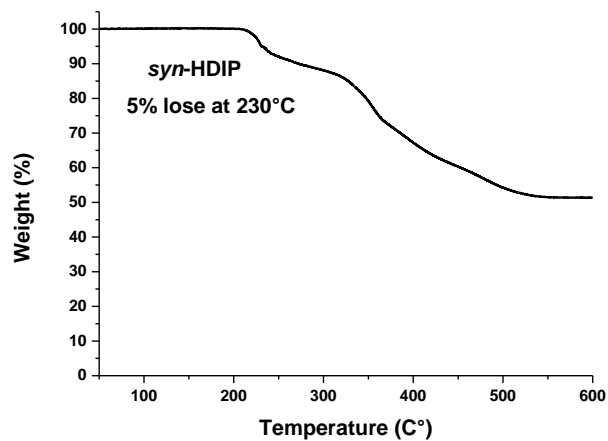
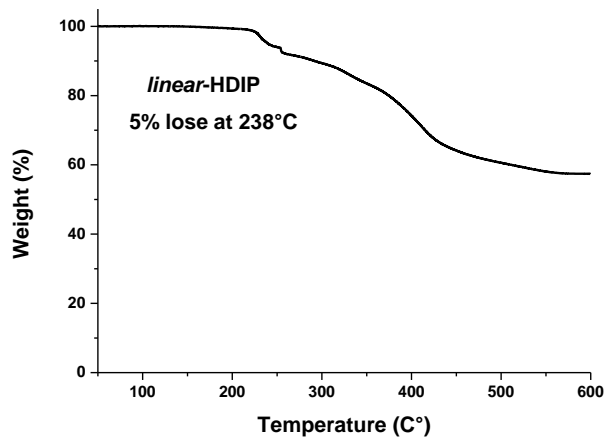
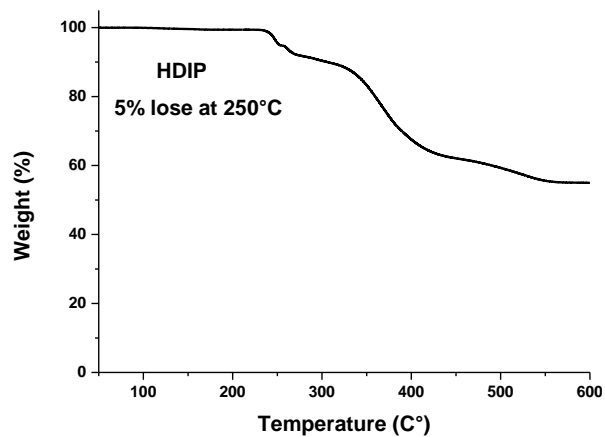
The stability tests were performed in 100 ml volumetric flask containing a toluene solution of the materials at a concentration of 26.6 μM . Air bubbling on the toluene solution for 30 min and 1 hour left with open bottle prior the dilution was done. All the samples were prepared at the same time and the volumetric flask with capped on were left on the bench with light on. Aliquots of 2.5 mL were taken at different times and were put in the cuvette for recording UV/vis absorption spectra.

Change of UV/vis absorption spectra over time (left) and plot of A_t/A_0 at their own λ_{max} nm vs time (right)





THERMOGRAVIMETRY ANALYSIS OF HDIP derivatives under N₂



THEORETICAL CALCULATIONS

The computations were mainly performed using the computer facilities at the Research Institute for Information Technology, Kyushu University. Molecular orbital calculations were performed using the program Gaussian 16 except for odd-electron density and NICS calculations.^{vii} The geometries were optimized at the B3LYP/6-311G(d,p) level for the singlet and UB3LYP/6-311G(d,p) for the triplet, and these optimized structures are used for the further calculations of the singlet and triplet, respectively, unless otherwise noted according to the literature.^{viii} The presence of energy minima for the geometry optimization was confirmed by the absence of imaginary modes (no imaginary frequencies). To numerically achieve accurate values, we have used a fine grid. The triisopropylsilyl (TIPS) groups were substituted with trimethylsilyl (TMS) groups. We adopted four model systems, which are main aromatic backbone without substituents (native FF series), with TMS-acetylene groups (FF series), with propane groups (native HDIP series), and with propane and TMS-acetylene groups (HDIP series) (Figure S1). The singlet biradical was investigated by re-optimizing the geometry using open-shell broken-symmetry calculations at the UB3LYP/6-311G(d,p) level. The structures were also optimized at the CAM-B3LYP/6-311+G(d,p), broken symmetry UCAM-B3LYP/6-311+G(d,p), and UCAM-B3LYP/6-311+G(d,p) for closed-shell singlet, open-shell singlet, and triplet, respectively.

The singlet biradical factor was also calculated by the natural orbital occupation number (NOON) of the LUMO in a projected spin-unrestricted Hartree-Fock (PUHF) calculation using 6-31+G(d,p) basis set.^{ix} The broken symmetry PUHF/6-31+G(d,p) calculations gave LUMO occupation number. According to the Yamaguchi scheme,^x the index for singlet biradical character is expressed as

$$y_i = 1 - \frac{2T_i}{1 + T_i^2}$$

where T_i is the orbital overlap between the corresponding orbital pairs and it can be presented using the NOON of HOMO and LUMO.

$$T_i = \frac{n_{HOMO} - n_{LUMO}}{2}$$

The diradical characters by the theoretical calculation are listed in Table S1.

The TD-DFT calculations were conducted at the B3LYP/6-311+G(d,p) level for the excited states calculations.

Odd-electron density distribution were calculated using the program Multiwfn^{xi}

NICS calculations were performed using Gaussian 09 and Aroma 1.0.^{xii} NICS values employ σ -only model to obtain the effect of the π contribution only. NICS(0) π_{zz} , NICS(1) π_{zz} , and NICS(1.7) π_{zz} , where the dummy atoms are positioned ring center at 0 Å, 1 Å, and 1.7 Å above the ring, respectively. The NICS values were estimated using the GIAO-B3LYP/6-311+G(d,p) methods for the structures calculated at the B3LYP basis set and the GIAO-CAM-B3LYP/6-311+G(d,p) methods for the structures calculated at the CAM-B3LYP basis set, and these data are summarized in Table S5 and S6.

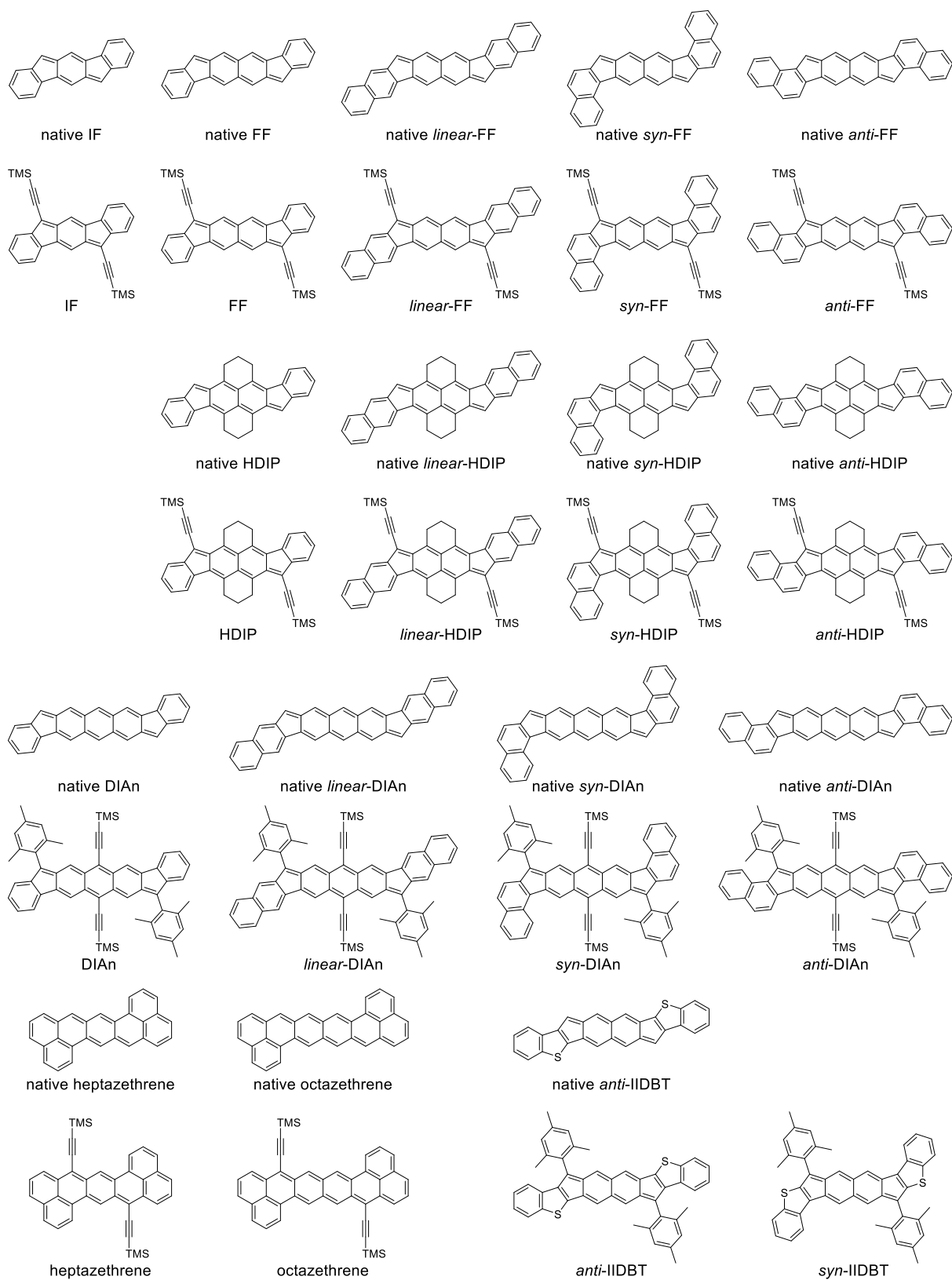


Figure S3. Chemical structures of the calculated molecules

Bond	X-ray	RB3LYP	RB3LYP – XR	UB3LYP
a	1.454 (2)	1.455	0.001	1.453
b	1.406 (2)	1.409	0.003	1.419
c	1.415 (2)	1.421	0.006	1.413
d	1.391 (2)	1.399	0.008	1.407
e	1.458 (2)	1.462	0.004	1.457
f	1.451 (2)	1.453	0.002	1.449
g	1.362 (2)	1.371	0.009	1.373
h	1.447 (2)	1.454	0.007	1.451

|RB3LYP-XR| corresponds to the bond length difference between the structure optimized at RB3LYP and the X-ray structure.

Bond	X-ray	RCAM-B3LYP	UCAM-B3LYP	RUCAM RCAM*0.45 +UCAM*0.55	RUCAM –XR
a	1.454 (2)	1.459	1.450	1.453	0.001
b	1.406 (2)	1.384	1.424	1.406	0.000
c	1.415 (2)	1.431	1.399	1.413	0.003
d	1.391 (2)	1.378	1.411	1.396	0.005
e	1.458 (2)	1.465	1.442	1.452	0.004
f	1.451 (2)	1.459	1.443	1.450	0.001
g	1.362 (2)	1.356	1.365	1.361	0.001
h	1.447 (2)	1.456	1.442	1.448	0.001

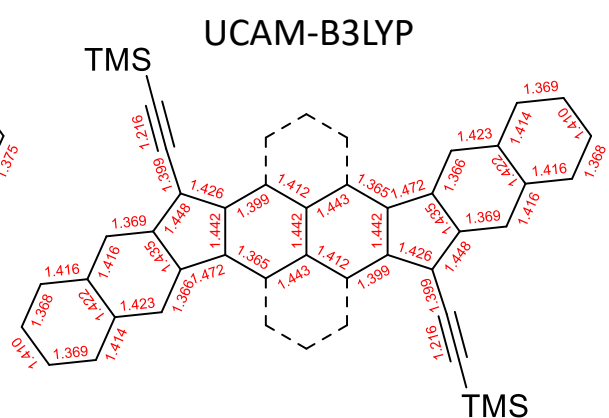
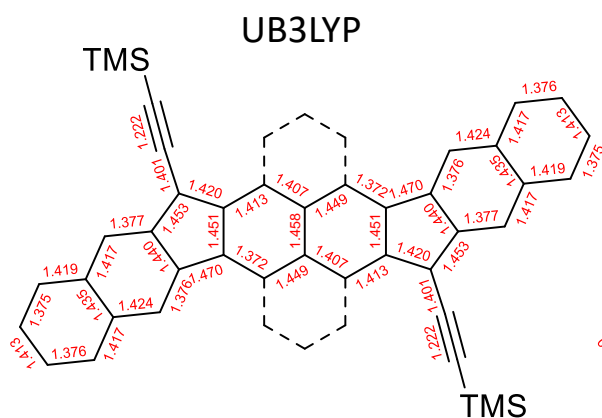
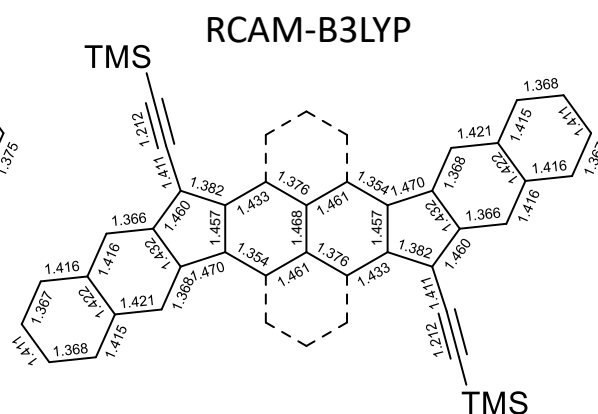
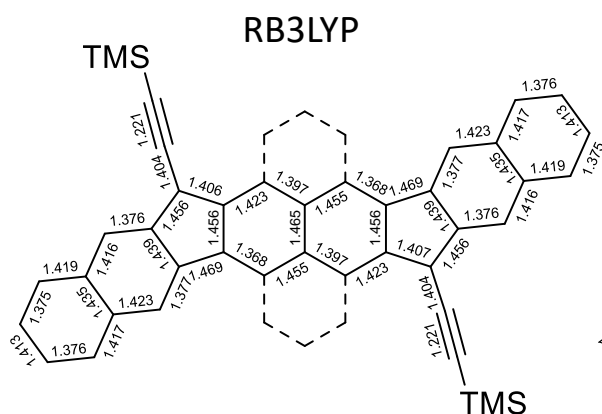
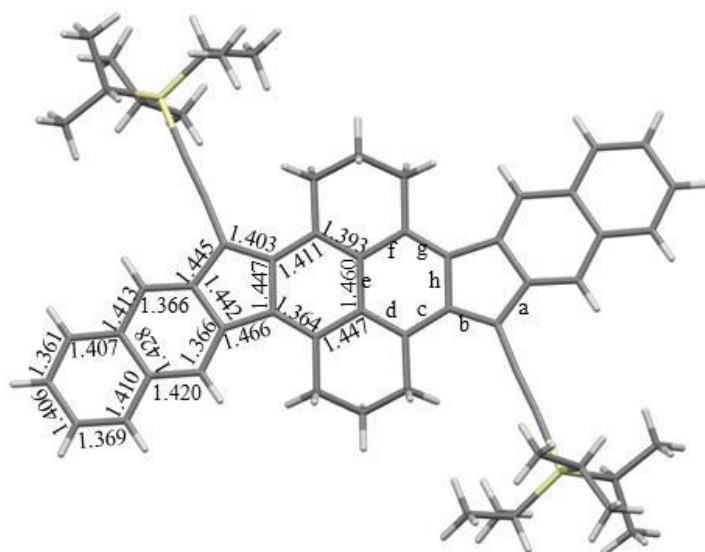
|**RUCAM**–XR| corresponds to the bond lengths difference between the resonance hybrid between CAM structures as RCAM*0.45 +UCAM*0.55 and the X-ray structure.

Accordingly, y_0 is in the range of 0.55 ± 0.05 by into account the standard deviation of the apical bond length.

y_0 is of 0.56 calculated at PUHF from R-BL3YP structure.

y_0 is of 0.54 calculated at PUHF from X-ray structure.

Linear-HDIP: Bond length comparison of X-ray structure and calculations



Bond	X-ray	RB3LYP	RB3LYP – XR	UB3LYP
a	1.445 (3)	1.456	0.011	1.453
b	1.403 (3)	1.406	0.003	1.420
c	1.411 (3)	1.423	0.012	1.413
d	1.393 (3)	1.397	0.004	1.407
e	1.460 (4)	1.465	0.005	1.458
f	1.447 (3)	1.455	0.008	1.449
g	1.364 (3)	1.368	0.004	1.372
h	1.447 (3)	1.456	0.009	1.451

|RB3LYP-XR| corresponds to the bond length difference between the structure optimized at RB3LYP and the X-ray structure.

Bond	X-ray	RCAM-B3LYP	UCAM-B3LYP	RUCAM RCAM*0.52 +UCAM*0.48	RUCAM–XR
a	1.445 (3)	1.460	1.448	1.454	0.009
b	1.403 (3)	1.382	1.426	1.403	0.000
c	1.411 (3)	1.433	1.399	1.417	0.006
d	1.393 (3)	1.376	1.412	1.393	0.000
e	1.460 (4)	1.468	1.442	1.456	0.004
f	1.447 (3)	1.461	1.443	1.452	0.005
g	1.364 (3)	1.354	1.365	1.359	0.005
h	1.447 (3)	1.457	1.442	1.450	0.003

|RUCAM–XR| corresponds to the bond lengths difference between the resonance hybrid between CAM structures as RCAM*0.52 +UCAM*0.48 and the X-ray structure.

Accordingly, y_0 is in the range of 0.48 ± 0.07 by into account the standard deviation of the apical bond length.

y_0 is of 0.58 calculated at PUHF from R-BL3YP structure.

y_0 is of 0.58 calculated at PUHF from X-ray structure.

Bond	X-ray	RB3LYP	RB3LYP – XR	UB3LYP
a	1.443 (2)	1.446	0.003	1.445
b	1.400 (2)	1.407	0.007	1.409
c	1.408 (2)	1.416	0.008	1.414
d	1.394 (2)	1.400	0.006	1.402
e	1.455 (2)	1.457	0.002	1.456
f	1.449 (2)	1.454	0.005	1.453
g	1.369 (2)	1.38	0.011	1.381
h	1.456 (2)	1.458	0.002	1.457

|RB3LYP-XR| corresponds to the bond length difference between the structure optimized at RB3LYP and the X-ray structure.

Bond	X-ray	RCAM-B3LYP	UCAM-B3LYP	RUCAM RCAM*0.47 +UCAM*0.53	RUCAM –XR
a	1.443 (2)	1.451	1.442	1.446	0.003
b	1.400 (2)	1.382	1.416	1.400	0.000
c	1.408 (2)	1.427	1.399	1.412	0.004
d	1.394 (2)	1.377	1.407	1.393	0.001
e	1.455 (2)	1.46	1.44	1.449	0.005
f	1.449 (2)	1.462	1.449	1.455	0.006
g	1.369 (2)	1.364	1.371	1.368	0.001
h	1.456 (2)	1.459	1.447	1.452	0.004

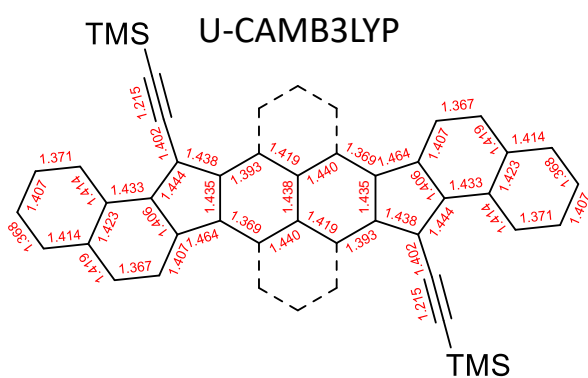
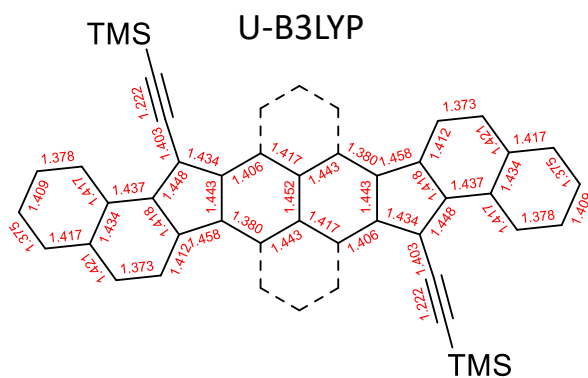
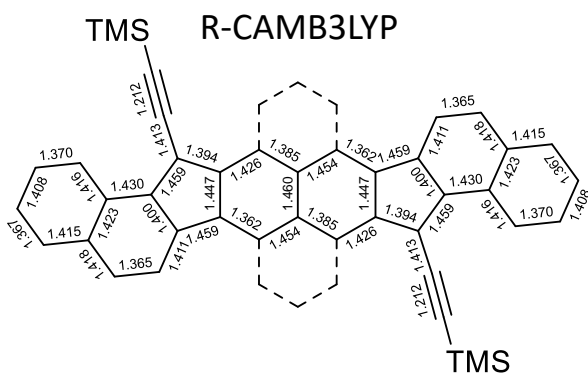
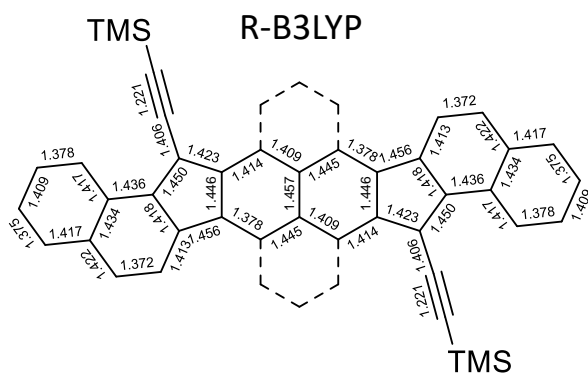
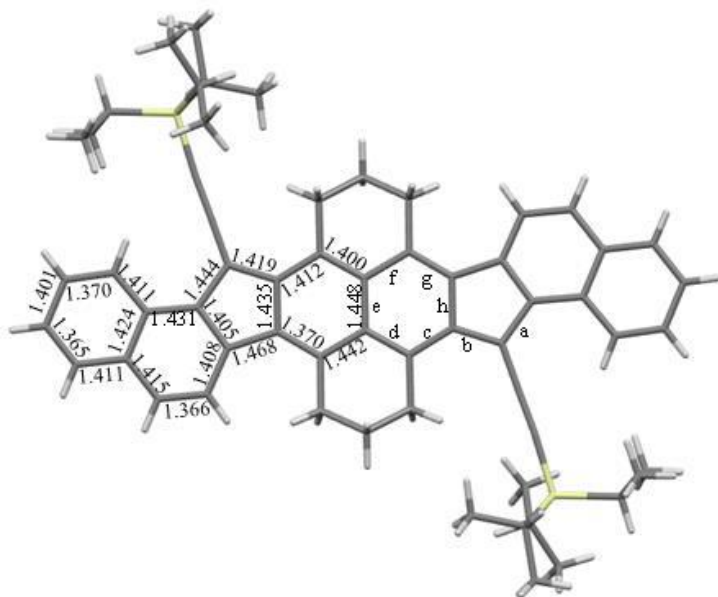
|**RUCAM**–XR| corresponds to the bond lengths difference between the resonance hybrid between CAM structures as RCAM*0.47 +UCAM*0.53 and the X-ray structure.

Accordingly, y_0 is in the range of 0.53 ± 0.05 by into account the standard deviation of the apical bond length.

y_0 is of 0.59 calculated at PUHF from R-BL3YP structure.

y_0 is of 0.56 calculated at PUHF from X-ray structure.

Anti-HDIP: Bond length comparison of X-ray structure and calculations



Bond	X-ray	RB3LYP	RB3LYP – XR	UB3LYP
a	1.444 (2)	1.45	0.006	1.448

b	1.419 (2)	1.423	0.004	1.434
c	1.412 (2)	1.414	0.002	1.406
d	1.400 (2)	1.409	0.009	1.417
e	1.448 (2)	1.457	0.009	1.452
f	1.442 (2)	1.445	0.003	1.443
g	1.370 (2)	1.378	0.008	1.38
h	1.435 (2)	1.446	0.011	1.443

|RB3LYP-XR| corresponds to the bond length difference between the structure optimized at RB3LYP and the X-ray structure.

Bond	X-ray	RCAM-B3LYP	UCAM-B3LYP	RUCAM RCAM*0.43 +UCAM*0.57	RUCAM-XR
a	1.444 (2)	1.459	1.444	1.450	0.006
b	1.419 (2)	1.394	1.438	1.419	0.000
c	1.412 (2)	1.426	1.393	1.407	0.005
d	1.400 (2)	1.385	1.419	1.404	0.004
e	1.448 (2)	1.46	1.438	1.447	0.001
f	1.442 (2)	1.454	1.44	1.446	0.004
g	1.370 (2)	1.362	1.369	1.366	0.004
h	1.435 (2)	1.447	1.435	1.440	0.005

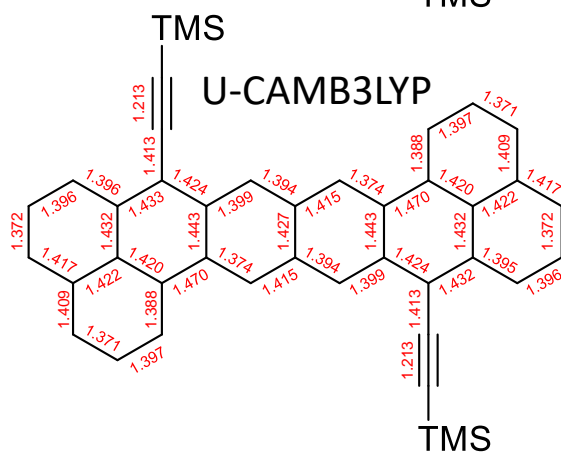
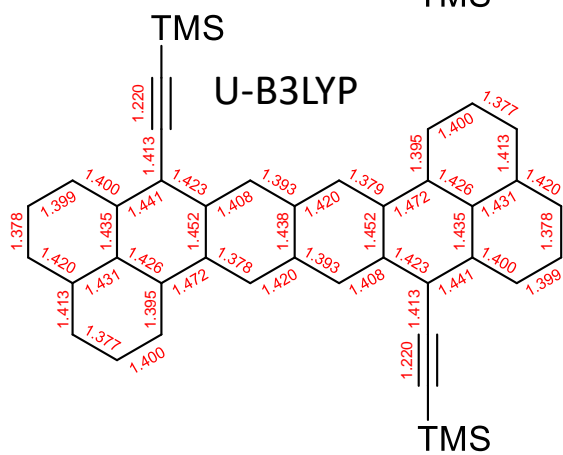
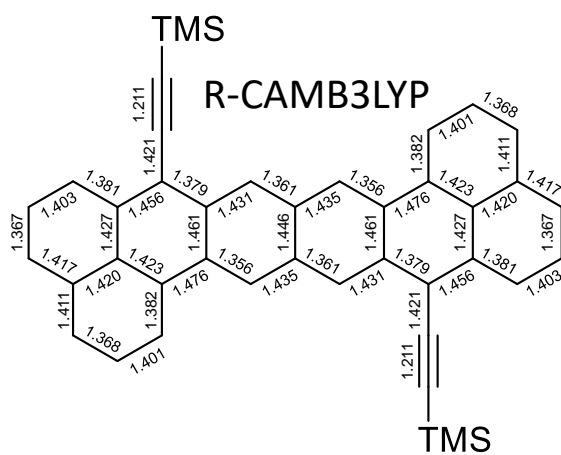
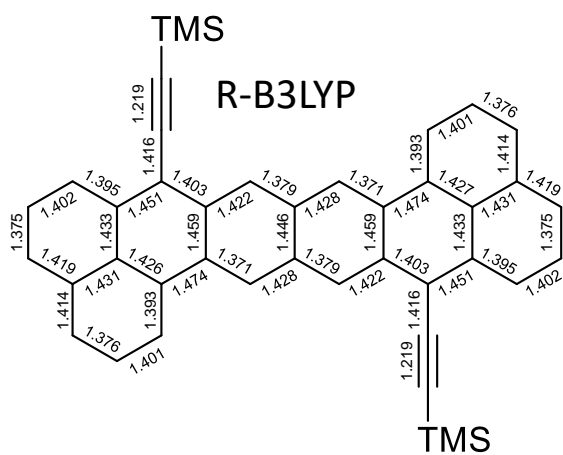
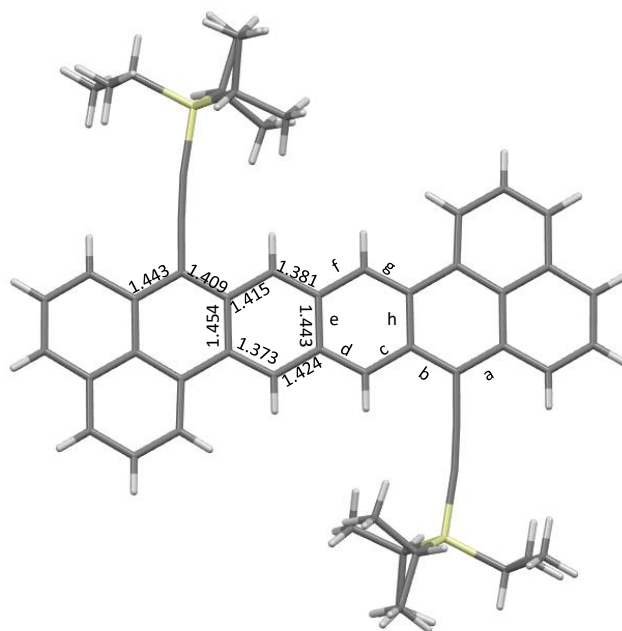
|RUCAM-XR| corresponds to the bond lengths difference between the resonance hybrid between CAM structures as RCAM*0.43 +UCAM*0.57 and the X-ray structure.

Accordingly, y_0 is in the range of 0.57 ± 0.05 by taking into account the standard deviation of the apical bond length.

y_0 is of 0.65 calculated at PUHF from R-BL3YP structure.

y_0 is of 0.62 calculated at PUHF from X-ray structure.

TIPS-octazethrene: Bond length comparison of X-ray structure and calculations



Bond	X-ray	RB3LYP	RB3LYP – XR	UB3LYP
a	1.443 (2)	1.451	0.008	1.441
b	1.409 (2)	1.403	0.006	1.423
c	1.415 (2)	1.422	0.007	1.408
d	1.381 (2)	1.379	0.002	1.393
e	1.443 (2)	1.446	0.003	1.438
f	1.424 (2)	1.428	0.004	1.42
g	1.373 (2)	1.371	0.002	1.378
h	1.454 (2)	1.459	0.005	1.452

|RB3LYP-XR| corresponds to the bond length difference between the structure optimized at RB3LYP and the X-ray structure.

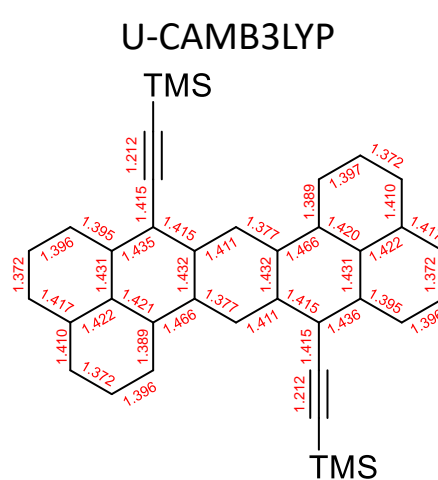
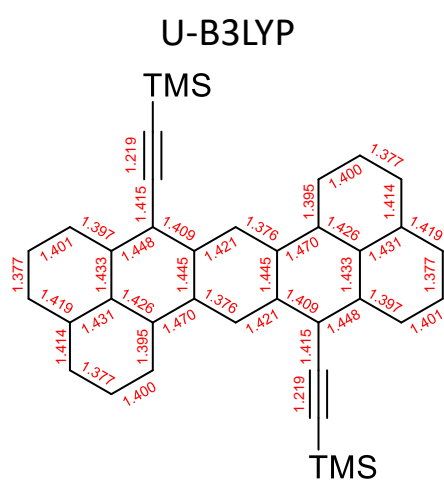
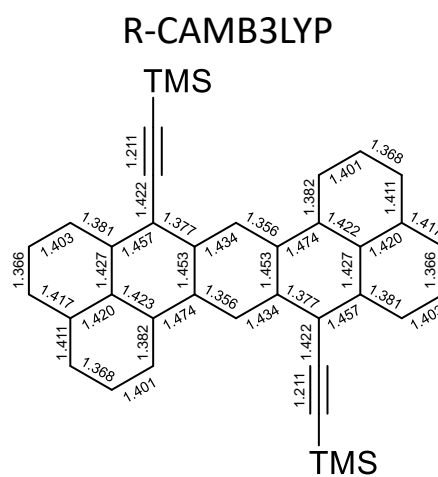
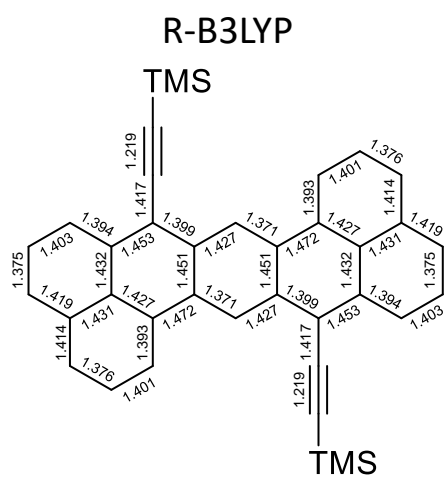
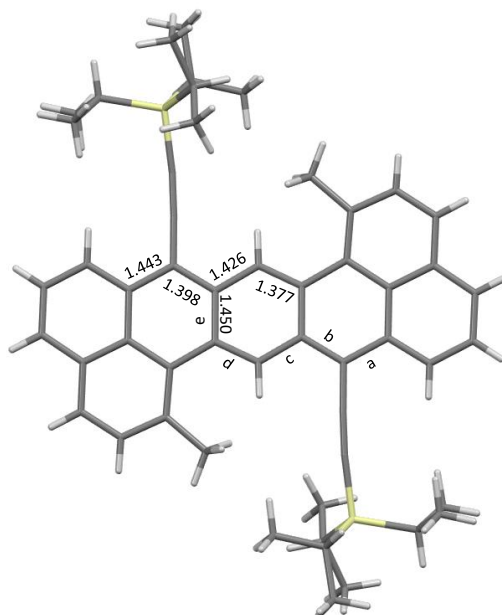
Bond	X-ray	RCAM-B3LYP	UCAM-B3LYP	RUCAM RCAM*0.33 +UCAM*0.67	RUCAM –XR
a	1.443 (2)	1.456	1.433	1.440	0.003
b	1.409 (2)	1.379	1.424	1.409	0.000
c	1.415 (2)	1.431	1.399	1.410	0.005
d	1.381 (2)	1.361	1.394	1.383	0.002
e	1.443 (2)	1.446	1.427	1.433	0.010
f	1.424 (2)	1.435	1.415	1.422	0.002
g	1.373 (2)	1.356	1.374	1.368	0.005
h	1.454 (2)	1.461	1.443	1.449	0.005

|**RUCAM**–XR| corresponds to the bond lengths difference between the resonance hybrid between CAM structures as RCAM*0.33 +UCAM*0.67 and the X-ray structure.

Accordingly, y_0 is in the range of 0.67 ± 0.05 by taking into account the standard deviation of the apical bond length.

y_0 is of 0.68 calculated at PUHF from R-BL3YP structure.

TIPS-heptazethrene: Bond length comparison of X-ray structure and calculations



Bond	X-ray	RB3LYP	RB3LYP – XR	UB3LYP
a	1.443 (2)	1.453	0.010	1.448
b	1.398 (2)	1.399	0.001	1.409
c	1.426 (2)	1.427	0.001	1.421
d	1.377 (2)	1.371	0.006	1.376
e	1.450 (2)	1.451	0.001	1.445

|RB3LYP-XR| corresponds to the bond length difference between the structure optimized at RB3LYP and the X-ray structure.

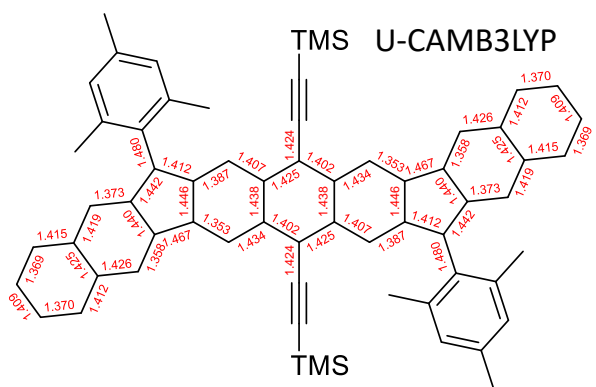
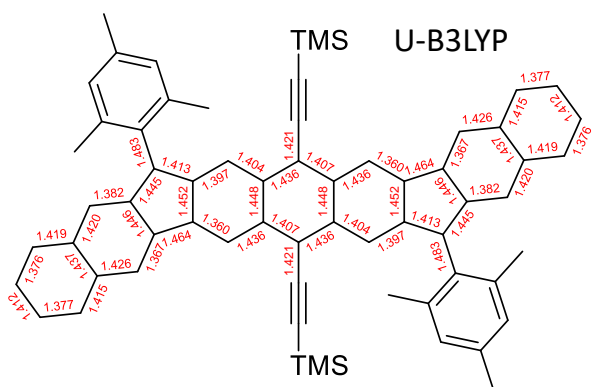
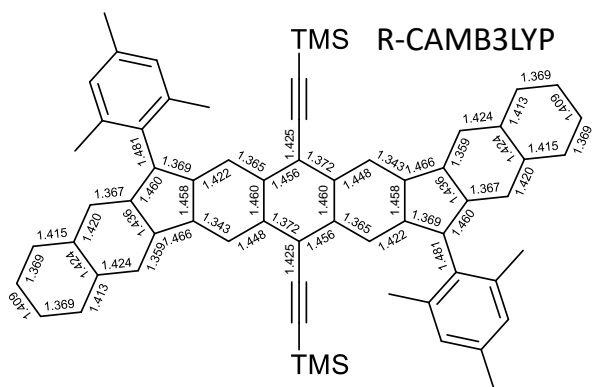
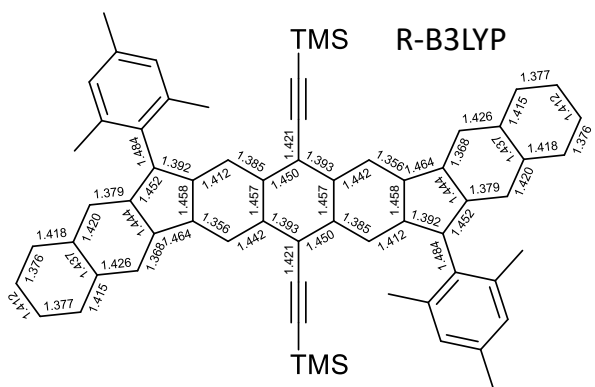
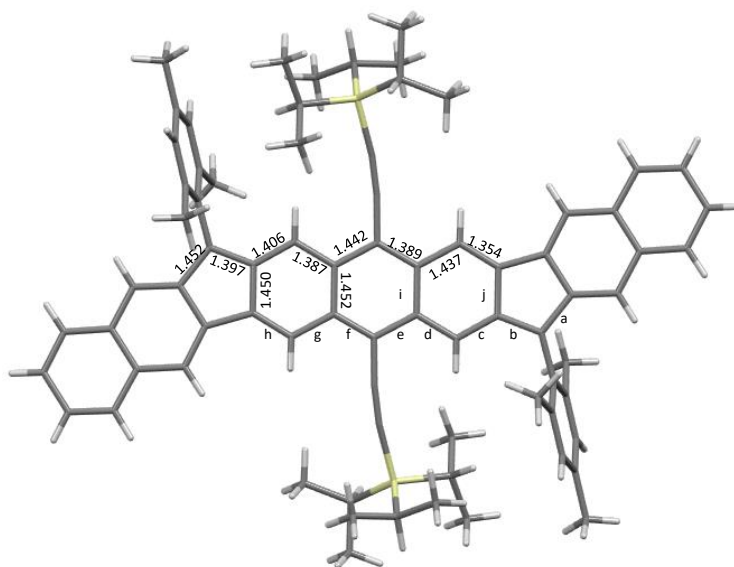
Bond	X-ray	RCAM-B3LYP	UCAM-B3LYP	RUCAM RCAM*0.44 +UCAM*0.56	RUCAM–XR
a	1.443 (2)	1.457	1.435	1.445	0.002
b	1.398 (2)	1.377	1.415	1.398	0.000
c	1.426 (2)	1.434	1.411	1.421	0.005
d	1.377 (2)	1.356	1.377	1.368	0.009
e	1.450 (2)	1.453	1.432	1.440	0.01

|RUCAM–XR| corresponds to the bond lengths difference between the resonance hybrid between CAM structures as RCAM*0.44 +UCAM*0.56 and the X-ray structure.

Accordingly, y_0 is in the range of 0.56 ± 0.05 by taking into account the standard deviation of the apical bond length.

y_0 is of 0.58 calculated at PUHF from R-BL3YP structure.

Linear-DIAN: Bond length comparison of X-ray structure and calculations



Bond	X-ray	RB3LYP	RB3LYP – XR	UB3LYP
a	1.452 (2)	1.452	0.000	1.445
b	1.397 (2)	1.392	0.005	1.413
c	1.406 (2)	1.412	0.006	1.397
d	1.387 (2)	1.385	0.002	1.404
e	1.442 (2)	1.450	0.008	1.436
f	1.389 (2)	1.393	0.004	1.407
g	1.437 (2)	1.442	0.005	1.436
h	1.354 (2)	1.356	0.002	1.360
i	1.452 (2)	1.457	0.005	1.448
j	1.450 (2)	1.458	0.008	1.452

|RB3LYP-XR| corresponds to the bond length difference between the structure optimized at RB3LYP and the X-ray structure.

Bond	X-ray	RCAM-B3LYP	UCAM-B3LYP	RUCAM	RUCAM–XR
				RCAM*0.35 +UCAM*0.65	
a	1.452 (2)	1.460	1.442	1.448	0.004
b	1.397 (2)	1.369	1.412	1.397	0.000
c	1.406 (2)	1.422	1.387	1.399	0.007
d	1.387 (2)	1.365	1.407	1.392	0.005
e	1.442 (2)	1.456	1.425	1.436	0.006
f	1.389 (2)	1.372	1.402	1.392	0.004
g	1.437 (2)	1.448	1.434	1.439	0.002
h	1.354 (2)	1.343	1.353	1.350	0.004
i	1.452 (2)	1.460	1.438	1.446	0.006
j	1.450 (2))	1.458	1.446	1.450	0.000

|RUCAM–XR| corresponds to the bond lengths difference between the resonance hybrid between CAM structures as RCAM*0.33 +UCAM*0.65 and the X-ray structure.

Accordingly, y_0 is in the range of 0.65 ± 0.05 by taking into account the standard deviation of the apical bond length.

y_0 is of 0.64 calculated at PUHF from R-BL3YP structure.

Table S1. Energies of converged wavefunctions (hartrees) and relative energies (kcal/mol) at the B3LYP/6-311G(d,p) and the biradical character (y_0) at the PUHF/6-31+G(d,p)

Compound	Closed-shell singlet (CS)	Open-shell singlet (OS)	Triplet	$\Delta E_{(os-cs)^a}$	$\Delta E_{s-T}^{b)}$	y_0
native IF	-769.52124942	-769.52124942	-769.49034105	0.00	19.40	0.28
IF	-1739.38280622	-1739.38280622	-1739.36320050	0.00	12.30	0.40
native FF	-923.18888752	-923.18900444	-923.17356793	0.07	9.69	0.48
native <i>linear</i> -FF	-1230.54513905	-1230.54529985	-1230.53075353	0.10	9.13	0.50
native <i>syn</i> -FF	-1230.53704651	-1230.53721199	-1230.52296173	0.10	8.94	0.55
native <i>anti</i> -FF	-1230.54382220	-1230.54431377	-1230.53183541	0.31	7.83	0.57
FF	-1893.05249659	-1893.05398597	-1893.04440163	0.93	6.01	0.58
<i>linear</i> -FF	-2200.40810469	-2200.40968699	-2200.40055400	0.99	5.73	0.59
<i>syn</i> -FF	-2200.40066681	-2200.40204899	-2200.39274993	0.87	5.84	0.64
<i>anti</i> -FF	-2200.40335095	-2200.40534341	-2200.39719645	1.25	5.11	0.67
native HDIP	-1156.72854260	-1156.72854260	-1156.70989822	0.00	11.70	0.46
native <i>linear</i> -HDIP	-1464.08405566	-1464.08405566	-1464.06713677	0.00	10.62	0.48
native <i>syn</i> -HDIP	-1464.05798717	-1464.05798734	-1464.03842845	0.00	12.27	0.51
native <i>anti</i> -HDIP	-1464.08311923	-1464.08311923	-1464.06734824	0.00	9.90	0.55
HDIP	-2126.58486864	-2126.58531503	-2126.57374924	0.28	7.26	0.56
<i>linear</i> -HDIP	-2433.93942087	-2433.94014249	-2433.92975057	0.45	6.52	0.58
<i>syn</i> -HDIP	-2433.91450704	-2433.91452257	-2433.90098567	0.01	8.49	0.59
<i>anti</i> -HDIP	-2433.93072698	-2433.93136220	-2433.92102161	0.40	6.49	0.65
native DIAn	-1076.85624712	-1076.85881937	-1076.84994738	1.61	5.57	0.61
native <i>linear</i> -DIAn	-1384.21210192	-1384.21484025	-1384.20626624	1.72	5.38	0.62
native <i>syn</i> -DIAn	-1384.20526975	-1384.20777358	-1384.19965657	1.57	5.09	0.67
native <i>anti</i> -DIAn	-1384.21222328	-1384.21536122	-1384.20815568	1.97	4.52	0.69
DIAn	-2744.88104284	-2744.88448685	-2744.87707957	2.16	4.65	0.62
<i>linear</i> -DIAn	-3052.23793645	-3052.24124909	-3052.23363228	2.08	4.78	0.64
<i>syn</i> -DIAn	-3052.22960530	-3052.23323423	-3052.22684354	2.28	4.01	0.68
<i>anti</i> -DIAn	-3052.23233266	-3052.23685485	-3052.23137688	2.84	3.44	0.71
native	-1076.90444272	-1076.90445862	-1076.88826202	0.01	10.16	0.53
heptazethrene						
heptazethrene	-2046.75379628	-2046.75425773	-2046.74198270	0.29	7.70	0.58
native	-1230.57027544	-1230.57212751	-1230.56185401	1.16	6.45	0.62
octazethrene						
octazethrene	-2200.41998699	-2200.42299252	-2200.41526878	1.89	4.85	0.67
native <i>anti</i> -IIDBT	-1872.06835017	-1872.06930443	-1872.05661519	0.60	7.96	0.60
<i>anti</i> -IIDBT	-2570.24747191	-2570.24864296	-2570.23672709	0.73	7.48	0.61
<i>syn</i> -IIDBT	-2570.24854268	-2570.24961174	-2570.23871638	0.67	6.84	0.66 ^b

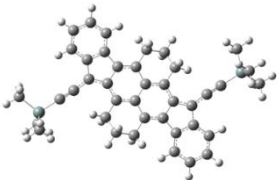
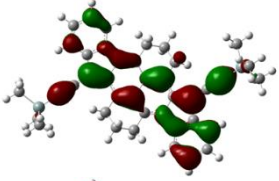
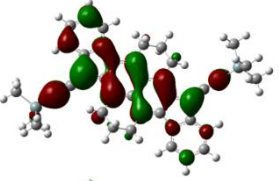
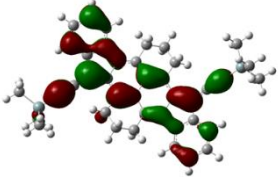
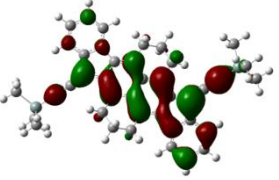
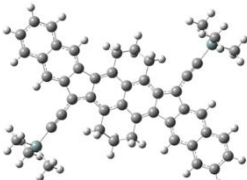
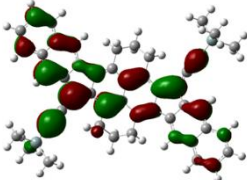
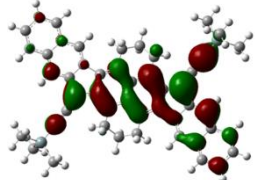
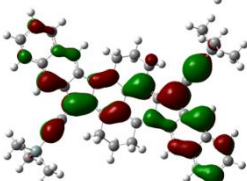
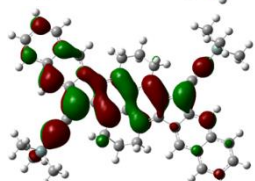
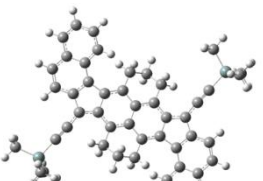
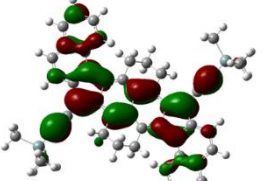
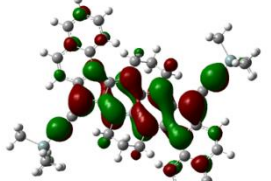
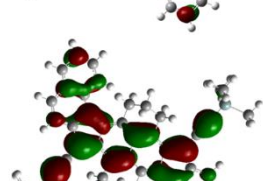
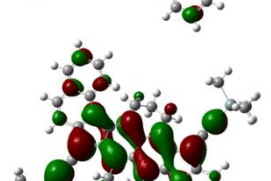
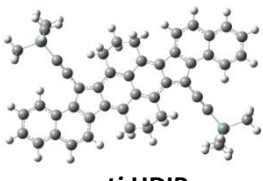
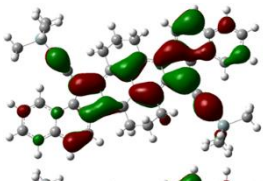
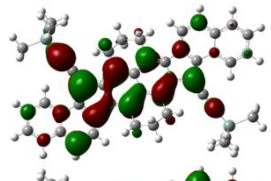
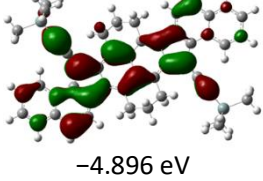
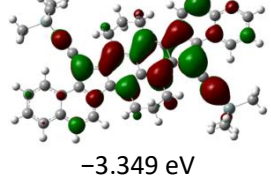
^a CS singlet energy minus OS broken symmetry singlet energy. ^b Unrestricted triplet energy minus singlet energy. ^bTaken from ref. 10k

Table S2. Energies of converged wavefunctions (hartrees) and relative energies (kcal/mol) at the CAM-B3LYP/6-311+G(d,p) and the biradical character (γ_0) at the PUHF/6-31+G(d,p)

Compound	Closed-shell singlet (CS)	Open-shell singlet (OS)	Triplet	$\Delta E_{(OS-CS)^a}$	ΔE_{S-T}^b
native IF	-769.0732628	-769.0732627	-769.0462274	0	16.96
IF	-1738.658809	-1738.660159	-1738.645013	0.85	9.50
native FF	-922.6489708	-922.6533314	-922.6413541	2.74	7.52
native <i>linear</i> -FF	-1229.829566	-1229.834487	-1229.82282	3.09	7.32
native <i>syn</i> -FF	-1229.821737	-1229.826584	-1229.81644	3.04	6.37
native <i>anti</i> -FF	-1229.827648	-1229.83387	-1229.825152	3.90	5.47
FF	-1892.23608	-1892.245729	-1892.238296	6.05	4.66
<i>linear</i> -FF	-2199.416364	-2199.42643	-2199.419002	6.32	4.66
<i>syn</i> -FF	-2199.408936	-2199.418743	-2199.412107	6.15	4.16
<i>anti</i> -FF	-2199.410665	-2199.422277	-2199.416573	7.29	3.58
native HDIP	-1156.058067	-1156.060068	-1156.045713	1.26	9.01
native <i>linear</i> -HDIP	-1463.237932	-1463.240735	-1463.227422	1.76	8.35
native <i>syn</i> -HDIP	-1463.213241	-1463.214228	-1463.199956	0.62	8.96
native <i>anti</i> -HDIP	-1463.236667	-1463.239675	-1463.228596	1.89	6.95
HDIP	-2125.638655	-2125.645083	-2125.636268	4.03	5.53
<i>linear</i> -HDIP	-2432.817853	-2432.825374	-2432.817051	4.72	5.22
<i>syn</i> -HDIP	-2432.794826	-2432.798787	-2432.789178	2.49	6.03
<i>anti</i> -HDIP	-2432.808872	-2432.816412	-2432.809202	4.73	4.52
native DIAn	-1076.22458672	-1076.23645822	-1076.22907545	7.45	4.63
native <i>linear</i> -DIAn	-1383.40488855	-1383.41747022	-1383.4099442	7.90	4.72
native <i>syn</i> -DIAn	-1383.3977314	-1383.41009682	-1383.40422381	7.76	3.69
native <i>anti</i> -DIAn	-1383.40385572	-1383.41773781	-1383.41261766	8.71	3.21
DIAn	-2743.56490649	-2743.57857523	-2743.57166282	8.58	4.34
<i>linear</i> -DIAn	-3050.74633106	-3050.7602359	-3050.75286788	8.73	4.62
<i>syn</i> -DIAn	-3050.73839664	-3050.75294294	-3050.74782001	9.13	3.21
<i>anti</i> -DIAn	-3050.74004091	-3050.75651663	-3050.75227925	10.34	2.66
native heptazethrene	-1076.28030160	-1076.28430459	-1076.26995009	2.51	9.01
heptazethrene	-2045.85629974	-2045.86299689	-2045.85162679	4.20	7.13
native octazethrene	-1229.85484398	-1229.86571016	-1229.85556919	6.82	6.36
octazethrene	-2199.43087659	-2199.44492911	-2199.43706064	8.82	4.94
native <i>anti</i> -IIBDT	-1871.43545589	-1871.44431405	-1871.43599431	5.56	5.22
<i>anti</i> -IIBDT	-2569.20275724	-2569.21238289	-2569.20456691	6.04	4.90
<i>syn</i> -IIBDT	-2569.20334655	-2569.21264788	-2569.20578774	5.84	4.30

^a CS singlet energy minus OS broken symmetry singlet energy. ^b Unrestricted triplet energy minus singlet energy

Table S3. Molecular orbitals at the B3LYP/6-311+G(d,p)

Compound		HOMO	LUMO
 HDIP	α -spin		
	β -spin	 -4.952 eV	 -3.260 eV
 <i>linear-HDIP</i>	α -spin		
	β -spin	 -4.863 eV	 -3.211 eV
 <i>syn-HDIP</i>	α -spin		
	β -spin	 -4.933 eV	 -3.348 eV
 <i>anti-HDIP</i>	α -spin		
	β -spin	 -4.896 eV	 -3.349 eV

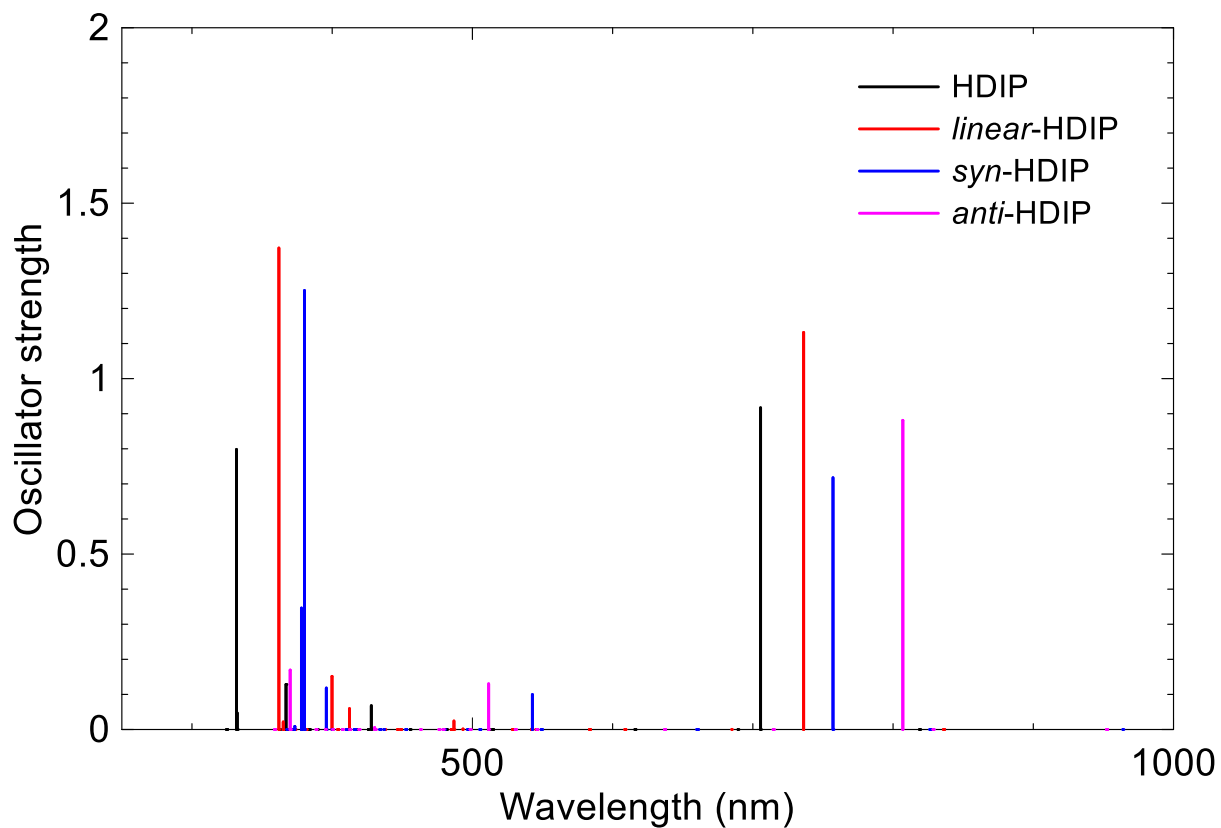


Figure S4. Simulated absorption spectra for HDIP derivatives at the TD-B3LYP/6-311+G(d,p)

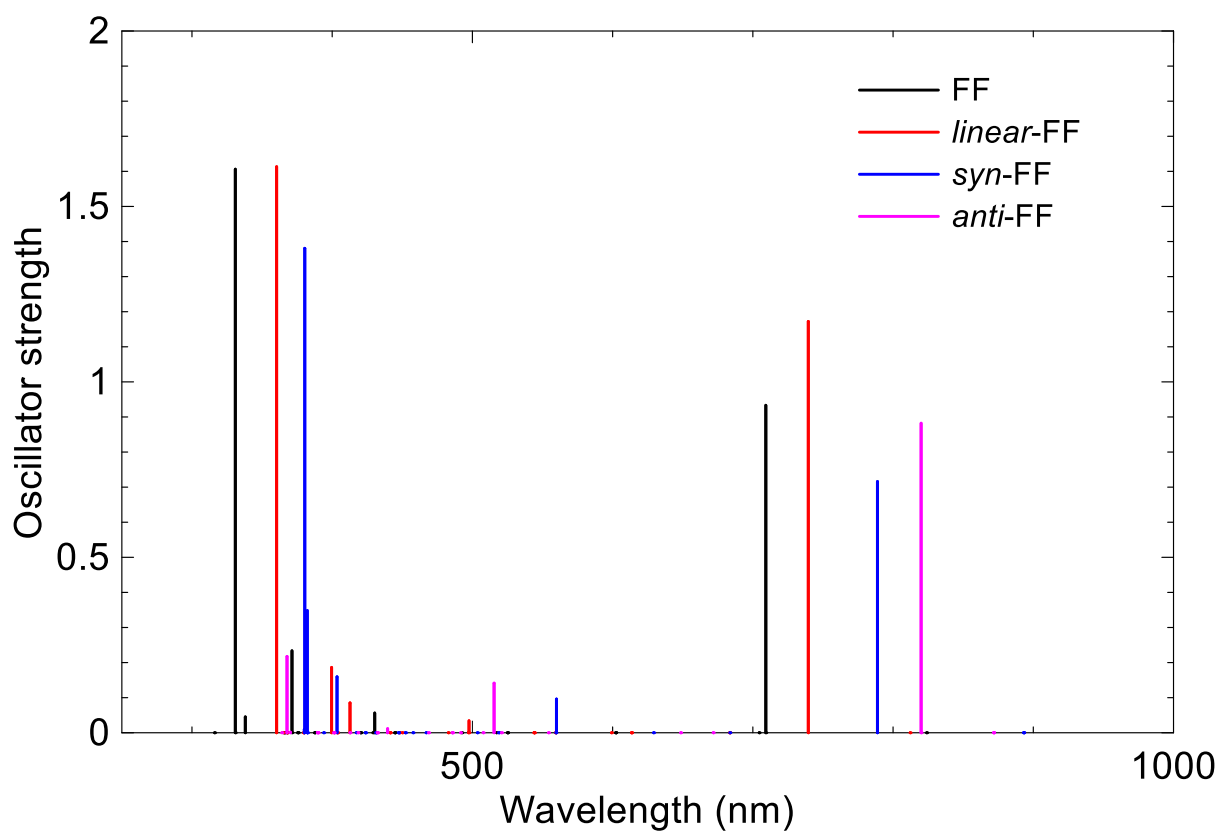


Figure S5. Simulated absorption spectra for FF derivatives at the TD-B3LYP/6-311+G(d,p)

Table S4. Calculated vertical excitation energies (VEE) for singlet excited states, wavelength, and oscillator strength (f) at the B3LYP/6-311+G(d,p) level

Compound	Excited states	VEE (eV)	wavelength (nm)	f	Compound	Excited states	VEE (eV)	wavelength (nm)	f
HDIP	1	1.757	705.49	0.9171	<i>linear</i> HDIP	1	1.685	735.88	1.1411
	2	1.798	689.45	0.0001		2	1.815	683.20	0
	3	2.576	481.36	0		3	2.343	529.08	0
	4	2.721	455.70	0		4	2.514	493.14	0
	5	2.897	427.94	0.0679		5	2.546	486.95	0.0244
	6	3.278	378.22	0.0263		6	3.007	412.31	0.0038
	7	3.344	370.75	0.0002		7	3.009	412.08	0.0565
	8	3.378	367.07	0.1284		8	3.103	399.53	0.1550
	9	3.422	362.34	0.0001		9	3.324	372.97	0
	10	3.731	332.32	0.0470		10	3.350	370.13	0.0013
	11	3.737	331.75	0		11	3.400	364.71	0.0002
	12	3.819	324.67	0		12	3.427	361.82	1.4020
<i>syn</i> HDIP	1	1.501	826.25	0	<i>anti</i> HDIP	1	1.496	828.53	0
	2	1.637	757.19	0.7178		2	1.537	806.95	0.8811
	3	2.284	542.80	0.0994		3	2.337	530.57	0
	4	2.453	505.36	0		4	2.424	511.60	0.1304
	5	2.584	479.82	0		5	2.488	498.36	0
	6	2.976	416.55	0		6	2.881	430.30	0.0054
	7	3.132	395.83	0.1182		7	3.005	412.60	0
	8	3.260	380.28	1.2512		8	3.136	395.36	0.0005
	9	3.279	378.11	0.3462		9	3.191	388.53	0
	10	3.321	373.37	0.0086		10	3.348	370.30	0
	11	3.336	371.70	0.0002		11	3.351	370.04	0.1694
	12	3.371	367.77	0.0002		12	3.454	358.92	0
FF	1	1.748	709.26	0.9332	<i>linear</i> FF	1	1.677	739.42	1.1720
	2	1.760	704.55	0.0001		2	1.814	683.41	0
	3	2.517	492.55	0		3	2.278	544.21	0
	4	2.788	444.67	0		4	2.492	497.59	0.0344
	5	2.881	430.34	0.0564		5	2.494	497.19	0.0011
	6	3.300	375.77	0		6	3.004	412.70	0.0850
	7	3.302	375.50	0.0003		7	3.072	403.67	0.0001
	8	3.339	371.34	0.2338		8	3.103	399.57	0.1865
	9	3.384	366.36	0.0001		9	3.368	368.11	0
	10	3.668	338.02	0.0451		10	3.371	367.75	0.0003
	11	3.747	330.92	1.6062		11	3.393	365.38	0
	12	3.921	316.19	0		12	3.440	360.40	1.6131
<i>syn</i> FF	1	1.388	893.09	0	<i>anti</i> FF	1	1.422	871.66	0
	2	1.572	788.89	0.7156		2	1.512	820.01	0.8825
	3	2.214	559.96	0.0961		3	2.380	520.85	0
	4	2.390	518.87	0		4	2.405	515.46	0.1412
	5	2.655	467.06	0		5	2.442	507.73	0
	6	2.876	431.17	0		6	2.821	439.52	0.0115
	7	3.073	403.46	0.1594		7	3.004	412.78	0
	8	3.242	382.42	0.0006		8	3.180	389.84	0
	9	3.243	382.30	0.0029		9	3.184	389.46	0.0003
	10	3.244	382.25	0.3482		10	3.350	370.15	0.0016
	11	3.259	380.48	1.3806		11	3.371	367.80	0.2174
	12	3.262	380.12	0.0098		12	3.405	364.18	0.0002

Table S5. NICS(0) π_{ZZ} , NICS(1) π_{ZZ} , and NICS(1.7) π_{ZZ} values at the GIAO-B3LYP/6-311+G(d,p) for native aromatic cores^a

CS singlet			OS singlet			Triplet					
Ring	NICS(0)	NICS(1)	NICS(1.7)	Ring	NICS(0)	NICS(1)	NICS(1.7)	Ring	NICS(0)	NICS(1)	NICS(1.7)
	π_{ZZ}	π_{ZZ}	π_{ZZ}		π_{ZZ}	π_{ZZ}	π_{ZZ}		π_{ZZ}	π_{ZZ}	π_{ZZ}
native FF											
A	2.35	1.61	-0.12	A	1.32	0.69	-0.59	A	-11.13	-11.38	-6.09
B	15.37	11.06	3.31	B	15.03	10.75	3.16	B	9.90	7.83	2.20
C	-23.94	-19.55	-10.82	C	-24.10	-19.69	-10.90	C	-19.40	-16.73	-9.50
native linear-FF											
A	-1.42	-1.78	-1.72	A	-2.45	-2.68	-2.19	A	-13.25	-13.11	-6.99
B	12.49	8.15	2.02	B	12.26	7.94	1.92	B	9.02	6.51	1.65
C	-22.95	-20.34	-11.66	C	-23.02	-20.40	-11.70	C	-16.29	-15.73	-9.26
D	-32.06	-27.23	-15.66	D	-32.14	-27.30	-15.69	D	-29.74	-25.23	-14.42
native syn-FF											
A	7.80	6.28	2.37	A	6.04	4.72	1.57	A	-14.80	-13.71	-7.80
B	25.66	19.79	7.23	B	24.66	18.91	6.81	B	14.68	11.36	3.53
C	-21.05	-18.58	-10.51	C	-21.27	-18.77	-10.64	C	-12.49	-12.55	-7.41
D	-30.70	-25.89	-14.93	D	-30.83	-26.00	-14.99	D	-26.91	-23.29	-13.24
native anti-FF											
A	7.02	6.01	2.22	A	3.84	3.20	0.78	A	-8.64	-10.34	-5.75
B	22.02	17.20	6.08	B	20.43	15.80	5.42	B	11.15	7.95	2.17
C	-21.28	-18.50	-10.52	C	-21.54	-18.73	-10.68	C	-13.70	-13.70	-8.25
D	-32.79	-27.56	-15.86	D	-32.90	-27.66	-15.91	D	-31.42	-25.93	-14.83
FF											
A	-0.61	-0.73	-1.45	A	-5.19	-4.76	-3.50	A	-13.20	-12.99	-7.04
B	14.61	10.52	3.00	B	13.28	9.32	2.38	B	9.24	7.24	1.77
C	-24.67	-20.00	-11.09	C	-25.43	-20.65	-11.46	C	-22.56	-19.27	-10.84
linear-FF											
A	-4.01	-3.74	-2.89	A	-7.85	-7.11	-4.61	A	-14.76	-14.24	-7.67
B	12.24	8.11	1.89	B	11.50	7.41	1.52	B	9.39	6.81	1.64
C	-23.54	-20.68	-11.89	C	-23.98	-21.06	-12.11	C	-19.54	-18.34	-10.65
D	-31.97	-27.12	-15.64	D	-32.33	-27.43	-15.81	D	-30.98	-26.27	-15.08
syn-FF											
A	4.36	3.54	0.84	A	-1.49	-1.65	-1.81	A	-17.35	-15.67	-8.95
B	23.92	18.39	6.51	B	20.92	15.75	5.23	B	13.45	10.27	2.84
C	-21.62	-18.93	-10.79	C	-22.51	-19.71	-11.29	C	-16.66	-15.82	-9.22
D	-31.32	-26.41	-15.24	D	-31.83	-26.85	-15.49	D	-28.75	-24.91	-14.20
anti-FF											
A	3.66	3.40	0.75	A	-3.44	-2.89	-2.45	A	-11.01	-11.43	-6.16
B	21.86	16.98	5.90	B	18.56	14.05	4.50	B	13.56	10.24	3.13
C	-20.65	-17.94	-10.27	C	-21.56	-18.74	-10.77	C	-17.48	-16.56	-9.72
D	-32.63	-27.46	-15.73	D	-32.99	-27.78	-15.90	D	-32.25	-26.93	-15.37

^a Ring positions are shown in the following drawings

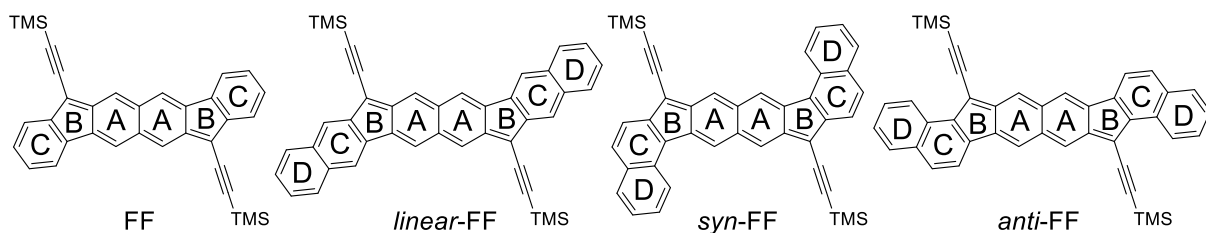
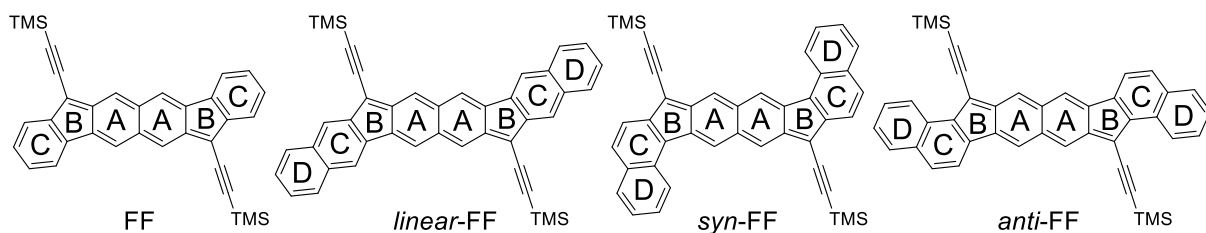


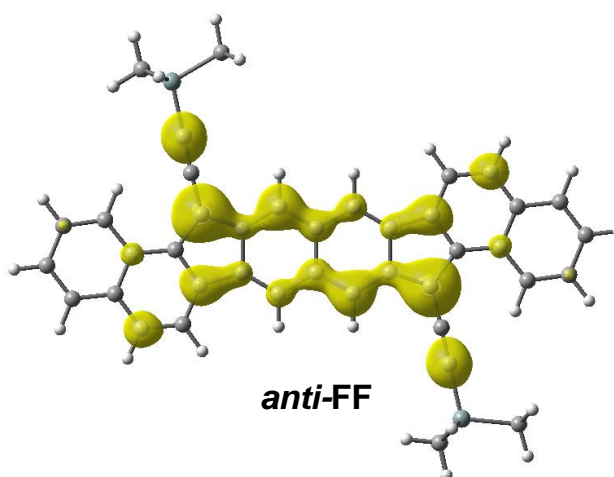
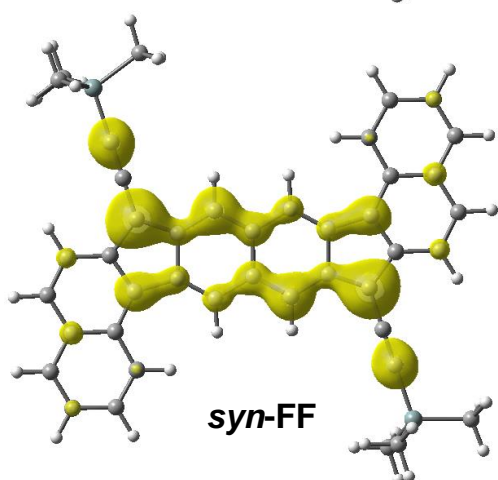
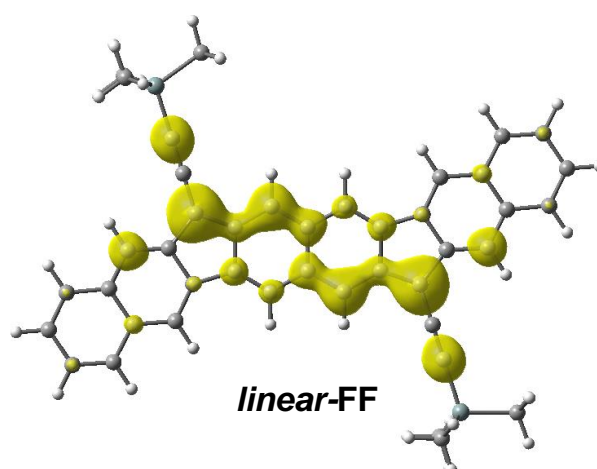
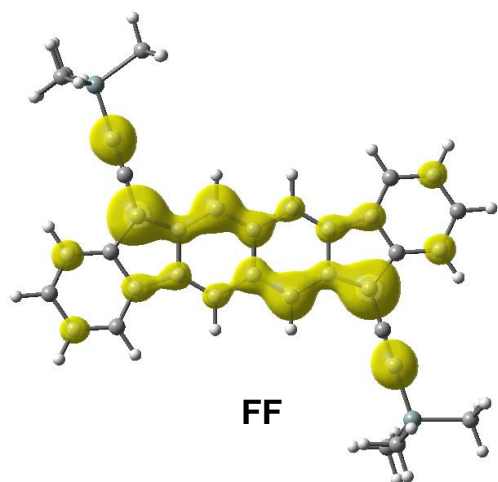
Table S6. NICS(0) π_{ZZ} , NICS(1) π_{ZZ} , and NICS(1.7) π_{ZZ} values at the GIAO-CAM-B3LYP/6-311+G(d,p) for aromatic cores^a

CS singlet			OS singlet			Triplet					
Ring	NICS(0) π_{ZZ}	NICS(1) π_{ZZ}	NICS(1.7) π_{ZZ}	Ring	NICS(0) π_{ZZ}	NICS(1) π_{ZZ}	NICS(1.7) π_{ZZ}	Ring	NICS(0) π_{ZZ}	NICS(1) π_{ZZ}	NICS(1.7) π_{ZZ}
native FF											
A	1.69	0.90	-0.48	A	-9.81	-8.98	-5.66	A	-14.97	-14.48	-7.75
B	11.97	8.14	1.82	B	11.72	7.87	1.59	B	9.60	7.92	2.08
C	-29.55	-24.25	-13.35	C	-27.85	-22.86	-12.64	C	-23.10	-19.44	-10.91
native linear-FF											
A	-0.57	-1.21	-1.31	A	-11.82	-10.78	-6.42	A	-16.55	-15.80	-8.43
B	10.84	6.75	1.37	B	10.81	6.65	1.18	B	8.30	6.37	1.47
C	-27.26	-23.93	-13.63	C	-24.75	-21.85	-12.54	C	-19.74	-18.15	-10.61
D	-34.69	-29.46	-16.92	D	-33.93	-28.80	-16.49	D	-31.84	-27.03	-15.44
native syn-FF											
A	5.18	3.93	1.07	A	-8.55	-8.01	-5.15	A	-19.83	-17.93	-10.32
B	19.69	14.72	4.68	B	17.41	12.74	3.72	B	13.41	11.36	3.63
C	-27.15	-23.66	-13.34	C	-24.15	-21.23	-12.12	C	-13.53	-13.68	-7.95
D	-33.47	-28.27	-16.29	D	-32.91	-27.80	-15.97	D	-31.70	-26.78	-15.33
native anti-FF											
A	5.14	4.27	1.24	A	-10.66	-9.41	-5.88	A	-13.53	-13.20	-6.96
B	16.72	12.65	3.78	B	14.64	10.80	2.90	B	11.47	9.87	3.10
C	-27.61	-23.81	-13.47	C	-23.32	-20.30	-11.65	C	-17.57	-16.04	-9.48
D	-34.93	-29.45	-16.98	D	-34.32	-28.84	-16.51	D	-33.45	-28.02	-15.97
FF											
A	-0.11	-0.41	-1.29	A	-16.02	-14.12	-8.42	A	-16.74	-15.86	-8.55
B	11.78	8.12	1.76	B	11.08	7.38	1.24	B	8.85	7.17	1.59
C	-29.72	-24.27	-13.40	C	-28.57	-23.33	-12.90	C	-26.28	-21.93	-12.22
linear-FF											
A	-2.42	-2.55	-2.18	A	-17.17	-15.12	-8.82	A	-17.72	-16.65	-8.92
B	10.75	6.84	1.31	B	10.63	6.60	1.00	B	8.32	6.32	1.29
C	-27.51	-24.01	-13.72	C	-25.64	-22.45	-12.88	C	-23.21	-20.90	-12.09
D	-34.56	-29.32	-16.88	D	-34.03	-28.85	-16.56	D	-33.03	-28.02	-16.08
syn-FF											
A	3.46	2.72	0.33	A	-14.56	-13.00	-7.79	A	-18.63	-17.07	-9.41
B	19.45	14.64	4.60	B	15.61	11.22	2.91	B	13.53	10.33	2.73
C	-27.14	-23.54	-13.33	C	-25.18	-21.98	-12.60	C	-17.70	-16.96	-9.74
D	-33.74	-28.51	-16.43	D	-33.60	-28.41	-16.32	D	-26.53	-23.72	-13.22
anti-FF											
A	3.61	3.26	0.56	A	-16.11	-13.89	-8.24	A	-15.24	-14.45	-7.66
B	17.96	13.68	4.18	B	14.26	10.30	2.55	B	11.54	9.55	2.73
C	-26.70	-23.01	-13.05	C	-23.72	-20.61	-11.85	C	-21.07	-18.92	-11.05
D	-34.92	-29.46	-16.88	D	-34.51	-29.07	-16.58	D	-34.11	-28.69	-16.35

^a Ring positions are shown in the following drawings



ODD-ELECTRON DENSITY MAPS FOR FF DERIVATIVES



OFET DEVICES

Bottom-gate/top-contact (BG/TC) OFETs were constructed on heavily doped n-type silicon wafers covered with thermally grown silicon dioxide (300 nm) which was cleaned by piranha solution. The silicon dioxide acts as a gate dielectric layer, and the silicon wafer serves as a gate electrode. The cross-linked PVP (poly-4-vinylphenol) was prepared by spin-coating from a solution of PVP (Aldrich 436224, Mw ~25,000, 1.0 wt%) and poly(melamine-co-formaldehyde) (Mn ~432, 1.0 wt%) in propylene glycol monomethyl ether acetate (PGMEA) at the rotational speed of 500 rpm for 5 s and then 4000 rpm for 60 s, followed by the cross-linkage at temperatures of 150 °C for 60 min under nitrogen atmosphere. Organic semiconductor layers were formed by drop-casting (see Figure S5) from a 0.1~0.2 wt% solution of HDIP derivatives with 1/4 wt% polystyrene (PS) in *o*-dichlorobenzene at 60 °C, followed by thermal annealing at 60 °C for ca. 30 min. Top-contact gold source-drain electrodes (50 nm) were deposited on PVP through a shadow mask with $L = 50, 100, 150$ and $200 \mu\text{m}$, and $W = 2000 \mu\text{m}$.

Bottom-contact/top-gate (BC/TG) OFETs were constructed on Corning's EAGLE glass substrates with the cross-linked PVP, which was prepared by spin-coating from a solution of PVP (10.0 wt%) and poly(melamine-co-formaldehyde) (10.0 wt%) in PGMEA at the rotational speed of 500 rpm for 5 s and then 4000 rpm for 60 s, followed by the cross-linkage at temperatures of 150 °C for 60 min under nitrogen atmosphere. Bottom-contact gold source-drain electrodes (50 nm) were deposited on PVP through a shadow mask with $L = 50, 100, 150$ and $200 \mu\text{m}$, and $W = 2000 \mu\text{m}$. Organic semiconductor layers were formed by drop-casting from a 0.05–0.1 wt% solution of HDIP derivatives with 1/4 wt% PS in *o*-dichlorobenzene at 60 °C, followed by thermal annealing at 60 °C for ca. 30 min. The CYTOP dielectric layer (450 nm measured by DektakXT™ Stylus Profiler) was spin-coated from a solution of CYTOP™ CTL-809M in CT-solv 180 from Asahi Glass at the rotational speed of 500 rpm for 5 s and then 1800 rpm for 120 s on top of the organic layer and then was dried at room temperature for 2 h. The Al gate electrode (50 nm) was formed by vacuum evaporation through a shadow mask.

The FET measurements were carried out at room temperature in a glovebox without exposure to air with a semiconductor parameter analyzer (B1500, Agilent). Mobilities (μ) were calculated in the saturation regime by the relationship: $\mu_{\text{sat}} = (2I_{\text{D}}L)/[WC_i(V_{\text{G}} - V_{\text{th}})^2]$ where I_{D} is the source-drain saturation current; C_i is the capacitance of the insulating layer; V_{G} is the gate voltage and V_{th} is the threshold voltage. The latter can be estimated as the intercept of the linear section of the plot of V_{G} ($I_{\text{D}})^{1/2}$. The reproducibility of the device performance of the presented devices was confirmed by measuring different samples fabricated on different days.

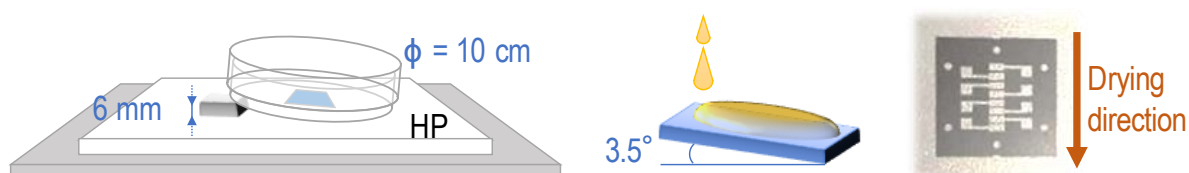


Figure S6. Schematic image of the drop-casting procedure. The substrates were placed inside the petri-dish with the saturated solvent vapor at 60 °C, then 30 μL of the semiconductor solution was drop-casted.

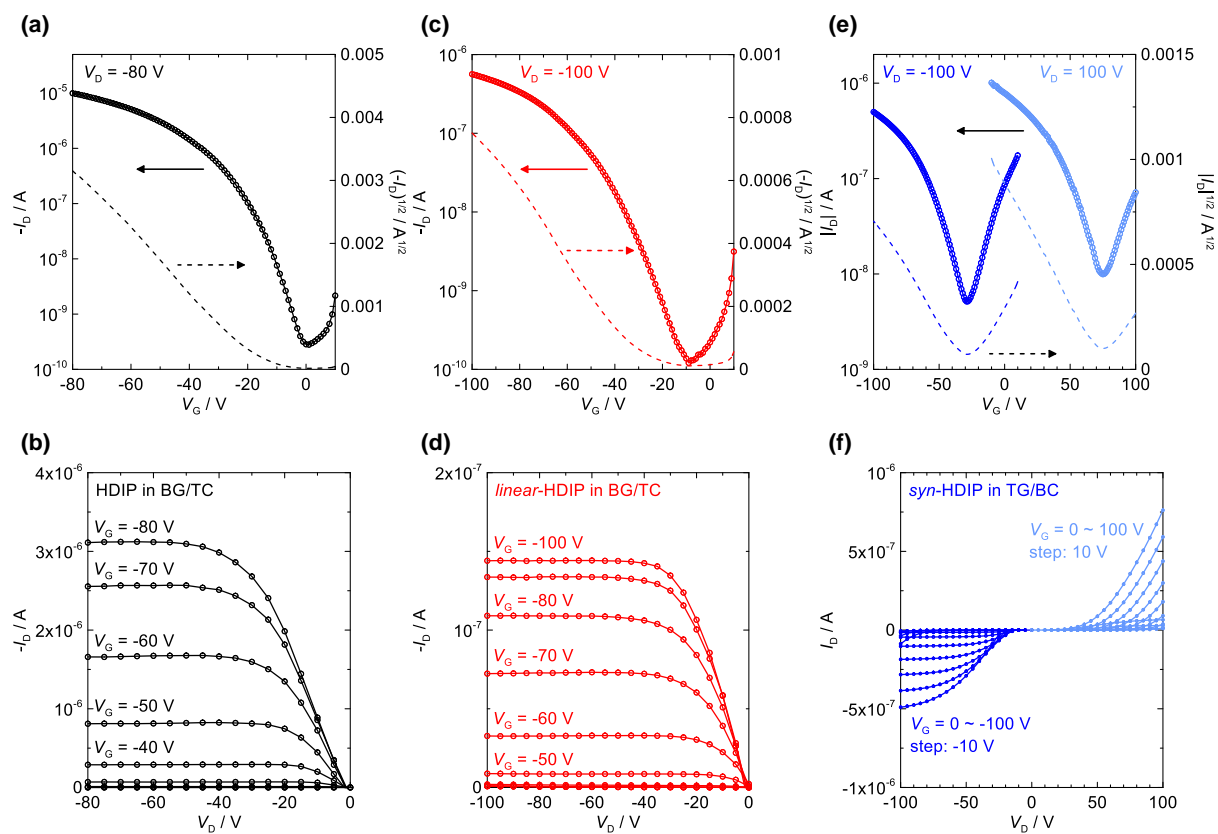
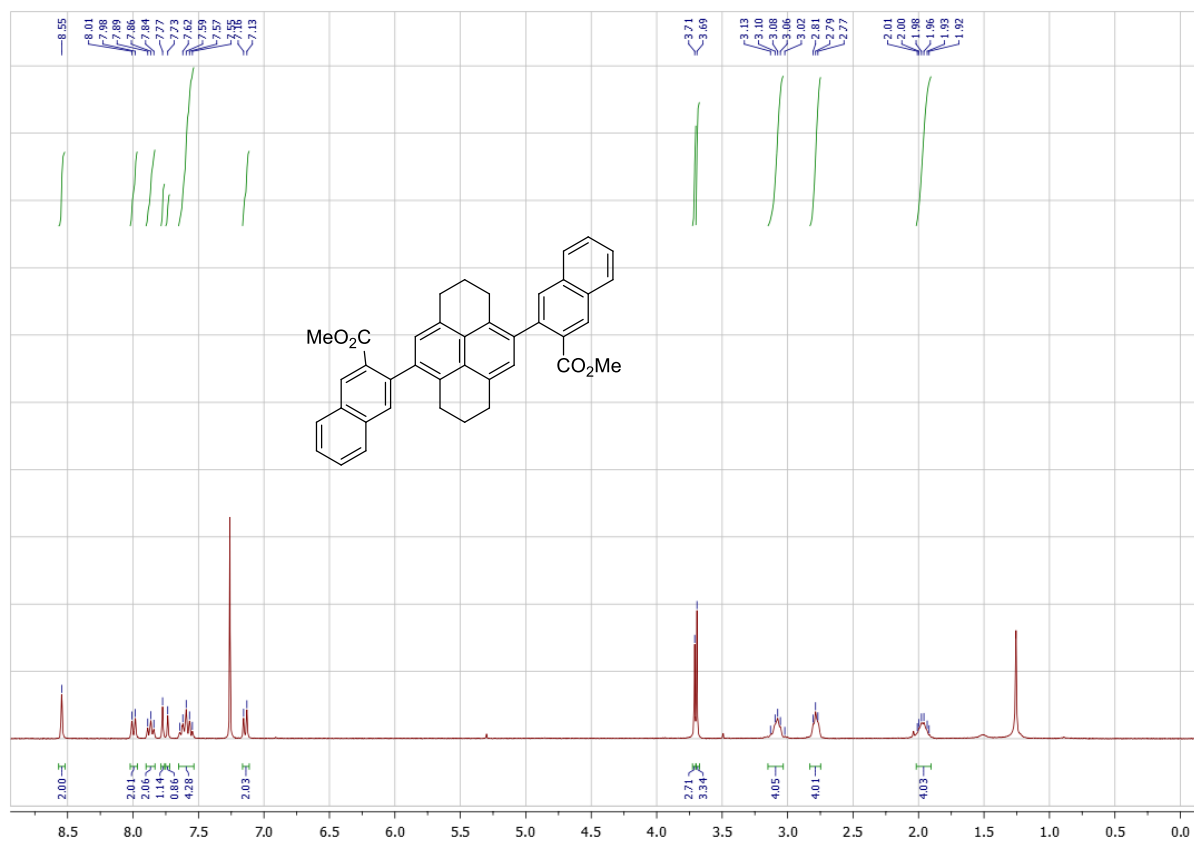
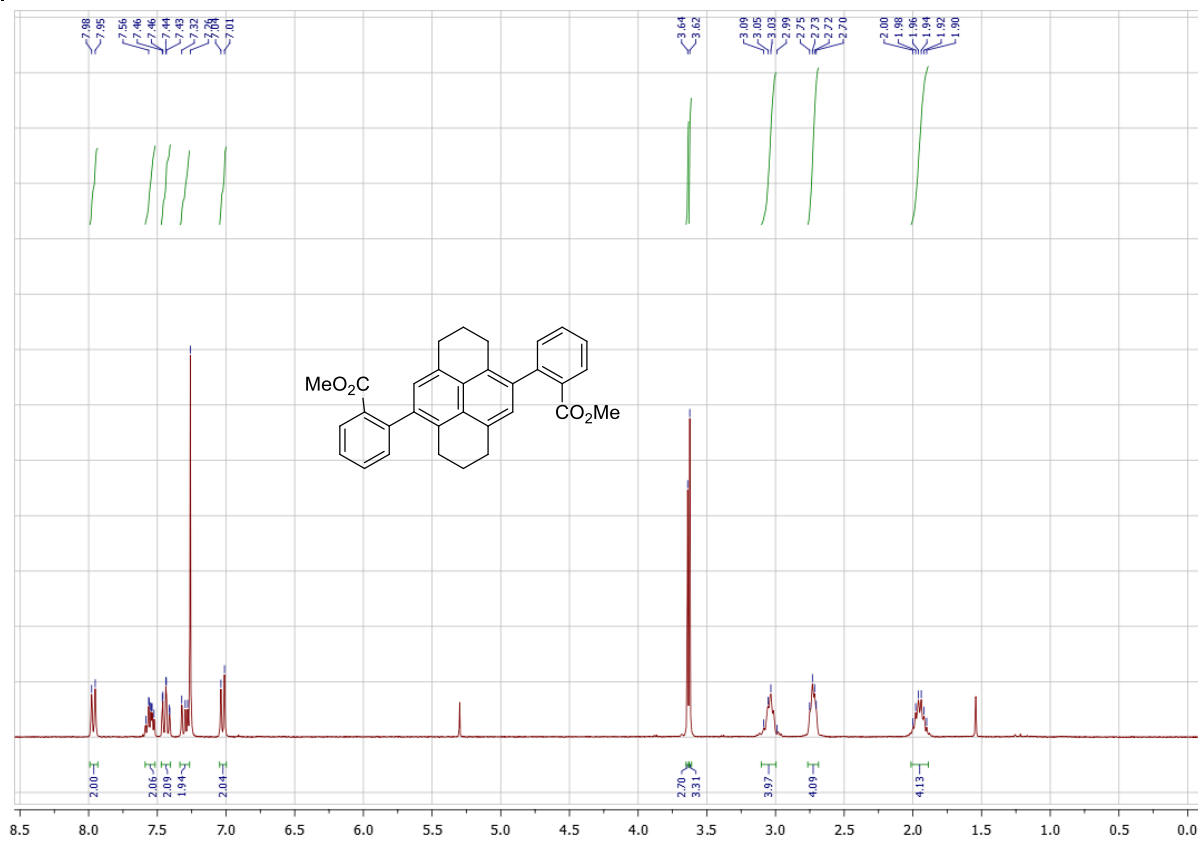
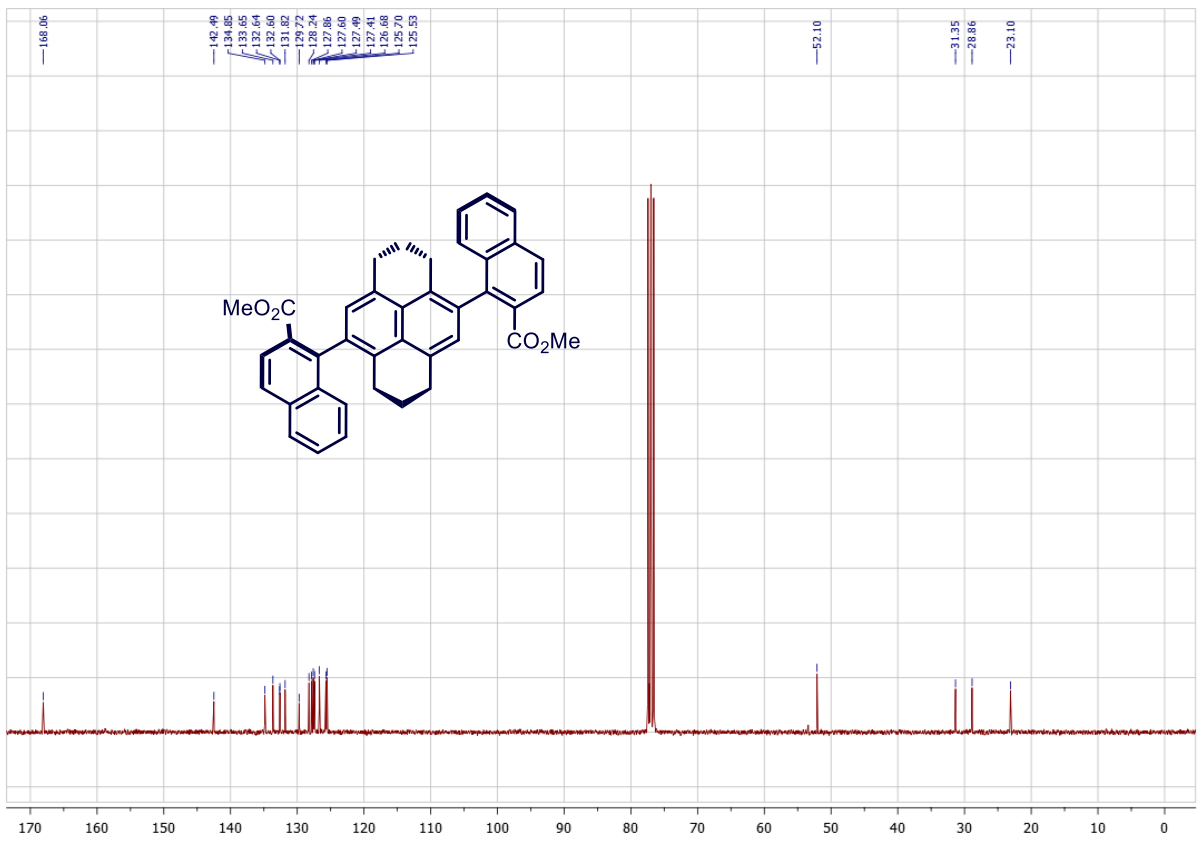
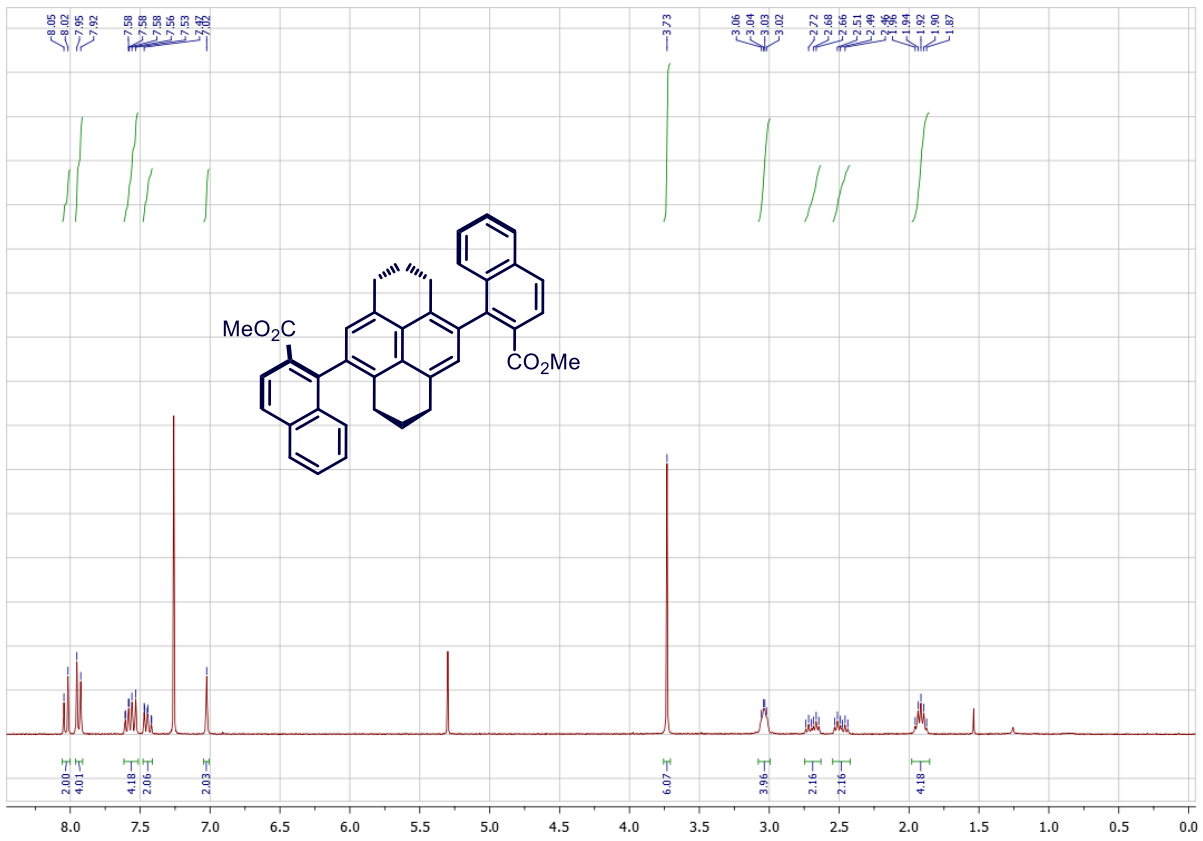
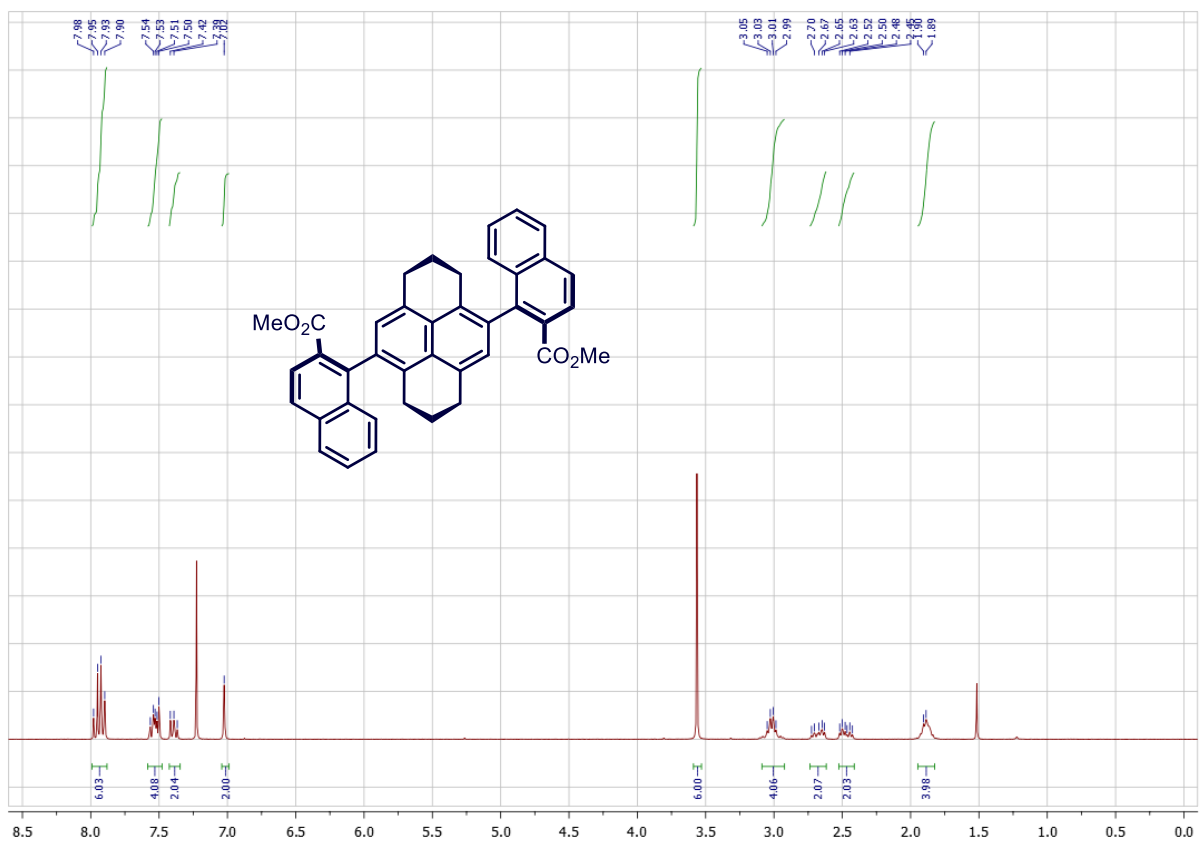


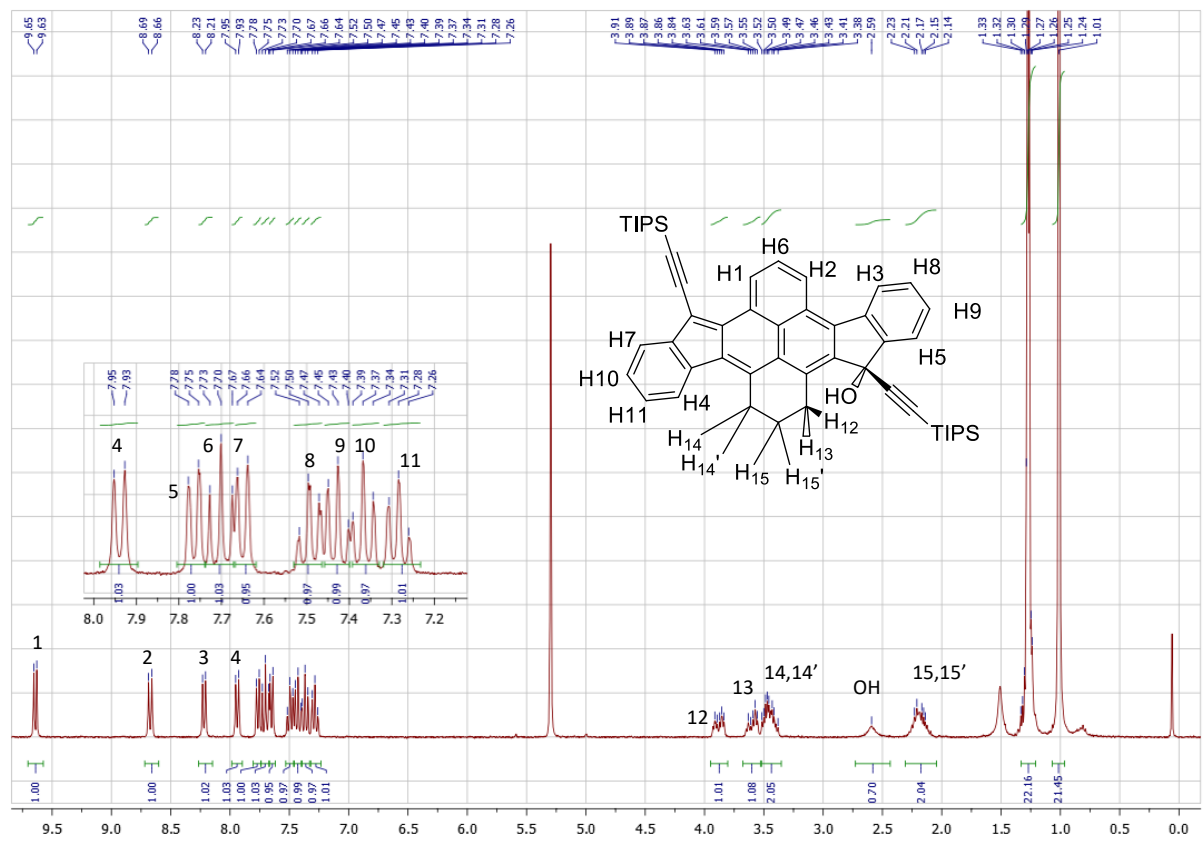
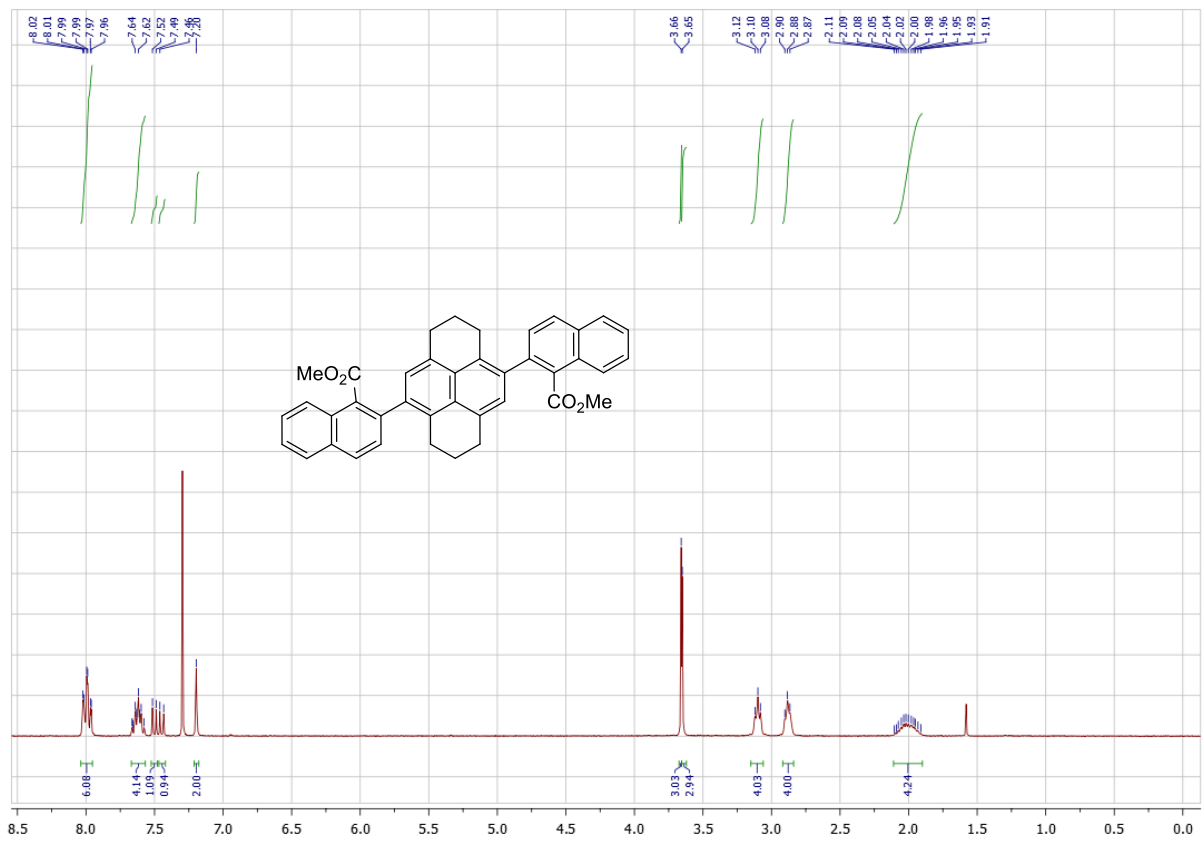
Figure S7. OFET devices of HDIP derivatives. (a) Transfer and (b) output characteristics of the BG/TC device with a drop-casted HDIP layer. (c) Transfer and (d) output characteristics of the BG/TC device with a drop-casted *linear*-HDIP layer. (e) Transfer and (f) output characteristics of the TG/BC device with a drop-casted *syn*-HDIP layer.

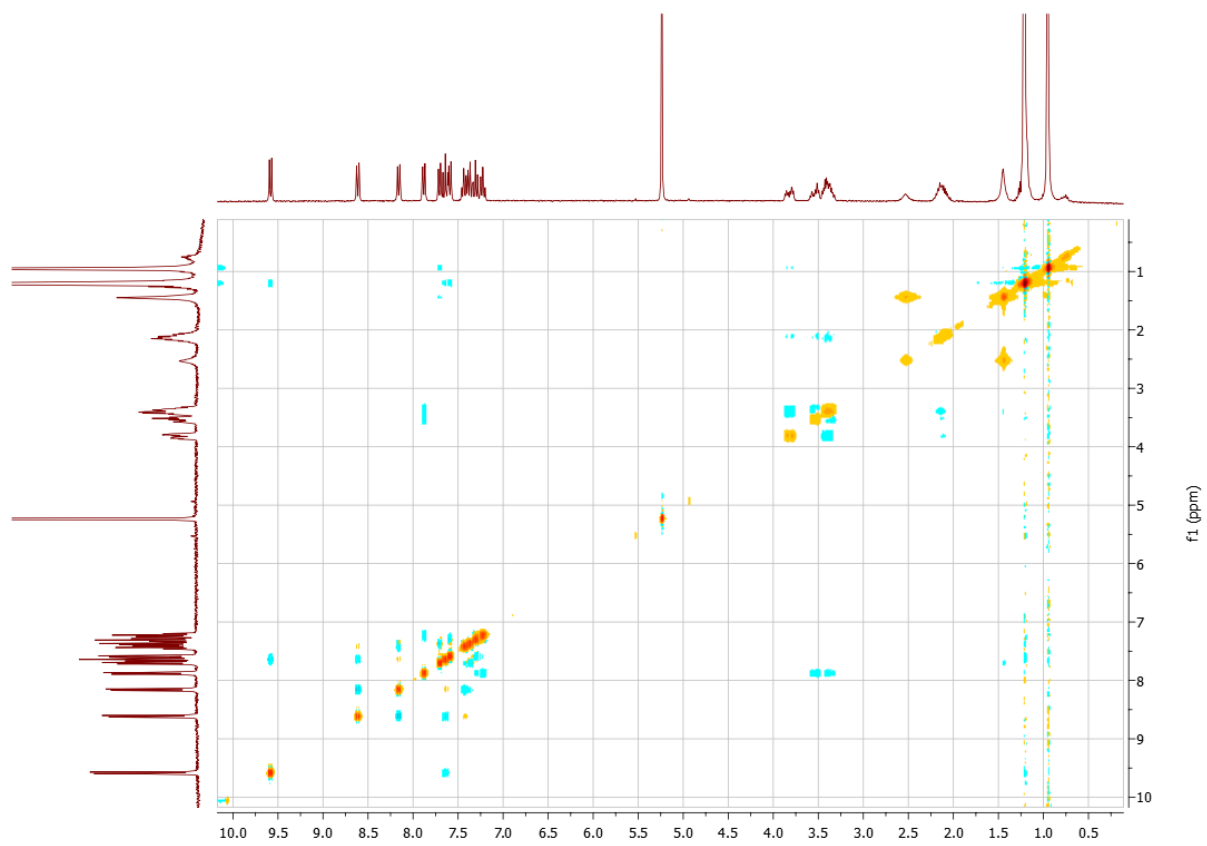
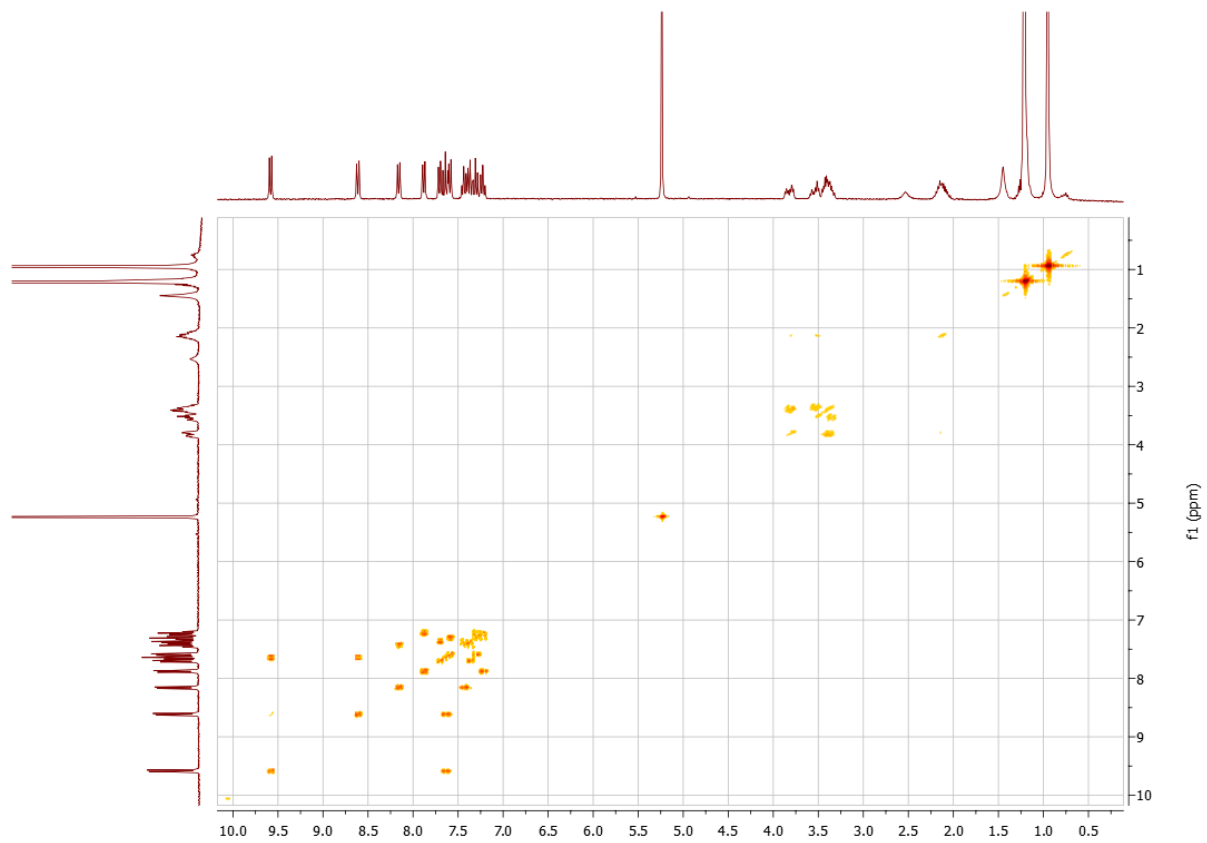
RMN SPECTRA

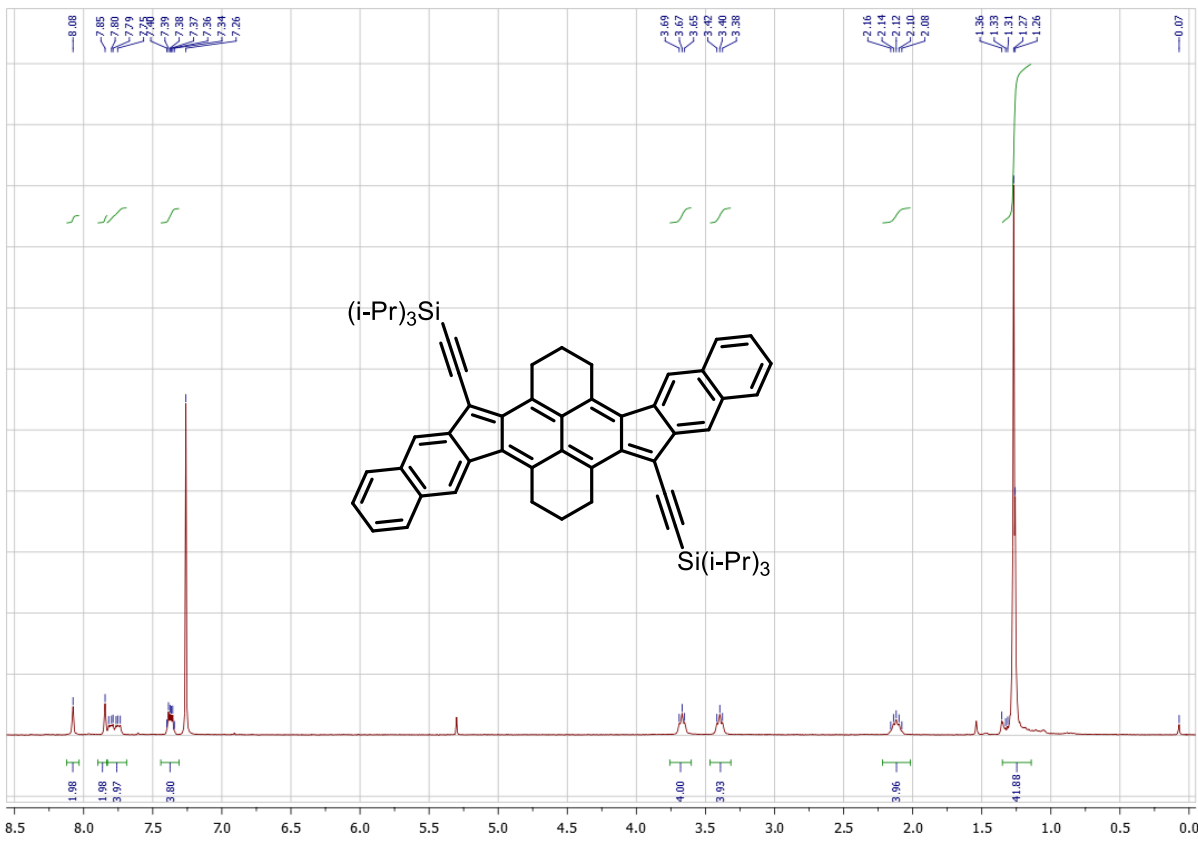
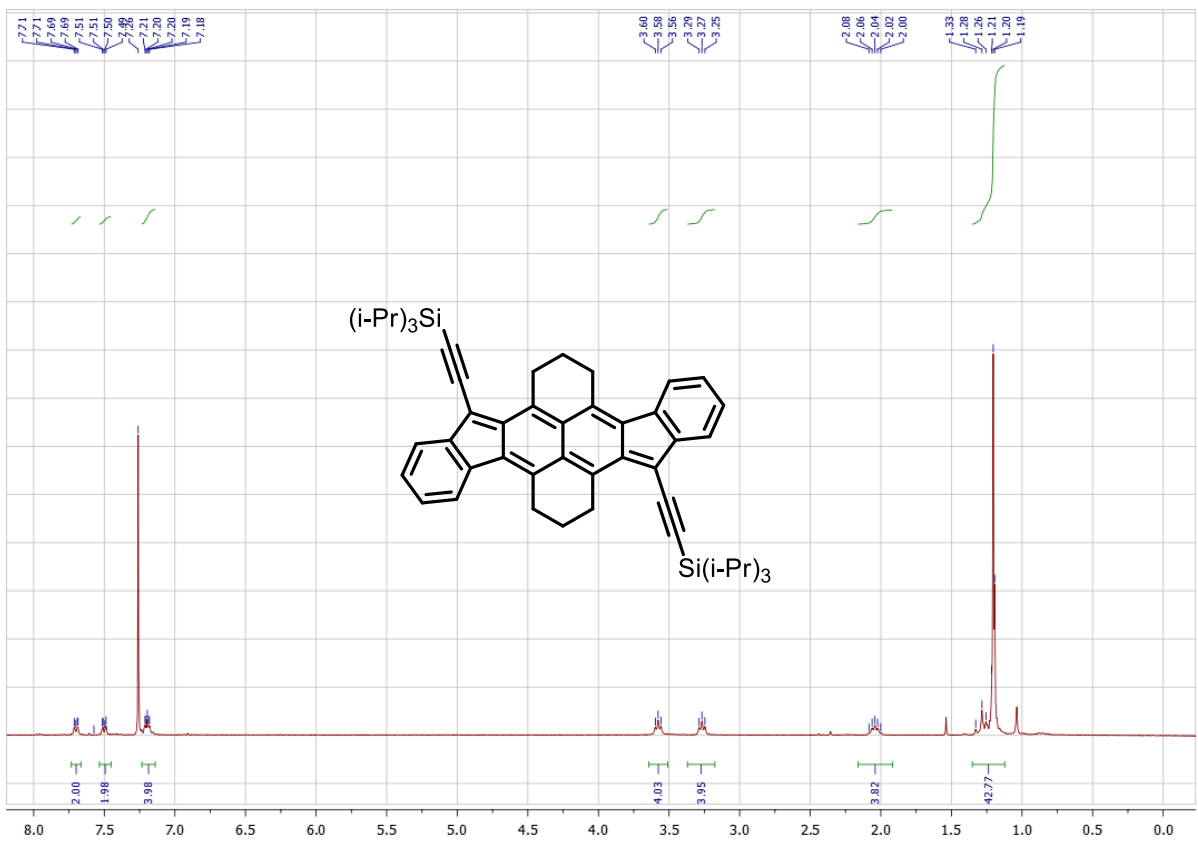


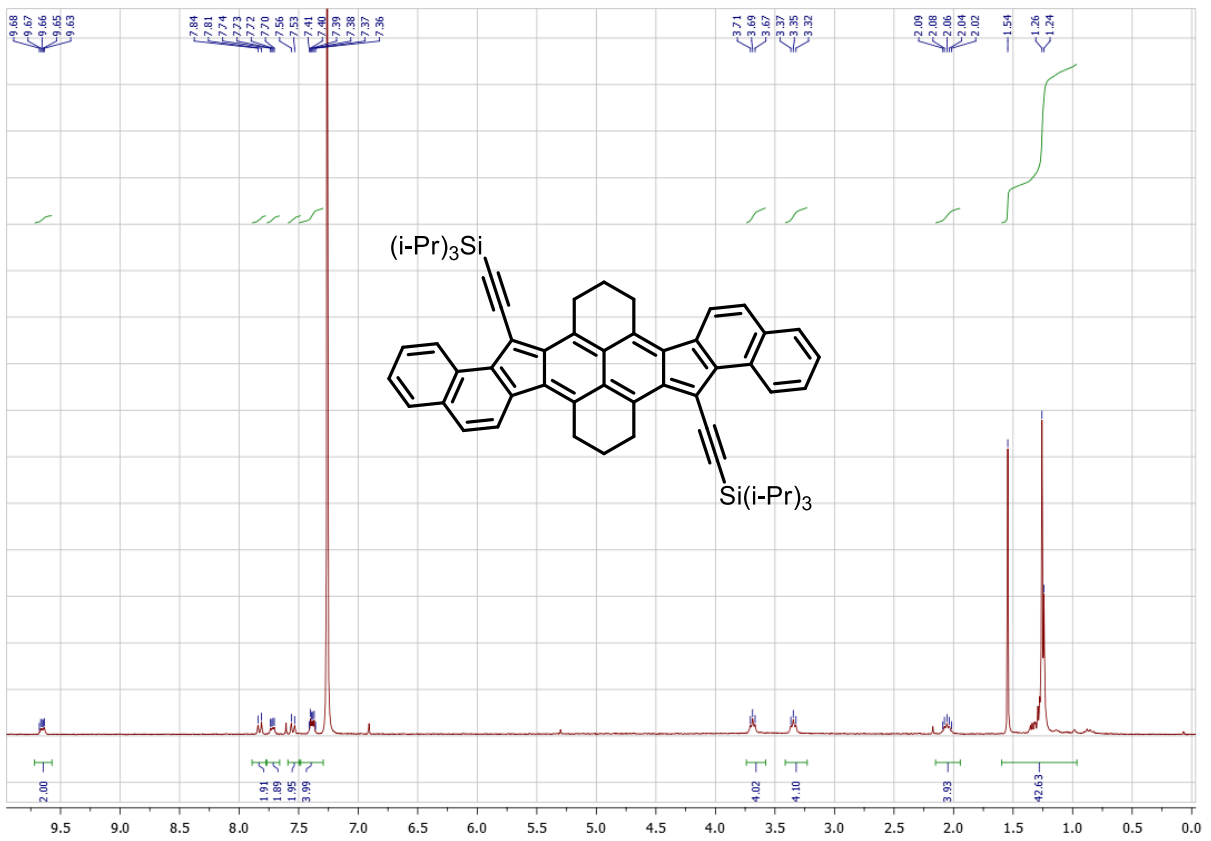
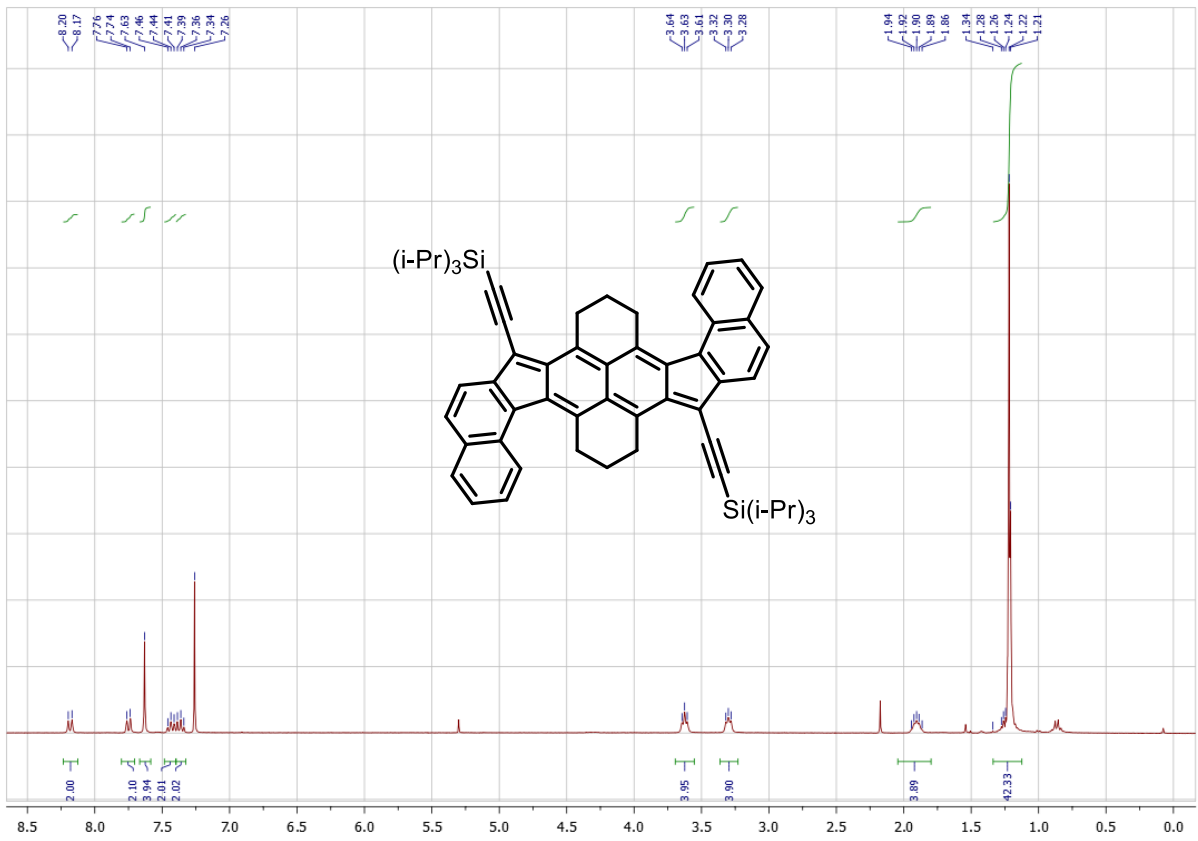




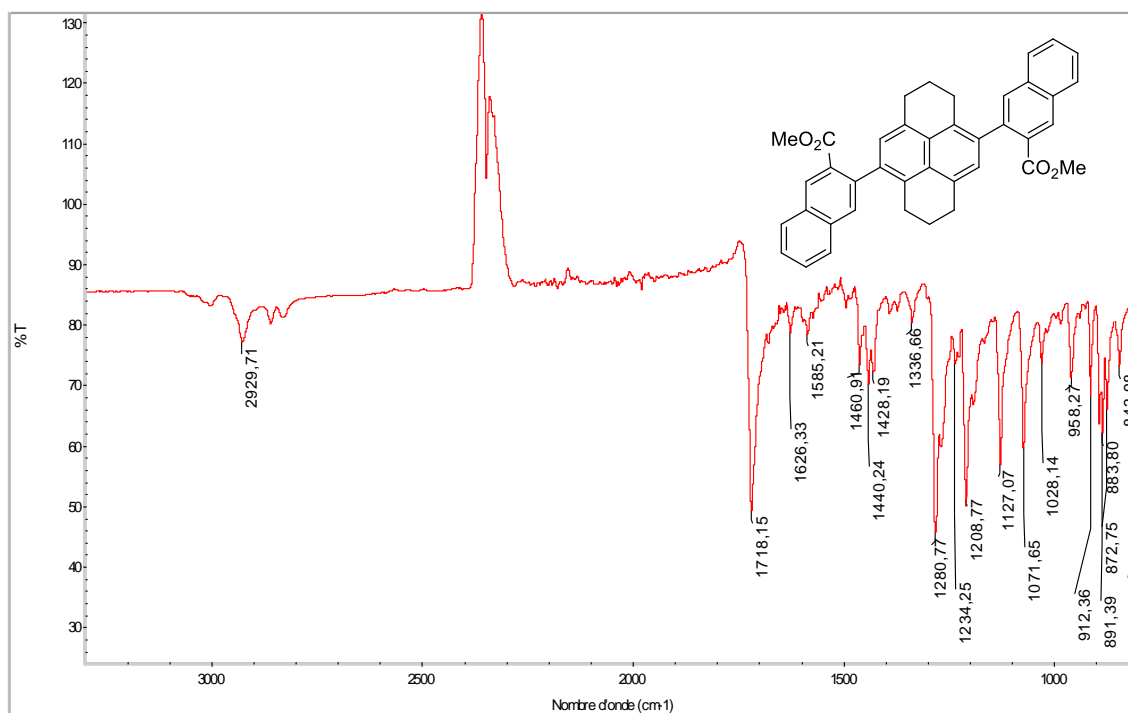
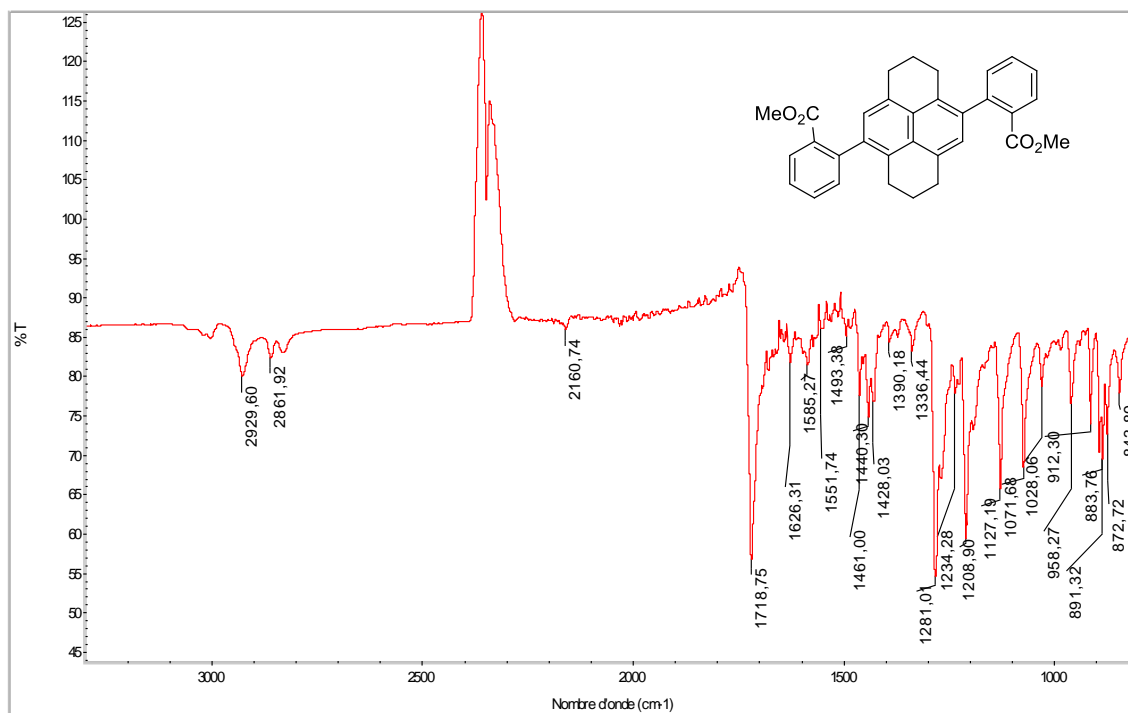


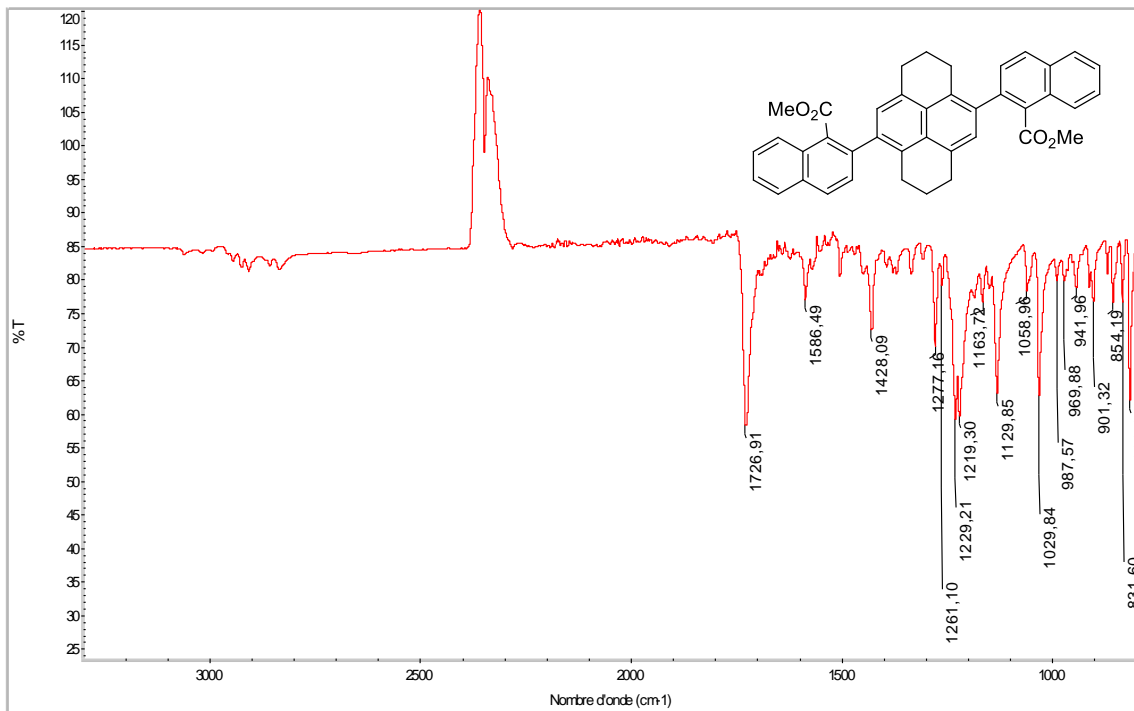
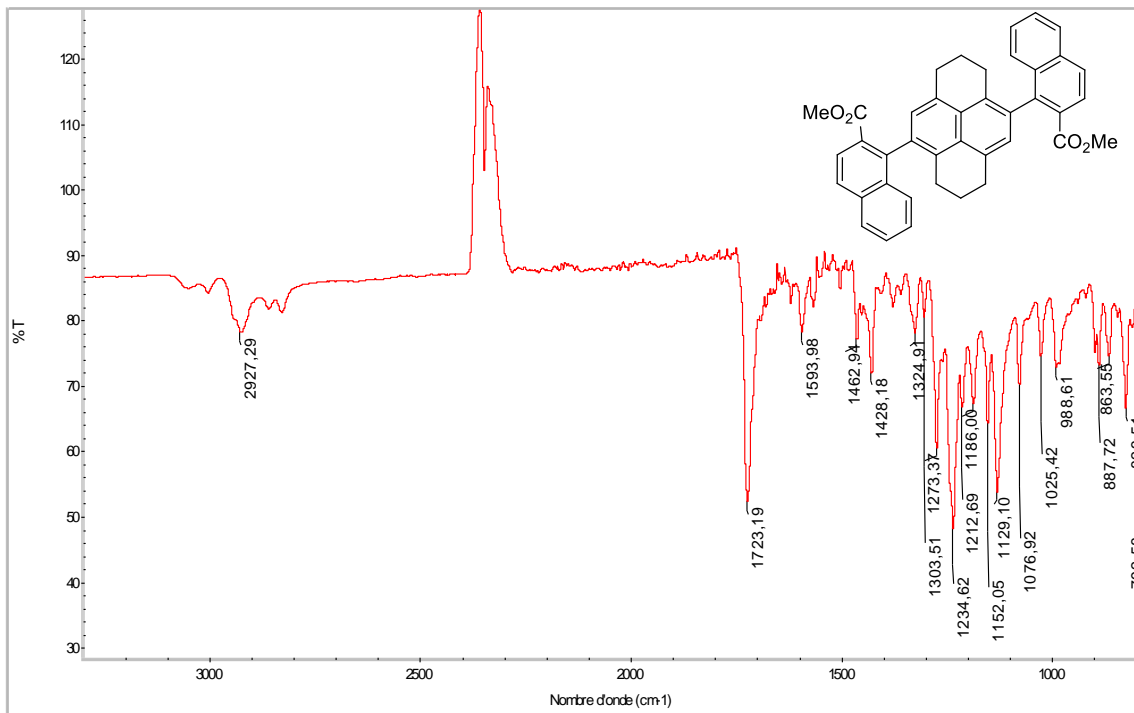


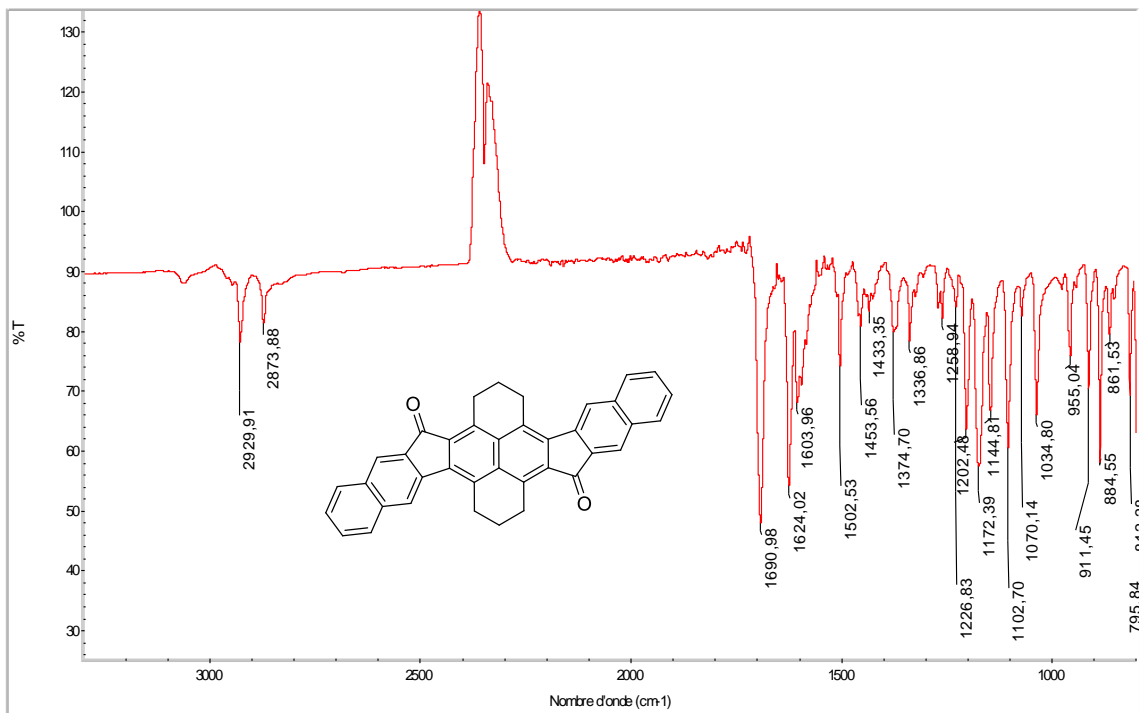
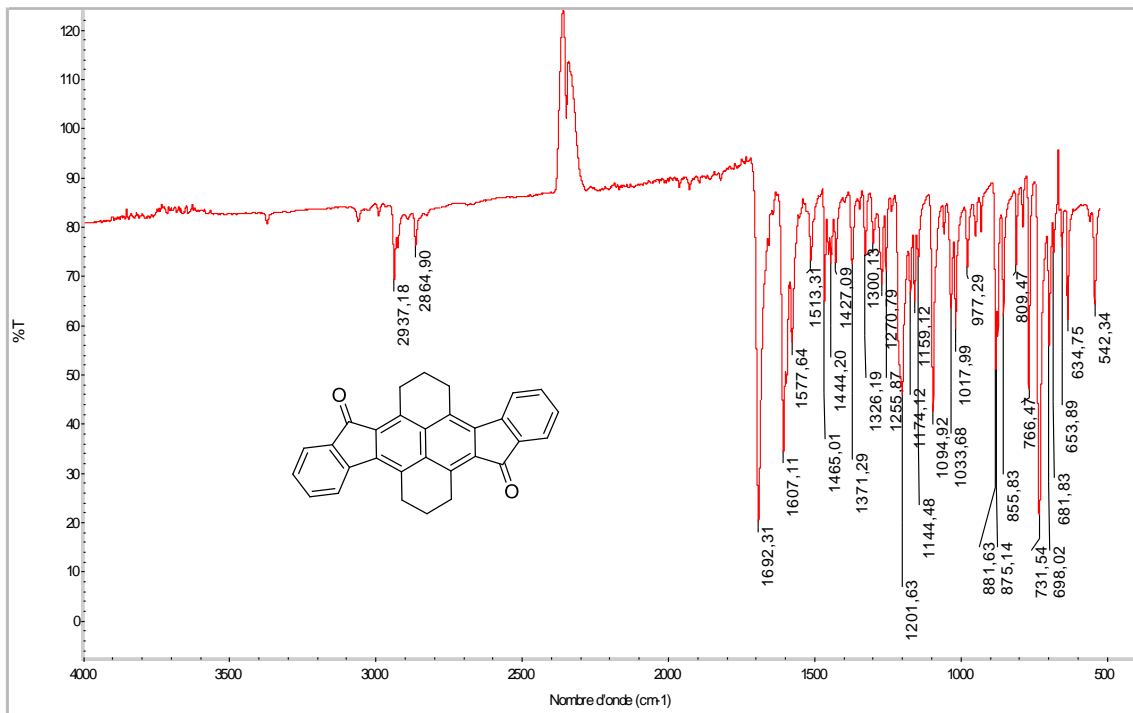


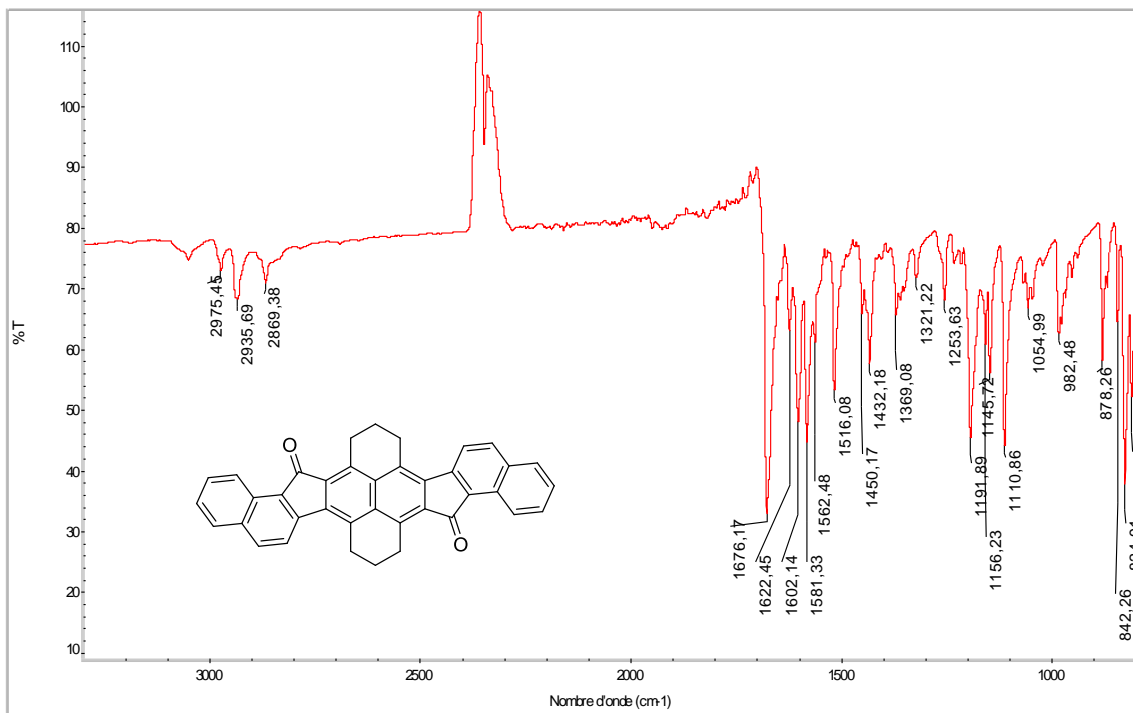
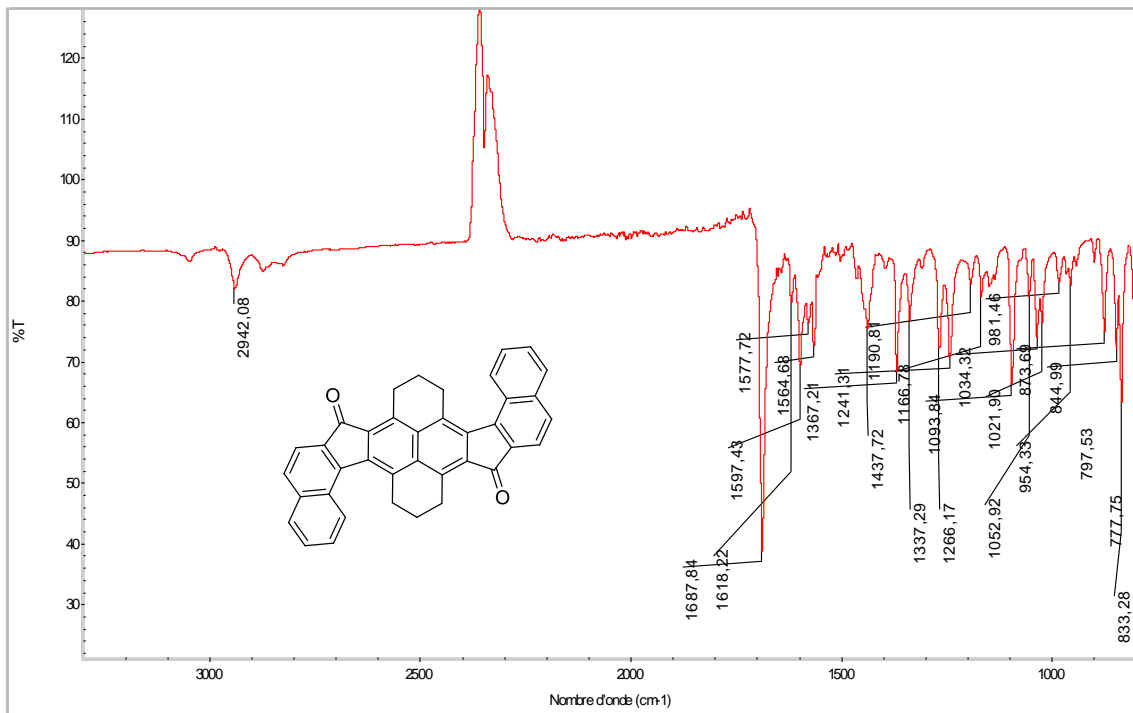


INFRARED SPECTRA

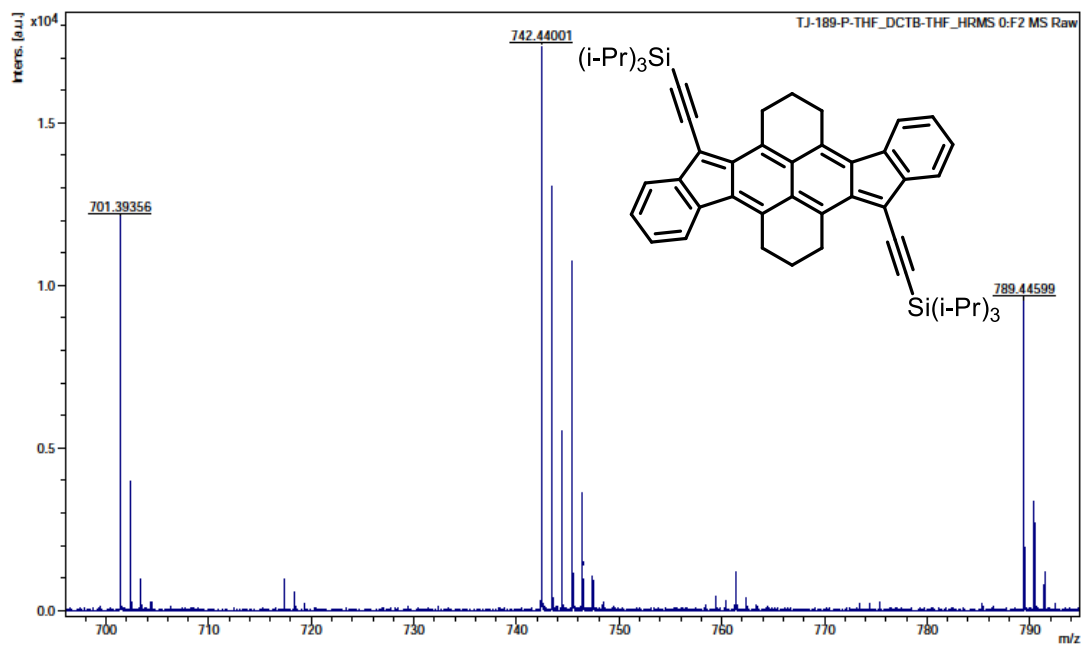
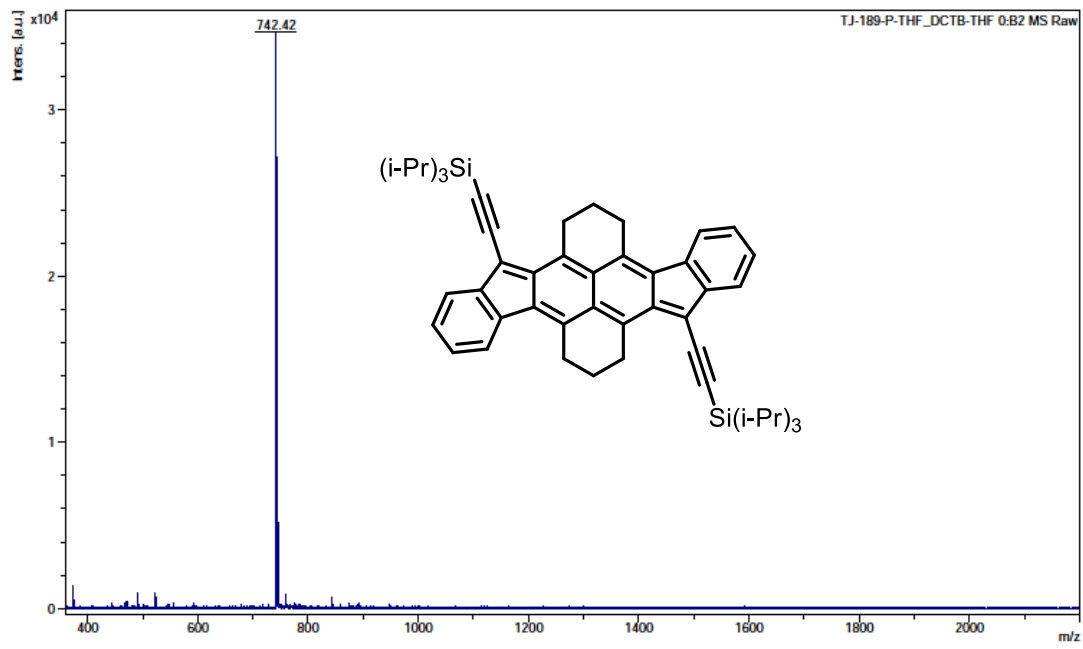


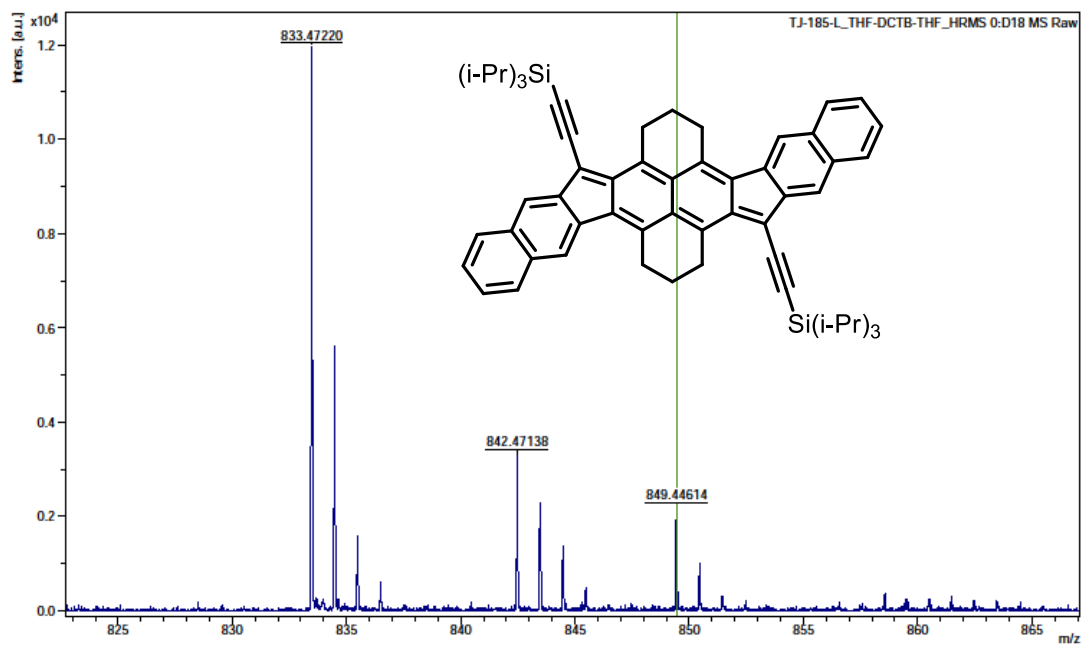
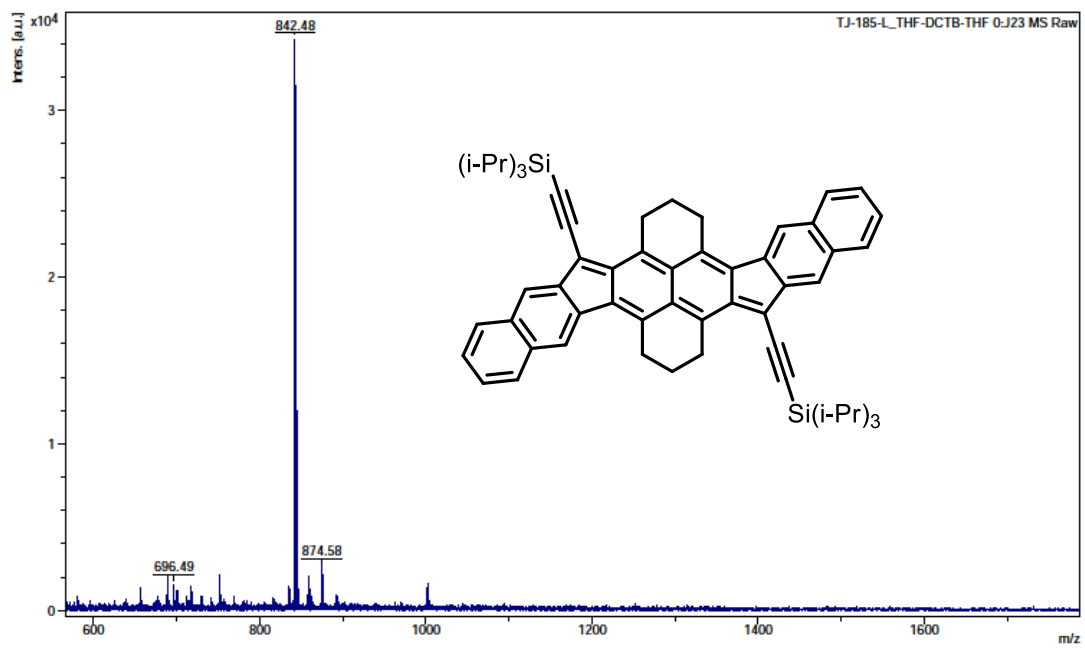


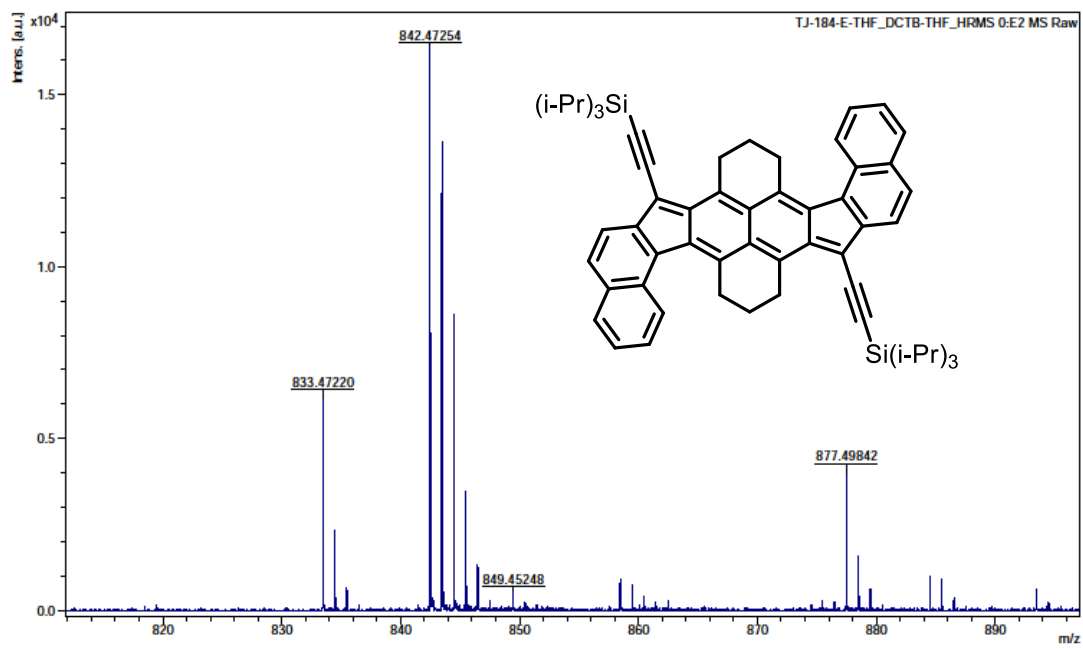
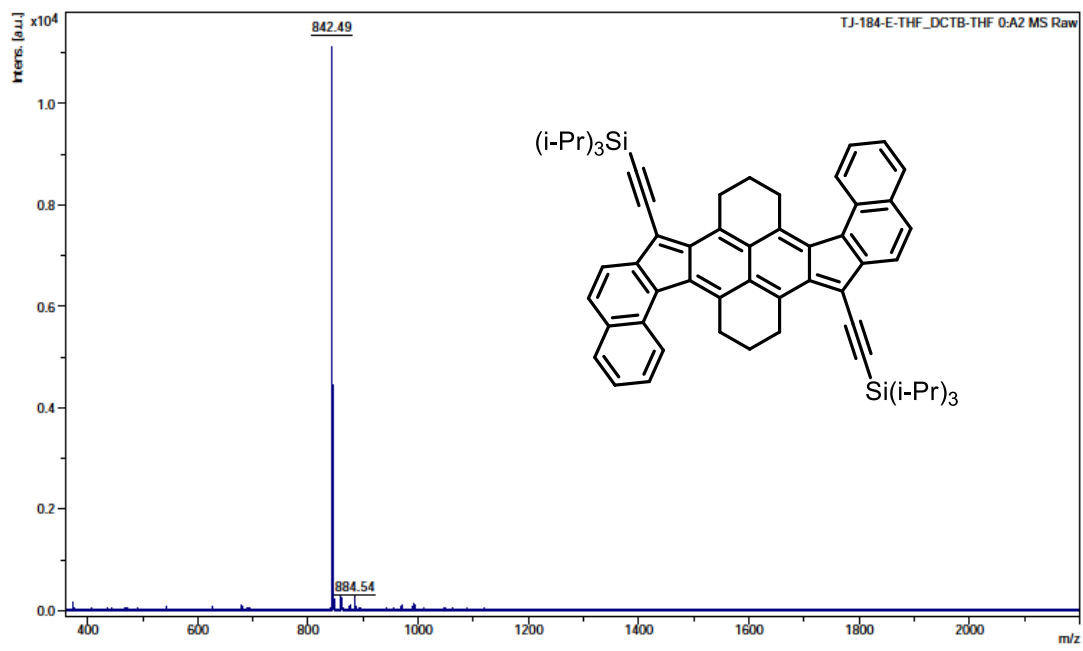


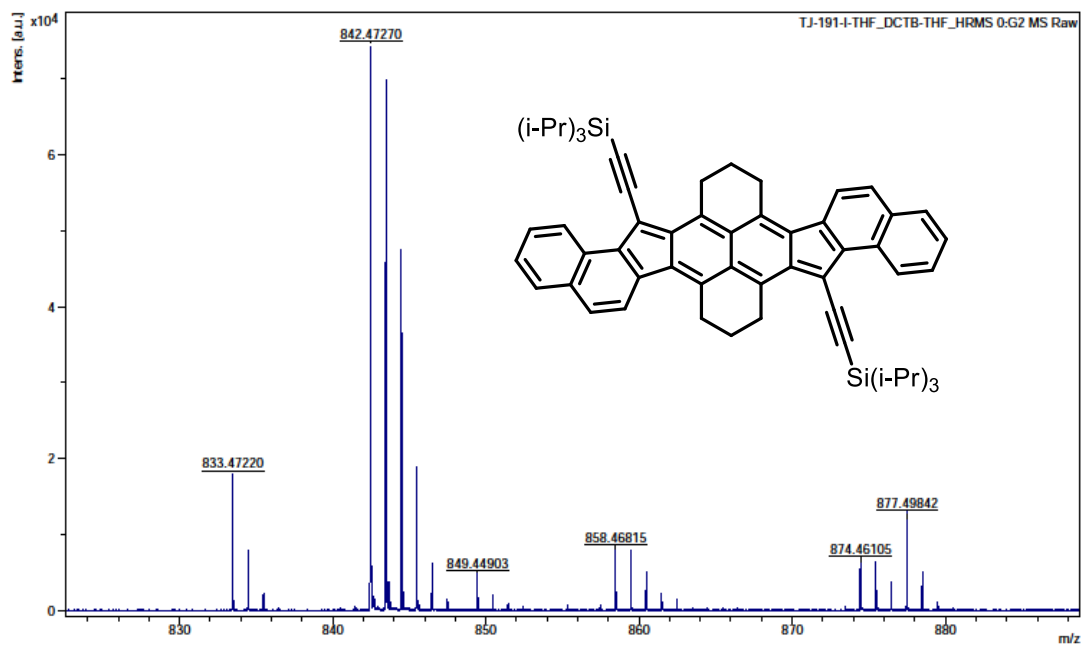
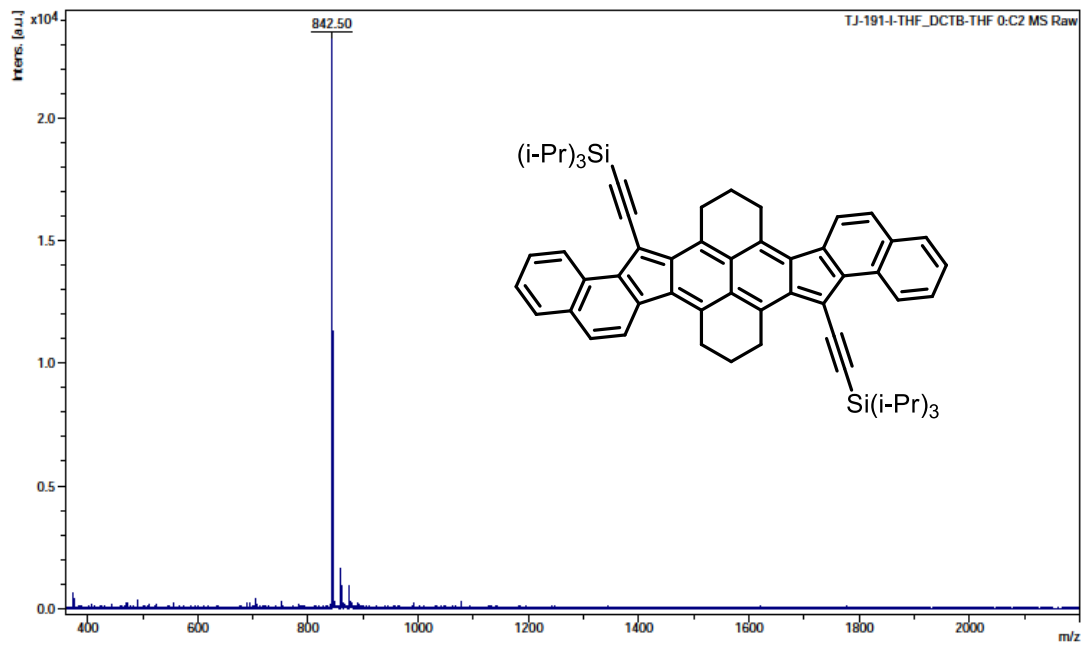


MALDI (TOF) of HDIP derivatives









REFERENCES

- ⁱ J. Lee and J. Park, *Org. Lett.*, 2015, **17**, 3960–3963.
- ⁱⁱ L. Ling, Y. He, X. Zhang, M. Luo and X. Zeng, *Angew. Chem. Int. Ed.*, 2019, **58**, 6554–6558.
- ⁱⁱⁱ Y. Xia, Z. Liu, Q. Xiao, P. Qu, R. Ge, Y. Zhang and J. Wang, *Angew. Chem. Int. Ed.*, 2012, **51**, 5714–5717.
- ^{iv} F. Krätzschar, M. Kaßel, D. Delony and A. Breder, *Chem. Eur. J.*, 2015, **21**, 7030–7034.
- ^v B. Ghaffari, S. M. Preshlock, D. L. Plattner, R. J. Staples, P. E. Maligres, S. W. Krska, R. E. Maleczka and M. R. Smith, *J. Am. Chem. Soc.*, 2014, **136**, 14345–14348.
- ^{vi} G. P. Eyer, K. R. Kittilstved and T. L. Andrew, *J. Phys. Chem. C* 2017, **121**, 24929–24935.
- ^{vii} Gaussian 16, Revision A.03, M. J. Frisch, G. W. Trucks, H. B. Schlegel, G. E. Scuseria, M. A. Robb, J. R. Cheeseman, G. Scalmani, V. Barone, G. A. Petersson, H. Nakatsuji, X. Li, M. Caricato, A. V. Marenich, J. Bloino, B. G. Janesko, R. Gomperts, B. Mennucci, H. P. Hratchian, J. V. Ortiz, A. F. Izmaylov, J. L. Sonnenberg, D. Williams-Young, F. Ding, F. Lipparini, F. Egidi, J. Goings, B. Peng, A. Petrone, T. Henderson, D. Ranasinghe, V. G. Zakrzewski, J. Gao, N. Rega, G. Zheng, W. Liang, M. Hada, M. Ehara, K. Toyota, R. Fukuda, J. Hasegawa, M. Ishida, T. Nakajima, Y. Honda, O. Kitao, H. Nakai, T. Vreven, K. Throssell, J. A. Montgomery, Jr., J. E. Peralta, F. Ogliaro, M. J. Bearpark, J. J. Heyd, E. N. Brothers, K. N. Kudin, V. N. Staroverov, T. A. Keith, R. Kobayashi, J. Normand, K. Raghavachari, A. P. Rendell, J. C. Burant, S. S. Iyengar, J. Tomasi, M. Cossi, J. M. Millam, M. Klene, C. Adamo, R. Cammi, J. W. Ochterski, R. L. Martin, K. Morokuma, O. Farkas, J. B. Foresman, and D. J. Fox, Gaussian, Inc., Wallingford CT, 2016.
- ^{viii} G. E. Rudebusch, J. L. Zafra, K. Jorner, K. Fukuda, J. L. Marshall, I. Arrechea-Marcos, G. L. Espejo, R. P. Ortiz, C. J. Gómez-García, L. N. Zakharov, M. Nakano, H. Ottosson, J. Casado and M. M. Haley, *Nat. Chem.*, 2016, **8**, 753–759.
- ^{ix} D. D. Dohnert and J. Koutecký, *J. Am. Chem. Soc.*, 1980, **102**, 1789–1796.
- ^x K. Yamaguchi, *Chem. Phys. Lett.*, 1975, **33**, 330–335.
- ^{xi} T. Lu and F. Chen, Multiwfn: A multifunctional wavefunction analyzer. *J. Comput. Chem.*, 2012, **33**, 580–592.
- ^{xii} A. Rahalkar, A. Stanger, Aroma: <http://chemistry.technion.ac.il/members/amnon-stanger/>; (b) A. Stanger, *J. Org. Chem.*, 2006, **71**, 883–893; (c) A. Stanger, *J. Org. Chem.*, 2010, **75**, 2281–2288; (d) R. Gershoni-Poranne and A. Stanger, *Chem. Eur. J.*, 2014, **20**, 5673–5688.